C-212

Final Report

DEVELOPMENT OF METHODS FOR ESTIMATING THE CHANGES IN MARINE SEDIMENTS AS A RESULT OF THE DISCHARGE OF SEWERED MUNICIPAL WASTEWATERS THROUGH SUBMARINE OUTFALLS

PART I - SEDIMENTATION FLUX ESTIMATION

****
*   *
* DRAFT COPY *
*   *
****

EPA Grant #: CR811182 - 01

Contracting Officer's Technical Representative:

Donald Baumgartner, Ph.D.

Submitted to:

United States Envirnomental Protection Agency (US-EPA)
Environmental Research Laboratory
Hatfield Marine Science Center
Ocean Discharge Division
Newport, Oregon

By:

Tareah J. Hendricks, Ph.D.
Southern California Coastal Water Research Project Authority
(SCCWRP)
646 West Pacific Coast Highway
Long Beach, California

January 22, 1987

SUMMARY

Some of the most evident impacts that accompany the discharge of sewered municipal wastewaters into the ocean environment are associated with the sedimentation of organically-enriched particles in the effluent. The increased fluxes of organic material and trace constituents to the ocean bottom can produce changes in the physical and chemical properties of the sediments around the outfall, and alter the abundance and community structure of the biota living near and within the sediments. The ability to predict the depositional rates and patterns of these particulates is a first step in relating changes to the characteristics of the effluent, the outfall system, and the receiving water environment. This report describes the development of a set of predictive "tools" that can be used to provide these depositional estimates.

Three levels of predictive capability are presented. At the lowest level, a "generic" depositional pattern is created for "typical" ocean conditions existing in the coastal waters of southern California. Additional tables and graphs are also developed to permit modification of the generic pattern for areas with faster or slower net flows, stronger or weaker variations in the flow, different wastefield elevations, and the effects of bottom slope.

These tables and plots were generated from the numerical simulation model "SFFT". This model was developed to provide estimates of depositional rates and patterns in an ocean of constant water depth, but with temporally varying currents. Approximate methods are presented to address the effects of a sloping bottom.

A second simulation model, "SEDF2D", was substantially modified and improved to provide estimates of sedimentation rates in areas with spatially variable water depth and flow fields. The validity of the model to reproduce sedimentaton rates and patterns was tested by comparing predicted rates and patterns with those estimated from cores collected in the White Point outfall area (Los Angeles County, California). Simulations with this model were also used to validate the predictions generated with SFFT, and to develop the method for adapting the SFFT and generic predictions to the case of a sloping bottom.

All of the models require information on the effluent particle settling speeds. A third model, "COAG", was developed to adapt the results of recently published laboratory-based studies of particle aggregation to ocean conditions. Results from this model are tested by incorporating them into the sedimentation predictions for the White Point outfall area.

The computational methods used in these models address major deficiencies in the method presently used in evaluating 301(h) waiver applications, and should provide substantially improved predictive capability.

TABLE OF CONTENTS

XII. FIGURES

XIII. APPENDICIES

XIII.1. Appendix A - Time-series of velocities for the simulations

XIII.2. Appendix B - "Generic" Pattern distributional probability matricies.

I. BACKGROUND

I.1. Overview

The characteristics of ocean sediments are the result of a complex interaction of a large number of dynamic physical, chemical, and biological processes. In broad terms, these processes can be subdivided into three groups: (1) water column processes, (2) interface and near-bottom processes, and (3) benthic processes. In reality, however, there is a certain degree of interaction between these groups. In this report, only the first group of processes, i.e. the initial sedimentation of particles to the ocean bottom, will be addressed.

Water column processes include (but are not limited to) advection and dispersion of the particles by ocean currents; the "creation" of new particles by phytoplankton growth, outfall discharge, fecal pellet production, and deposition at the air-water interface; transformation of particle characteristics by physical-chemical aggregation, microbial action, and biological uptake; and density driven sedimentation of particles through the water column. These processes are characterized by a wide range of time-scales and some of them, particularily the biological processes, can be dependent on the previous time-history of the receiving water environment. This temporal dependence introduces enoumous difficulties into the development of a "complete" simulation model of particle sedimentation.

In order to reduce the simulation task to a tractable problem, it is assumed that the major characteristics of particle sedimentation are determined by the three-dimensional movements of effluent particles in the absence of biological processes (some indications of the effects of biological activity can, however, be examined with the aggregation model COAG). In this restricted conceptual model, the sedimentation rates and patterns of the particles are determined by the gross properties of the ocean currents, the particle settling speeds, and the initial elevation of the particles above the ocean bottom.

I.2. Ocean Currents

The properties of the coastal ocean currents vary with depth and time. For southern California coastal waters, three catagories--"surface", "mid-water", and "near-bottom"--provide an operational, if coarse, breakdown of the flow regimes by depth. In this context, surface currents refer to motions of the mixed layer (typically 2-15m in depth), near-bottom currents refer to the flows whose properties differ from the mid-water currents as a result of interaction with the bottom (typically within 5 meters of the bottom) , and mid-water currents refer to the region between the bottom of the pycnocline and the near-bottom currents.

Ocean outfalls in the southern California area generate sub-

surface wastefields throughout most of the year. Thus the mid-water and near-bottom currents have the greatest influence on the dispersion and sedimentation of effluent particulates. The mid-water flows will, in general, play the most important role during the initial sedimentation; near-bottom currents will generally assume this role for resuspension and redeposition processes.

Figure 1 illustrates the temporal properties of "typical" mid-water currents (40m deep in 55m of water) off the coast of southern California. It is immediately evident that variations in the currents are substantially stronger than the mean flow. It is frequently convenient to subdivide these fluctuations into three catagories--tidal, sub-tidal, and super-tidal frequencies--according to the time-scales characterizing the fluctuations. For the purposes of discussion, tidal frequencies are defined to have periodicities ranging from 6 to 24.75 hours. Sub-tidal fluctuations are characterized by longer time-scales; super-tidal fluctuations, by shorter time-scales.

Figure 2 shows the cummulative variance for the longshore and cross-shore components of this flow as a function of increasing "time-scale" (or periodicity), and shows that the currents are described by a wide range of time-scales. Two differences between the longshore and the cross-shore components of the current are evident. First, most of the variance in the longshore component is associated with with the slowly varying, sub-tidal frequency, fluctuations; variations associated with these long time-scales are virtually absent in the cross-shore flow. This is a characteristic of all the mid-water, coastal flows in southern California. Secondly, the remainder of the fluctuations (except at the semi-diurnal tidal frequency of about 12 hours) are comparable in strength and temporal properties. This similarity is also a common characteristic of mid-water southern California coastal currents--in many cases, the semi-diurnal fluctuations are also comparable.

The presence or absence of fluctuations of sub-tidal periodicity has profound consequences for predicting advective transport along longshore and cross-shore directions. Comparisons of currents simultaneously measured at spatially separated moorings indicate that the sub-tidal fluctuations in the longshore motions are highly correlated ($r^2 = 0.9$) over length-scales of 5 kilometers (Hedricks, 1986), and moderately correlated ($r^2 = 0.25$) over length-scales of 20-30 kilometers (Winand, 1983).

In contrast, tidal fluctuations are uncorrelated, or only moderately correlated, ($r^2 = 0 \rightarrow 0.3$) over length-scales of 3-5 kilometers, and super-tidal fluctuations are essentially uncorrelated ($r^2 < 0.02$) over length-scales on the order of 1 kilometer.

As illustrated in Figure 2, sub-tidal fluctuations generally dominate the longshore motions. The high correlation of these fluctuations, combined with their importance to transport (because of the long time-scales), means that longshore advective

motions can probably be predicted with acceptable accuracy from a minimal number of current meter moorings (for the length-scales characterizing outfall-related sedimentation).

On the other hand, the short correlation length-scales characterizing the cross-shore motions indicate that a large number of curent meter moorings would probably be required to provide sufficient information to provide estimates of the cross-shore advective transport of wastewater. It also suggests that for the range of time-scales relevant to the initial sedimentation process, it may not be possible to use hydrodynamical-numerical models to deterministically estimate advective cross-shore transport. Therefore, it is likely that statistical methods will be required to estimate this cross-shore dispersion.

Net current speeds over periods on the order of a month typically range from about 1 to 7 cm/sec, with an average value of 4 cm/sec. Typical rms speeds for the variations in the longshore component of the flow range from 5 to 13 cm/sec; for the cross-shore motions, the rms speeds are on the order 3 to 6 cm/sec.

If the extent of the outfall-generated sedimentation field (e.g. outfall-related sedimentation rates in excess of natural sedimentation rates) is known, the time-scale characterizing the initial sedimentation process can be estimated. The longshore distances characterizing sedimentation fields off southern California range from substantially less than a kilometer for the smallest outfalls, to on the order of 16-18 kilometers for the "largest" outfall (the White Point outfall system has the largest historical mass emission rate of suspended solids). Using a net longshore movement of 4 cm/sec, the time-scale characterizing the sedimentation process for the largest mass emission is thus estimated to be on the order of 4-5 days. The time-scales characterizing the initial sedimentation fields around the smaller outfalls will obviously be much shorter.

If the initial elevation of the effluent particles above the bottom is know, the range of settling speeds dominating the flux of particles to the initial sedimentation field can be estimated from the time-scale associated with the field.

I.3. Wastefield Elevation / Settling Height

The distance the effluent particles must settle before reaching the ocean bottom is determined by the location and thickness of the wastefield and the local water depth.

Provided that the environmental parameters that govern the initial dilution process (e.g. discharge rate, outfall design, water column density stratification, ocean currents, effluent density, etc.) are synoptically known for a representative period of time, simulation models of initial dilution could be used to estimate the initial position of the wastefield in the water column. In practice, this information is virtually never available, and

"best guess" estimates of "representative conditions" are generally used for the simulation model inputs, or direct estimates of wastefield position are based limited direct observations.

This somewhat arbitrary procedure may be justified, to a degree, by an additional consideration. Even if the required environmental information were available, existing simulation models generally appear to do a poor job of estimating the thickness of the generated wastefield in the case of a density-stratified water column.

A final consideration is that the depth of an element of the wastefield generally varies with time following formation of the wastefield in response to internal waves, internal tides, and baroclinic adjustments of the water column. All of these considerations introduce considerable uncertainty in selecting appropriate choices of wastefield depth and thickness.

Based on initial dilution simulations for relatively low current speeds, and some direct observations, it is often assumed that a "typical" initial wastefield depth is equal to one-half the water depth at the outfall diffuser. This assumption is used in most of the simulations developed in this report. For the major outfalls, which discharge in water depths on the order of 55-60m, this means the wastefield forms approximately 30 meters above the bottom. A typical time-scale characterizing the sedimentation field associated with the White Point discharge was previously shown to be on the order of 4-5 days, hence most of the particles deposited in this field can be expected to have settling speeds in excess of about 0.005 -> 0.01 centimeters per second.

I.4. Settling Speeds

The mass distribution of particle settling speeds for effluent particles discharged into the ocean environment are not well described at the present time. Estimates of this distribution are often obtained from laboratory-based measurements using settling tubes.

Figure 3 shows the mass distribution of particle settling speeds for primary/advanced primary effluent from the White Point (Joint Water Pollution Control Project - Los Angeles County) and the Orange County (Orange County Sanitation District) treatment plants.

Measurements of the settling characteristics of the White Point effluent were made by Myers (1974) (black circles) and Herring and Abati (1978) (open circles). The Herring and Abati study also provided the data on the Orange County effluent (crosses). Considerable scatter in the results is evident (even in just the effluent from one plant). The "best-fit" approximation to this data set is indicated by the solid line (and is subsequently referred to as the "average" settling speed distribution). It is essentially the same as the settling speed distribution for

primary and advance primary treated effluent suggested in the sedimentation section of the EPA technical support document for 301(h) waiver applications (EPA, 1982).

It was previously estimated that for the White Point sediment field, most of the deposition is associated with particle settling speeds in excess of about 0.005 to 0.01 cm/sec. The settling speed distribution shown in Figure 3 indicates that approximately 14 to 19 percent of the discharged particles have settling speeds in excess of this value (for the Myers values alone, and the EPA distribution, the fractions are about 14-20 percent and 11-16 percent, respectively).

For the smaller sedimentation fields (e.g. smaller mass emission rates), the settling speeds of particles generating the initial sedimentaton field will usually be much greater (e.g. 0.1 -> 1 cm/sec). These fast settling particles may also be important in determining the "peak" sedimentation rates around the larger outfalls. Unfortunately, for a variety of reasons, the mass of particles associated with these fast settling speeds is generally not measured very well in settling column studies.

The validity of particulate settling speed measurements using settling tubes has been questioned because aggregation processes are probably not adequately simulated during those measurements. Studies have shown that particle settling speeds can be influenced by particle concentration (or dilution with sea water) and mixing within the column (e.g. Faisst, 197??; Cardoni, et.al., 1986). These variations in settling speed can be described in terms of aggregation processes.

In the "real world", aggregation may occur between effluent particles within the outfall, during the initial dilution process, and while settling in the ocean. In addition, aggregation may occur with natural particles during the initial dilution process and subsequent settling from the wastefield. Some investigators have attempted to evaluate the role of effluent-natural particle aggregation in settling column studies (e.g. Herring and Abati, 1978; Cardoni, et.al., 1986).

A number of investigators (e.g. Hunt, 1982; Hunt and Pandya, 1984; Farley and Morel, 1986) have studied aggregation processes using both mathematical methods and laboratory studies. These studies suggest that aggregation processes can be important for conditions that may occur around ocean outfally. They have also provided analytical descriptions of the effects of this process on particle removal. However, as in the case of the settling tubes, the laboratory environments used in these studies do not completely mimic the ocean environment (e.g. the initial dilution process, initial effluent particle size distribution, the range of natural particle sizes, intermittent shear associated with "patchy" turbulence, grazing by zooplankton, etc.). Thus it seems likely that both methods for estimating effluent particle speeds in the ocean environment contain the potential for substantial error.

I.5. Diffusion Processes

The spatial distribution of sedimenting effluent particles will be determined by the diffusion, as well as the advection, of those particles. In general, the characteristics of vertical exchange in the ocean differ greatly from those of horizontal exchange (here vertical and horizontal refer to exchange across and along isopycnal surfaces).

Vertical diffusion can be expected to influence sedimentation rates by producing changes in the thickness of the wastefield. This thickness will be determined by the "stretching" and "shrinking" of the distance between isopycnal (constant water density) surfaces resulting from the local, advectively-generated, "sources" and "sinks" of water, and the vertical exchange associated with molecular and turbulent diffusion.

Sedimentation rates may be expected to be significantly affected by these processes when changes in the thickness of the wastefield become comparable with the distance from the wastefield to the ocean bottom. A rough lower bound on the magnitude of the diffusivity required to produce these changes can be obtained from the combination of time-scale characterizing the White Point sedimentation field and the wastefield elevation. For a time-scale of 4 days, a settling height of 30m, and the assumption of "Fickian" diffusion, the minimum required diffusivity is on the order of 30 cm**2/sec. This value is substantially in excess of molecular diffusion values, or vertical eddy diffusion in density stratified waters, indicating that vertical diffusion effects can probably be ignored. They may, however, be significant for large discharges into density unstratified waters.

In a similar manner, horizontal diffusion can affect sedimentation patterns and rates through horizontal dispersion of the wastefield. Since density stratification of the water column does not directly suppress exchange along isopycnal surfaces, the eddy diffusivities are much larger than for vertical exchange.

In general, the effects of wastewater exchange along the axis of the wastefield can generally be expected to be relatively minor because of the small concentration gradients along this axis and the strength of the ocean currents in the longshore direction. Exchange associated with eddy diffusion transverse to the axis of the wastefield has the potential to be much more important due to the reduced length-scale characterizing the "width" of the wastefield (resulting in increased concentration gradients of effluent particles), and the relatively weaker cross-shore flows.

It was shown earlier that the coherence length-scales characterizing cross-shore motions are very short, hence in the absence of a detailed description of cross-shore flows, it may be most appropriate to treat all motions along this axis from a "diffusive" point of view rather than as an "advective" process.

I.6. Near-Bottom Currents

Measurements of currents within a few meters of the bottom in southern California coastal waters show substantial differences between motions in this layer and those characterizing the rest of the water column. In general, net flows and sub-tidal fluctuations are suppressed and super-tidal fluctuations are enhanced. As a result, transport rates are substantially reduced relative to the mid-water rates.

The near-bottom currents can influence the initial sedimentation of the particulates if they are sufficiently strong to "hinder" deposition of the particles. The statistical properties of the near-bottom currents can also affect deposition through generation of flow-induced micro-topography. In water depths characterizing most southern California outfalls (and away from reefs), the bottom topography seems to be primarly determined by the benthic fauna mor than by the near-bottom flows, so the influence of these flows on micro-topography can probably be neglected.

Measurements of sediment resuspension, however, indicate that near-bottom currents are frequently sufficiently strong to resuspend surface sediments (Hendricks, 1987). It is likely that deposition of effluent particles settling from the water column would also be inhibited during these resuspension periods. However, because of the short time-scales characterizing fluctuations in the near-bottom flows, and their reduced strength, the spatial distribution of effluent particles settling from the water column may not be significantly altered by these periods of hindered settling.

II. A SIMPLE SEDIMENTATION MODEL (SFFT)

II.1 Overview

SFFT is a simplified numerical simulation model of the sedimentation of effluent particulates. It uses a statistical approach to compute the dispersion of settling particulates in an environment with variable currents, but constant water depth.

The continuous discharge of particles is conceptually treated as a series of releases of "packets" of particles. It is assumed that the dispersion of particles associated with an individual packet can be described in terms of a "single parameter similarity distribution function". Examples of such distributions include the common "normal" (i.e. "Gaussian") and "uniform" ("top hat") distributions.

The probability distributions for both the longshore and the cross-shore directions are described in terms of a "dispersion" about the mean flow, and the displacement associated with the mean flow. Both of these quantities are functions of the elapsed time since discharge and the time-dependent properties of the currents along each axis. This "single packet" dispersion is generalized to the ensemble of packet releases by adding on the dispersion associated with changes in the mean flow from release to release.

Since a simple similarity distribution is used to describe the dispersion, the simulations are limited to the case of a flat bottom. Approximate methods for adapting these constant water depth results to situations with a simple sloping bottom are described later in Section VIII.

The evolution of the dispersion of packets of particles with increasing elapsed time since discharge is quantified in terms of the "variances" associated with the distributions along each axis. These variances are estimated by assuming: (1) the length-scales of the motion in Lagrangian and Eulerian reference systems have a 1:1 correspondence and, (2) temporal properties of variations in the ocean currents can be characterized through the use of a digital Fourier series transformation of a time-series of current measurements.

II.2. Conceptual Approach

The conceptual approach used in SFFT is perhaps most easily visualized by representing the dispersion and settling of particles continuously released from an outfall as consisting of a large number of sequential releases of "packets" of particles. Following discharge, each packet is advected by ocean currents and "spread" by eddy diffusion processes. SFFT uses a time-series of current measurements to estimate "ensemble-averaged" transport and spreading of the collection of packet releases.

Dispersion of "packets" of settling particles about the advective motion associated with the net (long-term) current velocity can be conceptually visualized as the result of three processes:

(1) dispersion from eddy diffusion processes associated with short-term velocity fluctuations (unresolved in the time-series),

(2) eddy-diffusion-like dispersion associated with velocity fluctuations that are of sufficient duration to be resolved in the time series and,

(3) the dispersion associated with variations in the elapsed time "mean" velocities (i.e. variations between the mean currents for fixed elapsed times but commencing at different times in the time-series of measurements).

This breakdown into various components can perhaps be clarified by a simple example.

II.2.a. Advection

Let us first consider the introduction of a "packet" of effluent particles into the water column at the location and depth corresponding to the initial formation of the wastefield. Let us also assume that we know precisely the average flow during the period of time following the introduction of the packet of particles into the water column (i.e. the elapsed time).

If there is no shear in the longshore or cross-shore flow fields, the location of the center of mass of this packet of particles can be precisely computed at the end of this period, and is equal to the product of the average velocity during this interval and the elapsed time. This displacement between the release point (the outfall terminus) and the location of this center-of-mass of the particles corresponds to the "advective transport" of the packet during this time interval.

II.2.b. Dispersion

In addition to this advection, there will be some "spreading" of the particles about their center-of-mass (Figure 4). This spreading is associated with fluctuations in the currents about their mean value during the time period since discharge. The "size" of this distribution can be quantified in terms of the variance of the distribution about its center-of-mass. In general, this variance (x, y) will be different in the longshore ("x") and cross-shore ("y") directions.In many cases, however, the distribution of the particles within the patch will maintain the same "shape" with the passage of time (although the overall size of the patch may grow and the concentration of

particles within the patch will decrease). In that case, the distribution of particles about their center-of-mass after some elapsed time period can be computed if the "shape" of the distribution and the two variances are known at each interval in time.

Some of current fluctuations will occur so rapidly, or are on such a small scale, that they will not be resolved in the time-series of current measurements. The dispersion associated with these fluctuations corresponds to the first process enumerated above.

Other fluctuations may be present that are resolved in the time-series, but are characterized by time-scales shorter than the elapsed time since discharge. The dispersion associated withe these fluctuations corresponds to the second process enumerated above.

If a second release is "made" beginning at a different time in the time-series, the same observations and calculations can be carried out for each elapsed time included in the analysis of the first release. In general, these observations will result in a new distribution function, a new variance, and a new mean velocity.

The computational procedure used in SFFT assumes that each time these measurements and calculations are carried out for the same elapsed time since discharge, the same distributional function and variance are obtained. Actually, this assumption is more restrictive than necessary. A computationally equivalent (but less restrictive) assumption requires simply that the distributional shapes and variances are independent of the mean velocity vector, and the collective distributions and variances can be represented by a single pair (longshore, cross-shore) of distributions and variances for each elapsed time.

Although the "spreading" of the patches may be similar from release to release, the mean velocity (averaged over the elapsed time period) will vary from release to release (i.e. V1,V2, ... Vn, in Figure 5). For the total set of releases, the ensemble-averaged advection of the collection of particles (and packets) is simply the time-dependent displacement based on the net current. It is calculated from the elapsed time since discharge and the net velocity vector for the entire time-series of current measurements (Ve in Figure 6).

If all possible releases with the same elapsed time are made for the entire period of the time series, a distribution of packet centers-of-mass will be obtained (represented by the ellipse in Figure 6). The distribution of the individual packet centers-of-mass about this ensemble center of mass will be generated by the variations in the "elapsed time mean velocities" about the ensemble net velocity. This distribution will have some "shape" and "variance" analogous to the particle spreading about the each

packet center of mass, and corresponds to the third of the three processes previously enumerated.

The distribution of particles of a particular "age" (i.e. elapsed time since discharge), averaged over a large number of releases (i.e. the duration of the time series) can now be estimated--provided that the distributional shapes are known, and the growth in the associated variances can be computed as a function of elapsed time.

For computational simplicity, it is assumed that the combined dispersion function (i.e. the combined particle and packet dispersions) can also be described by a similarity distribution function. We also assume that the variance for this distribution is related to the sum of the variances associated for the two individual dispersions (i.e. particle and packet dispersions). This assumption is valid when one of the two variances is much larger than the other--a condition that occurs frequently, but not all of the time.

This conceptual picture will be described from a mathematical point of view in the following sections.

II.2.b.i. Distinguishing "Particle Dispersion" from "Packet Dispersion"

Particle dispersion was defined as associated with current velocity fluctuations shorter than the elapsed time; packet dispersion was associated with velocity fluctuations with time-scales longer than the elapsed time.

The separation of velocity fluctuations into these two groups, characterized by their time-scales, is accomplished using a discrete Fourier series to transform the time series from "time-space" to "frequency-space" (for each spatial component):

$$u^x(t) = u_o^x + \sum_{j=1}^{\frac{N}{2}+1} u_j^x \cdot \sin\left(\omega_j t + \varphi_j\right) \qquad (1)$$

A similar series can be computed for the cross-shore ("y") component of velocity.

The "time-scale" characterizing each term in the series is operationally defined as the inverse of the angular frequency, , of that term:

$$\tau_j = \frac{1}{\omega_j} \qquad (2)$$

Particle dispersion is assumed to be related to velocity components with "periodicities" shorter than the elapsed time; packet

dispersion is associated with periodicities longer than the elapsed time:

$$T(\text{elapsed time}) > \frac{1}{\omega_j} \qquad (3)$$

With this distinction, the velocity series can be subdivided into three terms:

$$u^x(t) = u_0^x + \qquad (4a)$$

$$\sum_{j=1}^{m} u_j^x \cdot \sin(\omega_j t + \varphi_j) + \qquad (4b)$$

$$\sum_{j=m+1}^{N^*} u_j^x \cdot \sin(\omega_j t + \varphi_j) \qquad (4c)$$

where: $N^* = \frac{N}{2} + 1 \qquad \omega_m < \frac{1}{T} \leq \omega_{m+1}$

The first term is associated with the net velocity of the packet centers-of-mass; the second term, with "packet dispersion", and the third term, with particle dispersion about the packet center of mass.

II.2.b.ii. Variance - Particle Dispersion

The variance associated with particle dispersion is computed differently from the computation for the variance associated with packet dispersion.

Displacements associated with the short-term (particle dispersion) velocity fluctuations can be computed by integrating the terms in the second group of equation (4):

$$\{x(T)\} = \int_0^T \sum_{j=m+1}^{N^*} u_j^x \cdot \sin(\omega_j t + \varphi_j) \cdot dt \qquad (5a)$$

$$= -\sum_{j=m+1}^{N^*} (u_j^x/\omega_j)\left[\cos(\omega_j t + \varphi_j\right]_0^T \qquad (5b)$$

This dispersion is considered to be the result of random, and hence incoherent motions. Therefore the spatial variance associated with this group is equal to the sum of the squares of each of the amplitudes:

$$\sigma_{x,i}^2 = \sum_{j=m+1}^{N^*} (u_j^x/\omega_j)^2 \qquad (6)$$

From the assumption that a 1:1 correspondence esists between length-scales in a Lagrangian coordinate system and in an Eulerian coordinate system, it follows that the variance in an Eulerian reference frame (current meter mooring) is related to the variance of the particle dispersion (Lagrangian reference frame) by a simple proportional factor, β_{EL} :

$$\sigma_{x,1}^2 = \beta_{EL}^2 \cdot \mathcal{R}_{x,1}^2 \qquad (7)$$

This computed variance only includes fluctuations that have periodicities equal to, or in excess of, twice the sampling interval (i.e. the inverse of the Nyquist Frequency). In general, shorter period fluctuations (not resolved in the current meter record) will also contribute to the dispersion. The variance associated with these very high frequency fluctuations is estimated by assuming that the associated dispersion can be computed using a "difffusion velocity" representation (Okubo, 197):

$$\sigma_D^2 = (v_D \cdot t_D)^2 \qquad (8)$$

$$t_D = 2 \cdot \Delta t_s \qquad (9)$$

where the diffusion time is taken as twice the current meter sampling interval. Since the range of length-scales associated with these unresolved motions is fixed (i.e. resolved variations are explicitly computed in the model), the contribution of these unresolved motions to subseqent increases in the total variance (e.g. for longer elapsed times) should be expressed in terms of a "Fickian" ("random walk") growth rate instead of continuing the diffusion velocity representation:

$$\sigma_D^2 = \frac{1}{2} K_D T \qquad (10)$$

$$K_D = 2 v_D^2 \cdot t_D \qquad (11)$$

This variance is added to the variance computed from the Fourier series representation of the time series:

$$\sigma_{x,2}^2 = \sigma_{x,1}^2 + \sigma_D^2 \qquad (12)$$

II.2.b.iii. Variance - Finite Size Diffuser

Most modern outfalls terminate in an extended, multi-port diffuser. This finite length, in combination with the spatial spreading associated with the initial dilution process, produces a finite size (variance) for the particle distribution at the time of formation of the wastefield (i.e. an elapsed time = 0).

This initial variance, $\sigma_{x,o}$, can be computed (for both the longshore and cross-shore directions) and used in the simulation, if desired. It is simply added to the particle dispersion variance:

$$\sigma_{x,3}^2 = \sigma_{x,2}^2 + \sigma_{x,o}^2 \qquad (13)$$

II.b.2.iv. Variance - Packet Dispersion

The variance associated with packet dispersion must be computed somewhat differently. In the case of particle dispersion, each fluctuation in the Fourier series goes through one, or more, complete oscillations during the elapsed time period. Each term in the series has associated with it, a unique spatial distribution (Figure 7) and variance that is independent of the elapsed time, and depends only on the (velocity) amplitude of the term and its periodicity.

For the terms associated with packet dispersion, none of the fluctuations have completed a full cycle (i.e. they were explicitly separated from the short-period terms because they "look" like "mean" flows over this period). In order to compute the variance associated with these fluctuations, we again assume that the terms in the third group of equation (4) are uncorrelated. Then the rms (root-mean-square) velocity associated with this group is given by:

$$u_x(\text{rms}) = \left[\sum_{j=1}^{m} \left(u_j^x \right)^2 \right]^{1/2} \qquad (14)$$

The corresponding displacement variance is obtained by squaring the product of the rms velocity and the elapsed time:

$$\sigma_{x,p}^2 = \left(u_x(\text{rms}) \cdot T \right)^2 \qquad (15)$$

II.2.b.v. Combined Variance and Net Displacement

The overall variance describing the combination of particle and packet dispersion is obtained by simply adding the particle and packet dispersion variances (this is equivalent to assuming that the two processes are entirely independent):

$$\sigma_{x,\text{total}}^2 = \sigma_{x,p}^2 + \sigma_{x,3}^2 \qquad (16)$$

An analogous relationship can also be developed for the cross-shore motions. These two variances, in combination with their respective "distributional shapes", determine the (ensemble)

average spatial distribution of discharged particles about their (ensemble) center-of-mass after an elapsed time "T".

II.2.b.vi. Dispersion Probability Distribution Functions

In general, the probability distribution functions for the dispersive processes will be governed by the spectral characteristics of the ocean currents. For example, current fluctuations with a single frequency (e.g. the M2 tidal component) would give rise to the distribution shown in Figure 7, while Fickian diffusion (i.e. a "flat" spectrum) would be expected to give rise to a "normal" (Gaussian) distribution.

A normal distribution is used for dispersion along the longshore component in SFFT, while a modified top-hat distribution is used for cross-shore dispersion. For computational simplicity and speed, these distributions are approximated by four top-hat distributions (of varing width and magnitude) as illustrated in Figures 8a,b.

II.2.c. Particle Settling Speed Representation

The mass distribution of particle settling speeds must be supplied as input for the model simulation. The distribution is specified in terms of up to four straight line segments on a plot of the logarithim of the cummulative mass fraction of the particles with a settling speed > a reference settling speed, versus the reference settling speed (e.g. see Figure 3). This distribution can be estimated from a variety of sources (e.g. published information, distributions suggested by regulatory agencies, laboratory-based settling column studies, or from a particle settling speed models such as COAG--see Section IX).

This separation allows the basic framework of SFFT to be used for a variety of sources of information on the mass distribution of particle settling speeds. Thus the user is free to select the settling speed information that is deemed to be most appropriate for that area and effluent.

II.2.d. Particle Deposition

The sedimentation of effluent particles around the outfall can be computed using the advection-dispersion information (as a function of elapsed time) computed from the current meter time series, information on the mass distribution of particle settling speeds, and the initial elevation of the wastefield above the ocean bottom.

The basic procedure is to compute the (ensemble averaged) advection and dispersion of particles for a series of increasing elapsed times. Each elapsed time will have a corresponding settling speed (determined by the settling height). The mass of particles with settling speeds between each sequential pair of

elapsed times is "deposited" on the ocean bottom during each increment in elapsed time.

For accounting purposes, the simulation area is divided into a rectangular grid of cells. The set of cells receiving deposited particle mass during each elapsed time is computed from the location of the ensemble center-of-mass and its dispersion along the longshore and cross-shore directions. For computational simplicity, deposition into a cell is assumed to be uniformly distributed throughout the cell.

The mass fractions deposited in each cell are accumulated until the maximum elapsed time (i.e. the length of the time series) is attained. Output from the model consists of this matrix of probabilities for each simulation cell in a grid of 32 (longshore) by 16 (cross-shore) cells (it is assumed that the net cross-shore velocity is zero, so that the "other half" of the cross-shore distribution can be obtained by a "reflection" of the 16 cross-shore cells about their axis of symmetry).

Sedimentation rates can be obtained from these probabilities by multiplying them by the annual mass emission rate of suspended solids and dividing by the area of the grid cells. The sedimentation flux units are determined by the units used for the emission rate and area (e.g. mg/yr and cm**2 will yield a sedimentation rate in mg/cm**2/yr; gm/yr and m**2 will yield gm/m**2/yr). For depositonal probabilities expressed in terms of the fraction of the discharged mass deposited in each cell, mass emission of suspended solids in m-tons/year, and cell dimensions in kilometers, the sedimentation rate in mg/cm**2/yr is obtained from the relation:

$$S_F\left(\frac{mg}{cm^2\text{-}yr}\right) = 0.1\ \frac{\dot{M}\ (\text{m-tons dry susp. solids/yr})}{A\ (km^2)} \qquad (17)$$

For sedimentation rates expressed in terms of gm/m**2/yr, the values obtained from the previous equation should be multiplied by a factor of 10.

II.e. Treatment of "Fast" Settling Particles

The highest frequency (shortest "period") that exists in the Fourier series (equation (1)) is equal to twice the sampling interval (i.e. the "Nyquist period"). In many cases, this elapsed time is too long to spatially resolve the sedimentation associated with fast settling particles. In order to improve the spatial resolution in the immediate vicinity of the outfall, a maximum value for the minimum elapsed time is imposed on the simulation. This time is selected to be equal to the settling time for a settling speed of 1 cm/sec.

Multiples of this "max-min" elapsed time are used for the initial deposition calculations until a time equal to, or in excess of

the Nyquist period is obtained. During these early steps, it is assumed that the total variance is initially equal to the variance associated with the outfall diffuser length, and grows quadratically in time to attain the computed value at a time corresponding to the Nyquist period.

II.3. Computer Coding

The model is written in Microsoft Fortran-80. This compiler is a nearly complete implementation of the ANSI Fortran-66 standard, although complex number manipulations are not included. The complier also contains some extensions to the standard (principally in the area of disk operations).

The simulations have been carried out on microcomputers using the (Digital Research) CP/M-80 operating system. For a Z80 microprocessor running at a 4 megahertz clock rate, the first simulation for a current meter record containing 1024 observations (approximately 32 days at a 45 minute sampling interval) requires about 8-10 minutes of computation time. This time will vary with the dimensions of the cells and the strength of the net flow. Reductions in either quantity lead to increased computation times; conversely increased values reduce the computation time.

Three programs are used to carry out the initial simulation. The first program, VFFT, computes the Fourier transform of the time series, and the cummulative variances for both particle and packet dispersion. This information is stored in a disk file. The second program, CFFT, allows the mean velocities to be altered, combines various terms into a representative set of elapsed times, and computes the ensemble mean motion associated with each of these times. The time-series information is supplied to CFFT through the file created by VFFT, and the output from CFFT is also stored on a disk file. The third program, SFFT, "gets" information from the user about the dimensions of the grid cells, the initial elevation of the wastefield, the mass distribution of particle settling speeds (contained in a disk file) and the initial variance of the wastefield along each axis. It uses the information contained in the file created by CFFT to calculate the deposition probability for each cell. These probabilities are listed on a printer and stored in a third disk file.

This separation into three programs allows changes to be made in the net flows the distribution of settling speeds, or the wastefield elevation, without recalculating the Fourier transforms of the time-series of current measurements. In some cases, this can result in a two- to three-fold reduction in computation time for subsequent simulations.

Instructions for using the three programs (VFFT,CFFT,SFFT), and listings of the computer code, are contained in the separate report: "User Manual - SFFT".

II.4. Model Validation

The validity of the sedimentation rates and patterns generated from the model SFFT were tested by comparing them with the predictions generated with the sedimentation model SEDF2D. This process is discussed in Section VI.

III. SEDIMENTATION WITH VARIABLE WATER DEPTH - SEDF2D

III.1. Background

A number of techniques have been proposed to estimate the effects of bottom slope on particle deposition rates and patterns. Virtually all of these methods contain some conceptual difficulties.

III.1.a. EPA Technical Support Document Method

One suggested method is described in the technical support document for the 301(h) waiver applications (EPA, 1982). This method will be referred to as the "301(h) model". The method basically assumes that the settling height of the particles is independent of position within the simulation area (i.e. equivalent to assuming a constant wastefield and water depth), and hence is applicable to areas with either constant water depth, or where the slope of isopycnal surfaces matches the bottom slope.

In addition, a techniques is presented to modify the computation for areas where the bottom slope exceeds 5 percent (the significance of this slope is not discussed in the document).

In the case of a flat bottom, the model computes the horizontal transport distance for a particle with a settling speed, Vs, by assuming that the particles are dispersed within an area characterized by the average current speed in each of four directions (upcoast,downcoast,onshore,offshore). For an flow with an average speed of Va along one of these directions, and a settling height Ht, the dispersion distance in that direction is computed using the similarity relationship shown in Figure 9a.

In the presence of a sloping bottom, the suggested modification is equivalent to adding an "adjustment" to the velocity slope angle, , equal (for small slopes) to the slope angle of the bottom (see Figure 9b). For a slope of 5 percent, and the document suggested "default" cross-shore current speed of 3 cm/sec, the bottom slope angle is the same as the settling slope angle of a particle with a settling speed of 0.15 cm/sec. Thus a particle of that settling speed would only travel half as far inshore before being deposited.

Particles with slower settling speeds would travel farther inshore, but the maximum transport distance (for particles with "zero" settling speed) would be into a water depth equal to the wastefield depth (approximately 20 times the settling height, Ht). This reduction in the onshore dispersive length-scale would be expected to produce an increase in depositional rates inshore from the discharge point.

However, this computation is carried out for each of the transport directions to define the major and minor axes of the depositional ellipse. Therefore the length-scale characterizing cross-

shore dispersion is actually the sum of the dispersive distances computed for the onshore and offshore motions. Obviously bottom slope will increase the dispersion length for offshore transport. In fact, for a bottom slope of 5 percent, particles with a settling speed of approximately 0.15 cm/sec will move parallel to the bottom as it moves off shore and will not be deposited at all (see Figure 9c). Thus the offshore transport distance for particles with settling speeds slower than 0.15 cm/sec will essentially become infinity, the area of the corresponding ellipse will also tend to infinity, and the sedimentation rate of these particles with will become zero. (It is interesting to note that the settling speed for the group of fastest settling particles suggested for the calculation is only 0.10 cm/sec, hence the sedimentation of particles in an area with a bottom slope of 5 percent, or greater, would be calculated as zero).

In fairness, it should be noted that the document cautions that: "The applicant will have to exercise some judgement in developing the contours, especially in accounting for rapid depth changes offshore...", but no objective technique is presented and therefore the results are likely to be highly arbitrary.

III.1.b. "Transparent Bottom" Method

An alternate method of estimating sedimentation in areas with a sloping bottom has been developed by Koh (1982). In this model, the bottom is treated as a "transparent" boundary. Depositional fluxes are computed from a three-dimensional probability function (describing the spatial distribution of effluent particles in the water column) incorporating the settling speed of the particles. The time-dependent, probability function is estimated by assuming a "normal" distribution and computing the variances along each of the three axis as a function of elapsed time since discharge. Variances are generated by treating the dispersion as a diffusion-like process, with the (horizonntal) direction-dependent diffusivity estimated from auto-correlations computed from a time-series of current measurements.

An interesting feature of this model is that it predictes increased sedimentation rates offshore from the discharge point, and decreased sedimentation rates inshore. This is the opposite trend from that suggested by the 301(h) model. One possible explaination for this difference is that the "transparent" nature of the boundary means that particles are not "permanently" removed from the water column (or the calculation) after "deposition" on the "bottom". The presence of bottom slope can be expected to produce onshore-offshore asymmetries in the transfer of particles from the water column to the ocean bottom, with associated asymmetries generated in distribution function describing the concentration of particles in the water column.

There are a few other conceptual difficulties with this technique. For example, the cross-shore diffusivity is computed without any regard for the effects of the coastal boundary. Near the

boundary, the scale-lengths characterizing cross-shore motions can be expected to be reduced. The use of a spatially independent cross-shore diffusivity is equivalent to considering the bottom as "transparent" to water movements as well as particles (water parcels can be "viewed" as particles with zero settling speed in the method).

In summary, at least two sedimentation simulation models exist that predict intuitively disturbing characteristics for the sedimentation of particles in an discharge area with a sloping bottom. Moreover, while one model predicts that increased sedimentation rates will occur in shoaling water, the other model predicts the opposite trend will occur. Each model neglects aspects of the process that may be important in regulating the sedimentation rates and pattern. The 301(h) model neglects the effects of the temporal properties of the currents; the transparent boundary model neglects the asymmetries introduced into the water column distribution of particles associated with deposition on the bottom; and both models neglect the effect of a coastal boundary on the ocean currents and horizontal eddy diffusivity.

III.2. SEDF2D

III.2.a. An Overview

An alternate conceptual approach is used in the formulation of the sedimentation simulation model "SEDF2D". This approach uses a mix of statistical and quasi-deterministic methods. The effects of the coast on the ocean flow field are explicitly, if heuristically, treated in the simulation. Particles deposited on the bottom are permanently removed from the water column, so that any asymmetries in the particle spatial distribtuion function are implicitly included in the simulation. The penalty associated with this dependence on quasi-deterministic, quasi-Monte Carlo techniques (and less dependence on statistical techniques) is a substantial increase in the computation time required to carry out a simulation.

III.2.b. Transport

III.2.b.i. Longshore Transport

Longshore transport over distances in excess of 0.5 -> 2 kilometers in southern California coastal waters is likely to be dominated by the net flow and sub-tidal fluctuations. As noted in Section I.2 - Ocean Currents, these fluctuations are highly correlated over distances of at least 5 kilometers, and moderately correlated over distances of 25 kilometers. Both tidal and sub-tidal flows may be important over shorter distances, but the fluctuations of tidal frequency are increasingly correlated as the separation length-scale is reduced--hence the overall correlation for the set of fluctuations with time-scales important to the transport process will still be high.

Since longshore motions are usually highly correlated over distances comparable with, or in excess of, the sedimentation fields associated with all the southern California outfalls, the time-dependent movement of water parcels in this direction can generally be adequately estimated from current meter records collected at a small number of current meter moorings. In many cases, a single mooring may be adequate. Given that longshore transport can be deterministically estimated, it follows that the time-dependent statistical properties of longshore advective transport can be estimated from the ensemble of computed longshore motions.

III.2.b.ii. Cross-shore Transport

As was also noted in the Ocean Currents section, cross-shore motions are essentially uncorrelated over short length-scales (e.g. > 1 km). However, a limited number of comparisons of cross-shore movements estimated from current meter records with simultaneous observations of drogue movements suggests that the variance of the cross-shore motions measured by the two methods are comparable (Hendricks, 1983).

This similarity suggests that it may be possible to adequately estimate the time-dependent statistical properties of the cross-shore motions from current meter records. This hypothesis is the basis of the (statistical) algorithim used for cross-shore transport in SEDF2D. In particular, it is assumed that the time-dependent cross-shore distribution of particles resulting from advective-dispersive processes can be estimated from the ensemble of cross-shore motions computed from a set of progressive vector diagrams. The latter are generated from one, or more, time-series of current measurements.

III.2.b.iii. Joint Longshore and Cross-shore Transport

For an infinitesmal interval of time, the sedimentation of particles during that interval will depend not only on the local settling height (e.g. local water depth minus the wastefield depth) and the elapsed time, but also on the mass distribution of particle settling speeds present in the water column at the beginning of the interval. In the case of an area with spatially varying water depth, this distribution of particle speeds will be determined by the prior history of particle movements between the time they were discharged and the present time.

From a computational standpoint, this means that the spatial dependence of sedimentation cannot be simply computed from the product of the individual advective-dispersive, time-dependent probability distribution functions (even if they are statistically independent).

The computational scheme outlined so far, however, yields only these individual time-dependent probabilities. In order to in-

clude the effects of prior motions into the simulation process, the computational scheme must be modified. In particular, it is assumed that the set of two-dimensional movements computed from a current meter record (using progressive vector diagrams--PVD's) can be used to estimate both the time-dependent joint probability distribution function (longshore, cross-shore) and the prior histories of movement.

III.2.b.iv. Coastal Boundary Effects

III.2.b.iv.A. Artifacts

In general, PVD's computed from current meter records will show periods when packets of particulate-containing wastewater will be advected inshore of the coastal boundary. This transport obviously cannot occur in the real world.

This onshore transport can have profound effects on the estimated sedimentation rate--even if it occurs relatively infrequently. In the background section discussion of particle settling speeds, it was estimated that most of the significant sedimentation around ocean outfalls was likely to be associated with particles with settling speeds in excess of 0.05 -> 0.005 cm/sec. Roughly 15-20 percent of the discharged particles may have settling speeds in excess of 0.005 cm/sec, so roughly 80-85 percent of the discharged particles can be expected to be transported out of the outfall area. If however, onshore transport occasionally occurs across the coastal boundary, all of these particles will be "deposited" on the bottom close to the boundary (note: in this context, the "coastal boundary" can be considered as the isobath terminating the isopycnal surfaces bounding the particle field in the water column). Thus the "coast" would act more like a filter than as a barrier.

III.2.b.iv.B. Coping with the Effects of "Coastal Boundaries"

In order to mitigate the generation of artifacts associated with the computational scheme developed this far, an additional boundary condition is introduced into the simulation process. This condition requires that there be no normal component of flow across the boundary and is equivalent to the boundary condition used in hydrodynamical-numerical models. In this case, however, a heuristic algorithim, rather than the momentum and continuity equations, is used to estimate the resulting flow field.

It is assumed that at some distance offshore from the "coast", the influence of the boundary on the currents is negligible. Inshore of this "reference" distance, however, the effects of the coastal boundary become increasingly important. In particular, the algorithim used in the model assumes that the cross-shore component of the current diminishes in a linear fashion from the reference distance to the boundary. Within the influence distance of the effective coast, the longshore component of onshore

motions is considered to be parallel to the coast; outside this zone of influence, the longshore component is essentially considered to be parallel to the isobath corresponding to the diffuser depth.

It was found that some ad-hoc differences were required between the treatments of onshore versus offshore flows in order to avoid "attachment" of the flow to a divergent region of the coast. In the absence of this distinction, flow within the influence of the boundary would "follow" the coast around the corner illustrated in Figure 10a. The presence of viscosity, however, generally leads to separated flow (and possible eddy generation) as shown in Figure 10b. The differences between flow patterns in areas of convergent versus divergent bathymetry would normally result from the momentum and continuity equations in hydrodynamical-numerical models for a fluid with finite viscosity.

Since this algorithim modifies the flow pattern in a non-uniform manner, the "continuity condition" for fluid flows will generally be violated within the zone of influence of the coast. However, particle mass is strictly conserved with the computational scheme used in the model, hence the generation of non-physical "sinks" or "sources" of water mass by the algorithim does not generate corresponding "sinks" and "sources" of particle mass.

The primary effect of the lack of water mass conservation is the introduction of errors in the estimated advective-diffusive residence time of the particles within this region. Since the boundary-associated modification of the flow field is applied to the cross-shore component of the flow, while longshore movements generally play the major role in determining residence times, errors in the residence time associated with these boundary modifications can generally be regarded as "higher order" effects.

There may, however, be some instances when cross-shore motion dominates over longshore transport over the time-scales required to carry effluent from the outfall to the vicinity of the boundary. During these periods, this assumption will not be valid, and artifacts may be introduced into the predicted sedimentation rates and pattern (an example is presented in Section IV for the San Diego outfall simulation). During these periods, additional information (e.g. from additional current meter moorings) may be required if the flow is two-dimensional, or the model may not simulate the actual flow field if it is three-dimensional (e.g. "cellular" flows).

III.2.c. Computational Scheme

The sedimentation of particles from an outfall continuously discharging wastewaters is treated as a series of sequential releases of "packets" of wastewater particles. Each packet is "introduced" into the water column at T=0 (zero elapsed time) at the location of the outfall diffuser, and at a depth correspond-

ing to the mean depth of the wastefield. A time-series of current meter measurements is used to estimate the subsequent motion of the packet of particles as it moves through the simulation area. Each subsequent "release" of a particle packet occurs one sample time later in the current meter record.

At each step in the computation of the movement of the particles, the proximity of the packet to the "coastal boundary" is calculated. The bathymetry is supplied to the model in the form of a matrix of water depths at the corners of a grid of "cells" defining the simulation area (for reasons of computational speed, memory requirements, and spatial resolution, two grids are actually used--see Figure 11 in Section IV - SEDF2D Simulations).

The first step in the depth estimation process is to compute which cell(s) contains the beginning and ending points for the PVD segment currently being calculated. This (trial) end point is computed assuming that there is no effect associated with the coastal boundary. The "coastal boundary" is chosen to correspond to the isobath associated with the "mid-depth" of the "field" of settling particles present in the water column at the beginning of the time step. For example, at the beginning of the release, the effective "coast" corresponds to the initial wastefield depth. Thus, as particles approach the ocean bottom, they also approach the "effective" coast--no matter what the water depth is at the point of deposition.

Since particles with different settling speeds will occupy different regions of the water column for the same elapsed time, each release of particles is actually treated as the release of a set of particle "groups". The range of settling speeds within each group is limited, and there are enough groups contained in the release to represent the full range of settling speeds of interest. Sedimentation, including the effects of the coastal boundary on the advective-dispersive flow, is computed separately for each settling speed group.

Once the depth of the isobath corresponding to the particle field depth is computed, and the cells containing the "trial" end points of the PVD segment are known, the location of the "effective" coastal boundary can be calculated. This information is used to determine if either end of the PVD segment lies within the zone of influence of the coastal boundary. If not, the "trial" PVD segment becomes the "actual" PVD segment and the location of the packet at the end of this time step is known. If either end lies within the "zone of influence", the algorithim modifying the cross-shore flow is used to obtain the (estimated) actual movement.

After establishing the locations of the two ends of a PVD segment, the depth of the water at the end of the PVD segment is computed. The minimum particle settling speed required to reach the bottom during the current time step is calculated from this depth and the elapsed time since discharge. All the particles in the water column that have a settling speed in excess of this

minimum speed are assumed to be deposited during this time step.

For accounting purposes and simplicity, the deposited particles are assumed to be uniformly distributed within the cell containing the PVD mid-point. The deposited mass is added to any mass previously deposited in the cell, and the mass distribution of particle speeds remaining in the water column is modified to reflect this depositional "loss".

This computation proceeds, using successive observations from the time-series of current observations, until either all the particles have been deposited, or the packet of undeposited particles moves outside the simulation area. When either of these conditions occurs, a new release of particles is made, beginning one sample time later in the time-series than the previous release.

Eventually, releases have been made corresponding to each sample time in the time-series (actually releases are discontinued prior to the end of the time-series to ensure that no biases are introduced because of the limited amount of time available for the packet to move out of the similation grid). The simulation is then complete, and the resulting matrix of numbers (normalized by the number of releases) represents the fraction of a unit mass of discharged material that is deposited in each cell. Actual sedimentation rates (e.g. gm/m**2/yr) are obtained by multiplying by the appropriate annual mass emission rate (e.g. gm/yr) and dividing by the cell area (e.g. m**2).

III.2.d. Comparison of Current Version with Previous Versions

The version of the model described in this report (Ver. 5.2.01, and to a degree, intermediate versions of the form 5.1.X) represents an evolution of an earlier model (Ver. 4.2; Hendricks, 1983). It includes modifications designed to address conceptual and computational defects that became apparent in the earlier version. The principal defect was the failure to take into account the changing location of the "effective" coastal boundary as the particles settled through the water column. This flaw sometimes resulted in overestimates of the sedimentation rate inshore from the discharge, and underestimation of offshore sedimentation rates.

A substantial change was required in both concept and computational approach to incorporate this modification to the model. For example, "packets" of particles released in the earlier versions contained the full complement of particle settling speeds. As noted in the previous discussion, a set of packets, each containing a restricted band of settling speeds, is used in the present version. This change substantially increased the computation time required to carry out a simulation.

On the other hand, some benefits also accrue from carrying out sedimentation simulations for individual groups of settling speeds. The initial output from the model is a actually a set of

probability matricies--each member of the set corresponding to one of the settling speed groups. The combined probability matrix is obtained by accumulating the probability matricies for each group, using a weighting for each component equal to the fraction of the total mass of discharged materials represented by each settling speed range. Once the component (settling speed subgroup) probabilities have been calculated, sedimentation rates and patterns for other settling speed distributions can easily and quickly be estimated by recombining the component probabilities with different weightings.

At the same time that these modifications were being carried out, the algorithim used to estimate flow in the vicinity of the coastal boundary was modified to provide improved estimates. For example, within the "zone of influence", "longshore" and "cross-shore" motions now correspond to motions parallel and perpendicular to the "effective coastal boundary", respectively. In previous versions, they referred to motions along and across the isobath corresponding to the water depth at the point of discharge.

In addition, the estimation of the endpoint of a PVD segment within the zone of influece is computed by integrating the change in the cross-shore component of the flow from the beginning point and the endpoint of the longshore component of the motion. Previous versions used a combined finite-difference estimation and iteration procedure.

Modifications and additions were also made to the model to permit the use of current meter data simultaneously collected from multiple moorings within the simulation area. This allows the model to be used for a greater range of bathymetric and flow conditions. Data from up to eight moorings can be used in the simulation. The moorings supplying the flow estimation information for each grid cell are specified so that unusual flow conditions can be accomodated. The relative contributions of of the data from each specified mooring (computed at each time step) are estimated from the distance between the PVD beginning point and the mooring location.

III.2.e. Limitations on the Bathymetry

The position and orientation of the "effective coastal boundary" is estimated from depth values along the pair of cross-shore transects bounding the ends of the cells containing the PVD beginning and end points. Adjustments within the "zone of influence" of this boundary are computed from this distance and the orientation of the isobath. This means that the simulation does not "look ahead" for changes in the bathymetry. As a result, the effects of the coastal boundary on the flow may be underestimated when there are abrupt changes in the isobaths--such as may occur around submarine canyons. Therefore, enhanced sedimentation in the vicinity of bathymetric features of this type should be regarded with some skepticism (examples are shown

in Section IV - SEDF2D Simulations).

The boundary algorithim may also fail if the depth does not monotonically increase (or remain constant) with increasing offshore position. These problems can be mitigated, to a degree, by an appropriate modification of the cell alignments, or by (artificially) modifying the bathymetry to ensure this condition.

A final deficiency of the boundary algorithim is that for reasons of speed, it is assumed that after the modification has been made to the flow vector, the PVD segment endpoint remains in the same cell(s) as the "trial" endpoint. However, since the orientation of the "longshore" axis is rotated to align with the orientation of the coastal boundary subsequent to generation of the "trial" PVD segment, there is a finite probability that the modified endpoint may reside in the next transect of cells. In that case, the boundary modification based on the trial endpoint will fail to make the "correct" modification--if the orientation of the coastal boundary changes between the two transects. Based on simulations carried out with the model, this source of error does not appear to significantly change sedimentation patterns or rates for typical oceanographic conditons.

IV. SEDF2D SIMULATIONS

IV.1. Overview

SEDF2D was used to predict sedimentation patterns for five southern California ocean outfalls:

1. White Point (JWPCP - Los Angeles County)
2. Orange County (Orange County Sanitation District)
3. Encina (Carlsbad Sanitation District)
4. Oxnard (Ventura Sanitation District)
5. Point Loma (City of San Diego)

One of the purposes of these simulations was to explore the sedimentation rates and patterns for outfalls situated in areas with differing bottom slopes and bathymetric conditions. The characteristics of the simulations for each discharge site are summarized in Table I (along with a summary of some of the sedimentation features predicted for each area). The time-series of velocities used for each simulation area are shown in Appendix A.

IV.2, White Point (Palos Verdes) Simulation

The White Point outfall system presently discharges about 350 MGD of primary and secondary treated effluent through two outfalls ("90-inch" and "120-inch") terminating in 55-62 meters of water off the Palos Verdes headland. It is operated by the Joint Water Pollution Control Project of Los Angeles County.

Effluent was first discharged through a shorter outfall (terminating in shallower water) in 1939. As the flow through the outfall system increased, additional outfalls were added. In 1956, the 90-inch (upcoast, terminating in a wye diffuser) was placed in operation to replace the shallower outfalls. In 1961, the 120-inch outfall (downcoast, dog-leg diffuser) was also placed in operation. Effluent flow rates and mass emission of suspended solids increased until the 1970's, when additional treatment resulted in reduced suspended solids emissions in spite of the increasing flow.

Approximately 85 percent of the total mass of suspended solids discharged through the system has been through the two deep water outfalls. Since the 90-inch outfall was placed in operation 15 years before the 120-inch outfall, and for a period of time it also carried higher concentrations of suspended solids that the 120-inch, the bulk of the suspended solids discharged through the two outfalls has been through the 90-inch outfall.

From 1956 until 1981, the average annual mass emission rate of suspended solids was 113,000 metric-tons. Maximum emissions, in the range of 160,000 to 180,000 m-tons/yr, occurred in the early 1970's.

Figure 11 shows the general area around the two outfalls, their

location, the bathymetry of the area, and the grid(s) of cells used for the simulation(s). This is an interesting area to simulate because of the rapid change in water depth with increasing offshore distance, and because of the variations in the width of the nearshore shelf with longshore location. Submarine canyons (Redondo, upcoast; San Pedro, downcoast) lie at each end of the simulation area. Thus the simulation algorithim used to treat currents near a coastal boundary should be well "exercised" in this simulation.

The mass distribution of suspended solids measured by Myers (1974) was used for the simulation (solid circles in Figure 3) since it was felt that these measurements were made with an effluent that best represented the average properties during the 25 year simulation period from 1956 to 1981.

Figure 12 shows the predicted sedimentation pattern for the two White Point outfalls corresponding to a combined mass emission rate of 113,000 m-tons per year (the Station "dots" and labels also shown will be discussed in Section V - SEDF2D Test/ Validation). The predicted peak sedimentation rate is on the order of 500-600 mg/cm**2/yr (5000-6000 gm/m**2/yr), and occurs in the immediate vicinity of the 90-inch outfall diffuser. Sedimentation rates for other mass emission rates can be obtained from the simulated rate of 113,000 m-tons/yr by a simple scaling of the sedimentation rate isopleth values. The sedimentation field is relatively narrow and tends to follow the isobath corresponding to the diffuser depth.

Emery (1964) estimated that the (net) sedimentation rate of natural particulates in this general area (in the absence of a discharge) to be about 10 mg/cm**2/yr. Sedimentation rates in excess of this value are predicted to occur in a thin band along a ? ? kilometer section of the coast. The total area enclosed within the 10 mg/cm**2/yr isopleth at this discharge rate is about 30 square kilometers.

Figure 13 shows the distribution of surface sediment biological oxygen demand (BOD) and volatile solids content (VS), as well as the distribution of Infaunal Index values (a measure of benthic community structure) observed in the simulation area in 1978. These distributions were obtained from sediment grab samples. A comparison of these patterns with the predicted simulation pattern indicates a considerable degree of (qualitative) similarity. This similarity suggests that the modeling technique is capable of reproducing at least the general features of the flow and sedimentation fields. A detailed (quantitative) comparison between the predicted and "observed" sedimentation rates is presented in Section V.

IV.3. Orange County (Newport Beach) Simulation

The area around the Orange County outfall, the associated bathymetry, and the outline of the simulation grid(s) is shown in

Figure 14. In contrast to the White Point area, this system discharges on a relatively wide nearshore shelf. Again submarine canyons (San Gabriel, upcoast; Newport, downcoast) bound the simulation area. The outfall terminates in about 55m of water.

The average mass distribution of particle settling speeds (solid line) shown in Figure 3 was used for this simulation. The mass emission rate was assumed to be 33,000 m-tons/year.

Figure 15 shows the predicted sedimentation pattern. The peak sedimentation rate occurs in the immediate vicinity of the outfall diffuser and is on the order of 90 mg/cm**2/yr. A comparison of this pattern with that obtained for the White Point area shows the restrictions on cross-shore transport that are associated with increased bottom slope. This restricted transport probably also accounts for part of the ? ?-fold increase in the sedimentation rate (normalized by mass emission rates) at White Point, relative to the Orange County discharge. The area of the Orange County sediment field with a predicted sedimentation rate of effluent particles in excess of 10 mg/cm**2/yr is computed to be about 6 square kilometers.

Note that a "hot spot" of sedimentation is predicted to occur downcoast from Newport Canyon. As noted in the previous section, the limitations on the ability of the simulation model to deal with rapid changes in water depth around submarine canyons introduce uncertainty into the validity of this sedimentation feature.

IV.4. Encina (Carlsbad) Simulation

The Encina outfall discharges a mixture of primary and secondary treated sewage through an outfall terminating in about 46 meters of water. The discharge area, bathymetry, and grid outline(s) are shown in Figure 16. The bottom slope is intermediate between those found at the White Point and Orange County outfalls, but a submarine canyon (Carlsbad Canyon) is located only about 4 kilometers upcoast from the outfall.

The mass emission rate of suspended solids used for the simulation is 1070 m-tons/year. A mass distribution of effluent particle settling speeds corresponding to the 301(h) model distribution was used for the simulation.

The predicted sedimentation rates and pattern are shown in Figure 17. As in the case of Newport Canyon for the Orange County simulation, deposition is suppressed as particles pass over the submarine canyon, but enhanced in the area downstream from the it. Again, the validity of this enhanced sedimentation in the vicinity of the submarine canyon is open to question.

The peak sedimentation rate is about 28 mg/cm**2/yr, and occurs in a small area (ca. 0.03 km**2) in the immediate vicinity of the diffuser. The area of the sedimentation field with depositional rates in excess of 10 mg/cm**2/yr is only about 0.19 square

kilometers.

IV.5. Ventura (Oxnard) Simulation

Figure 18 shows the discharge area and bathymetry for the Oxnard outfall. The site is distinguished by both the relatively shallow water and the proximity of the diffuser to Hueneme Submarine Canyon.This outfall annually discharges about 925 m-tons of suspended solids from an outfall terminating in relatively shallow water (15.3m). The 301(h) model mass distribution of settling speeds was used for the simulation.

Figure 19 shows the predicted depositional pattern and rates for this discharge. As before, the presence of the canyon modifies the sedimentation rates and pattern--although not as much as might be expected since the net current was downcoast. The peak sedimentation rate is about 13 mg/cm**2/yr (0.12 km**2), and the area with depositional rates in excess of 10 mg/cm**2/yr is estimated to be about 0.38 square kilometers. This area is about twice as large as that associated with the Encina discharge, which has a comparable mass emission rate. Part of this increase is probably associated with the reduced settling height of the particles from the wastefield to the ocean bottom (e.g. 8 meters vs. 21 meters).

IV.6. Point Loma (San Diego) Simulation

The discharge area and bathymetry for the Point Loma outfall is shown in Figure 20. This area is characterized by moderate bottom slope, but with relatively uniform bathymetry (in the longshore direction) and no submarine canyons. The outfall terminates in about 64 meters of water and annually discharges effluent containing about 17,600 m-tons of suspended solids. The 301(h) model mass distribution of particle settling speeds was used for the simulation.

The predicted depositional pattern is shown in Figure 21. It is somewhat unusual in that an area with substantially increased depsitional rates is predicted to occur upcoast and inshore from the outfall.

The generation of this inshore "peak" is predominantly associated with a two week period within the two month long time-series of current measurements. During this period, the currents are weak and two major reversals in the longshore component of the currents occur. The currents at a depth of 40m (used for the simulation) show both onshore and upcoast flow of moderate speed during this entire two-week period (Figure 22).

In the discussion of the formulation of SEDF2D, it was noted that the failure to satisfy the continuity condition for fluid mass could lead to errors in the residence times of particles in the

grid cells. In general, these errors are small since the longshore component of the currents is substantially greater than the cross-shore component, and only the latter is modified near the boundary.

During this particular period at Point Loma, however, this condition is clearly not satisfied, and errors in the residence times may be large. In the extreme case of a direct onshore flow, for example, the cells inshore from the outfall will be "sinks" for the effluent particles, as well as water mass, since there is no mechanism (i.e. longshore transport) to carry them out of the cell. Therefore, it is important to be aware of the assumptions incorporated in the model so that features of the predicted sedimentation pattern that may be due to failure of the modeling assumptions can be identified as suspect.

In this particular case, flows measured at another depth (15m), as well as at an intermediate depth (28m) at a different mooring (42m of water), show considerable differences in the net motions from those observed at the 40m depth. This suggests that during this period, the flow in the area was probably complex. Possibly if data had been available from other, suitably placed moorings, a more representative prediction could have been generated for this period.

Figure 23 shows part of the deposition pattern predicted for the month-long time-series of current measurements containing this anomalous two-week period of onshore flow. In this simulation, the sedimentation rates in the vicinity of the 30 meter isobath (the effective coast) are on the order of ?? mg/cm**2/yr, and substantially exceed the sedimentation rates predicted for the immediate area of the outfall diffuser (??? mg/cm**2/yr).

In contrast, Figure 24 shows the pattern for the other month of current measurements. In this case, the peak sedimentation rate is about 53 ?? mg/cm**2/yr (0.5 km**2) and occurs in the vicinity of the diffuser. Sedimentation rates in excess of 10 mg/cm**2/yr occur over an area of about 6.5 km**2 at an emission rate of 17,600 m-tons/yr of suspended solids.

This latter pattern is probably more representative of the actual sedimentation pattern and rates occurring in this area. Increased sedimentation can, however, be expected to occur during the period of onshore flow observed during the second month of observations--even if not at the rate indicated by the model. More current measurements would have to be examined to see if this onshore flow condition occurs frequently. If so, more moorings, or possibly a more sophisticated model, would be required to adequately estimate the sedimentation rates and pattern.

This example serves to illustrate that, as with other simulation models, some care must be used in interpreting the results generated by the model when unusual environmental conditions are present.

IV.7. Simulation Summary

The basic sedimentation characteristics for each of the simulated discharge areas are summarized in Table I.

Table I
Simulation Parameters

Location	Sett Spd.	Mass Emission	Sett. Ht.	Max. Rate	Area	Area > Nat.Rate
White Pt	MYR	113,000	15-30	505	0.25	30
OrangeCo	AVG	33,000	30	90	0.5	6
SanDiego	EPA	17,600	30	53	0.5	6.5
Encina	EPA	1,070	11	28	.03	.19
Oxnard	EPA	925	8	13	.12	.38

where:
Sett.Spd. refers to the settling speed dist.
EPA -> 301(h) model (F = .0175/Vs**.41)
AVG -> Avg. (Fig.3) (F = .0190/Vs**.43)
MYR -> Myer (1974) (F = .0142/Vs**.50)
Mass Emission is in metric-tons of suspended solids per year.
Settling Ht. is in meters.
Max. Rate is the maximum sedimentation rate in mg/cm**2/yr
Area is the area corresponding to the maximum sedimentation rate in square kilometers
Area > Nat. Rate is the depsoitional area (km**2) with a rate in excess of 10 mg/cm**2/yr

V. SEDF2D TEST/VALIDATION

V.1. Overview

Two techniques were considered for testing the sedimentation rate predictions generated by SEDF2D: (1) direct measurements of sedimentation rates using "sediment traps" and, (2) measurements of the accumulation of outfall related materials. Sediment trap measurements were rejected in favor of accumulation rate estimates for a number of reasons.

First of all, the conceptual approach in the model is based on an ensemble averaging process. Thus it is necessary to measure the flux rates and patterns for a sufficiently long period of time so that the fluxes measured in the traps are representative of the average flux rates.

In addition, it would be difficult to determine if differences between observed and predicted sedimentation rates are the result of: (1) not satisfying the averaging criteria during sediment trap study, (2) employing current meter records for the simulation that were not representative of typical flow conditions or, (3) fundamental deficiencies in the simulation model.

Another difficulty is associated with the characteristics of sediment traps. Although they appear to yield fairly reproducable sedimentation rates (and thus are probably suitable for inter-site comparisons), the magnitude of the sedimentation rates measured with them are frequently questioned at the levels of accuracy required for a definitive test of the sedimentation predictions.

The final problem is associated with signal-to-noise ratios. For the major outfalls, the peak (spatial--temporally averaged) sedimentation rates are on the order of 100 mg/cm**2/yr (see Section IV - SEDF2D Simulations). Sediment traps placed near the bottom, in water depths comparable with the outfall diffusers, collect particles at rates that correspond to "apparent" sedimentation fluxes on the order of 2000-4000 mg/cm**2/yr. These increased rates are apparently associated with resuspension and redeposition of sediment particles. Since these measured fluxes are substantially in excess of the expected effluent particle sedimentation flux, it would be necessary to utilize a set of traps at varying heights to assist in separating resuspension-related fluxes from effluent-related sedimentation.

The separation of resuspension-related deposition from effluent particle sedimentation might be relatively straight-forward provided that the wastefield is always above the set of traps. However, as the strength of the currents increases, the equilibrium depth of the wastefield increases and, conversely, the settling height decreases. The location of the wastefield in the water column may also vary in time as isopycnal surfaces are displaced upward and downward by internal waves, internal tides, and baroclinic processes. This variability greatly increases the

difficulty in separating sedimentation processes from resuspension processes.

Measurements of the accumulation rate of effluent-related materials on the ocean bottom provide an alternate method of estimating sedimentation rates. This method has the advantage that the properties of the sediments are generally the result of "averaging" fluxes (through bioturbation of the sediments) over a longer period of time than could reasonably be achieved with sediment traps.

Difficulties associated with the method include: (1) uncertainty about the precise location of the "discharge horizon" in sediment cores (due to bioturbation) and, (2) the accumulation actually reflects the combination of a variety of processes including sedimentation, resuspension, and non-conservative mechanisms such as the mobilization of effluent "tracers", or the uptake or "decay" of organic material, etc.

These difficulties can be mitigated, to a degree, if a test site can be identified where resuspension and redistribution processes are minimal, and where large masses of effluent-related materials have accumulated. Both of these considerations suggest that the best site will involve an outfall discharging a large mass of solids over a long time into "deep" water. Discharge into deep water might be expected to reduce the magnitude and frequency of sediment resuspension. In addition, for a given length-scale characterizing the dispersion of resuspended particles, the resuspension related effects on the outfall-generated sedimentation field will be minimized if the field is "large" compared with the resuspension length-scale. Large mass emission rates, over a long period of time, will maximize the accumulation of effluent-related material in the sediments, increasing the depth of the "discharge horizon", and minimizing the error associated with the "smearing" of this horizon by bioturbation.

V.2. Comparison with Cores from Palos Verdes

The White Point outfall system (described in Section IV.2.) meets all three criteria---"deep" discharge, large annual mass emission rate, and a long period of discharge. The discharge area is shown in Figure 11, and the predicted sedimentation rates and pattern are shown in Figure 12. In addition to satisfying the three criteria listed above, this discharge area also includes a variety of bathymetric features (moderately steep bottom slope, shelf width varying with longshore position, curvature in the isobaths, and the presence of submarine canyons). These bathymetric features should provide a good test of the simulation capability of SEDF2D.

V.2.a. Estimation of Accumulated Organic Material

Cores were collected at 17 locations in this discharge area in

1981 as part of a cooperative study by JWPCP and SCCWRP. The gravity coring device used to collect the samples is described in Bascom (1982). The station locations are indicated by the "dots" in Figure 12. The accompanying numbers (e.g. "8C") identify the stations (the number designates the longshore position of a cross-shore transect; the letter, the water depth). JWPCP personnel analyzed the core, in depth increments of 2 cm, for wet mass, percent water, and percent volatile solids. A subset of cores and depths were also analyzed for organic carbon and total DDT. This data set is discussed in Stull, et.al. (In press).

A subset of 12 cores was used to esimate the accumulation of outfall-related organic material, as measured by volatile solids. The primary cores in this set were collected along the 60m isobath (JWPCP "C" stations"), secondary cores were collected along the 305m isobath (JWPCP "A" stations). We did not use the core from station 8A (or stations 8B and 8Z - not shown in Figure 12) since there is evidence that material was redistributed as the result of a "slump".

Figure 25 shows the distribution by "depth" of volatile solids in the core from stations 9C. In this figure, and in the subsequent text, "depth" is expressed in terms of cummulative dry-grams of particulate mass per square centimeter, eliminating the effects of compaction during coring and providing a convenient set of units for testing modeling predictions expressed in terms of mass fluxes. The physical depth of this core was 20 centimeters.

The influence of the outfall discharge on the organic content of the sediments is seen as an increase in volatile solids concentration at depths of less than 7-10 gm/cm**2. Below that depth, the volatile solids concentration is relatively constant at about 4-5 percent.

The concentration of volatile solids in natural sediments (in the absence of the outfall discharge) is estimated from the "deep" sediments in each core. The mass of natural and effluent-related particulates deposited in the sediments is assumed to be equal to the mass of particles above the "horizon" separating increased levels of volatile solids from the underlying natural levels. Some uncertainty is introduced into the precise location of this horizon by the bioturbation occurring during the period when those sediments were near the surface. Myers (1974) has estimated that extensive mixing of the surface sediments extends to a (physical) depth of about 5 centimeters. From the characteristics of the surface sediments in the core data, we estimate that the corresponding bioturbation depth, expressed in mass/area units, is about ? ? gm/cm*2.

The accumulation of organic material represents the combined sedimentation of natural and effluent particles after taking into account the loss of material due to biochemical "decay".

Myers (1974) found that the organic material in effluent particulates could be divided into refractory (resistant to decay)

and non-refractory fractions. Based on studies of the effects of decay in both laboratory simulations and in the ocean environment, he found that the concentrations of volatile solids were reduced by 20 to 35 percent by decay. Most of the loss occurred relatively rapidly (upper and lower bounds for the decay coefficient were estimated to be 0.22 and 0.05 per day, respectively). The total duration of the studies ranged from 20 to 78 days. In most of the experiments, the decay process was essentially complete after an elapsed time of about 1 week. Myers estimated that a "representative" reduction in the concentration of organic carbon was about 25 percent.

Based on these results, it was assumed that the primary loss of organic material occurs relatively rapidly--either while the particles are settling in the water column, or while residing in the "surficial" sediments (Hendricks, 1987). Some additional loss of organic material may occur while incorporated into the "permanent" sediments, but the decay rate for this process appears to be quite slow, especially if anaerobic conditions exist in the subsurface sediments (Myers, 1974). Therefore, the loss of additional material (in excess of the loss observed in the Myers study) is likely to be minor.

If the concentrations of natural and effluent particle volatile solids after decay are known, the masses of both effluent-related and natural particulates accumulated above the "discharge horizon" can be calculated. Average accumulation rates for the period between commencement of discharge through the deep outfalls (1956) and collection of the cores (1981) can be estimated by dividing by this time (25 years).

The volatile solids concentration of natural particulates (after decay), Cn, is estimated from the concentrations in the "deep" portion of the core. The average volatile solids for material above the discharge horizon, Cen, is computed from the accumulated volatile solids (Mvs) and total masses (Mt):

$$Cen = \frac{Mvs}{Mt} \qquad (18)$$

Let Ceo be the concentration of volatile solids in the effluent particles prior to decay, and Ce be the concentration after decay (i.e. the concentration of "refractory" volatile solids). Then:

$$C_e = S_e^o / S_e^T \qquad (19)$$

$$C_n = S_n^o / S_n^T \qquad (20)$$

and:

$$C_{en} = (S_e^o + S_n^o) / (S_e^T + S_n^T) \qquad (21)$$

where:

S_e^o = sedimentation of effluent-related organic

material (after decay)

S_e^T = sedimentation of total effluent-related material (after decay)

S_n^a = sedimentation of natural organic material (after decay)

S_n^T = sedimentation of total natural material (after decay)

The ratio of total effluent-related sedimentation rate to total natural sedimentation rate, R_T, is then given by:

$$R_T = \frac{S_e^T}{S_n^T} = \frac{Ce - Cen}{Cen - Cn} \qquad (22)$$

and the total accumulated mass, M_T, is given by:

$$M_T = S_{en}^T \cdot \Delta T = (S_e^T + S_n^T) \cdot \Delta T \qquad (23)$$

where ΔT is the duration of the discharge (i.e. 25 years). It follows that the two average sedimentation rates can be obtained from the core properties from the relations:

$$S_n^T = \left[\frac{R_T}{1 + R_T}\right](M_T/\Delta T) \qquad (24)$$

$$S_e^T = \left[\frac{1}{1 + R_T}\right](M_T/\Delta T) \qquad (25)$$

Assuming that the change in volatile solids associated with decay in the effluent particles is known, the sedimentation rate in the absence of decay can be computed:

$$S_e^T(\text{no decay}) = S_e^T(\text{decay}) \cdot \frac{1 - \gamma(1 - F_i)}{\gamma F_i} \qquad (26)$$

where:

Fi = fraction of inorganic material in the effluent particles

γ = refractory fraction**

= Ce(t-> ∞)/Ce(t=0)

This analysis was carried out for the cores collected along the main portion of the sediment field (except station 8A -- as noted earlier). The corresponding estimated outfall-associated sedimentation rates are listed in Table [illegible] for refractory fractions, Fi, of 0.6, 0.7, and 0.8 (Myers' values range from 0.64 to 0.77).

** Note: This is not the same as the mass refractory fraction of organic material (m(t-> ∞)/m(t=0))

Table 2

Estimated Outfall-Associated Sedimentation Rates
(in mg/cm**s/yr, multiply by 10 for gm/m**2/yr)

	Core Station	Refractory fraction 0.60	0.70	0.80
	*******	****	****	****
60m	0C	17	13	9
	1C	97	72	53
	3C	186	136	101
	6C	310	228	169
	7C	466	344	255
	8C	628	463	344
	9C	97	72	54
	10C	13	10	7
305m	1A	17	13	9
	3A	46	34	25
	6A	104	77	57
	10A	~0	~0	~0

V.2.b. Comparison with Predicted Rates

Figure 13 shows the predicted sedimentation rate and pattern for the White Point outfall area for an annual mass emission rate of 113,000 m-tons.

Figure 26 quantitatively compares the predicted (average) sedimentation rates for each core station along the 60m isobath ("C" stations) with the rates inferred from analysis of the sediment cores. The flux rates estimated from the cores are based on a (concentration) refractory fraction equal to 0.75 (the value used by Myers in his decay rate analysis).

Near the outfall, and for a couple of kilometers upcoast (Stations 8C, 7C, and 6C), the predicted sedimentation rates are comparable with the values estimated from the cores. Downcoast from the outfall (Stations 9C and 10C), the comparisons are less certain because of the large gradients (100-fold reduction in sedimentation rate over distance of 4 kilometers), but the general pattern of the reduction is reproduced quite well. In the region from 3 to 12 kilometers upcoast from Station 8C, the comparisons are less decisive. The predicted distributions exhibit substantial "hills" and "valleys" in the longshore variation of sedimentation rate. It is difficult to determine if these features are "real"; are a result of the limited current meter data; or indicate deficiencies in the similation technique. To some degree, these sedimentation features, if real, can be expected to be "smeared out" in the actual sediments through the

processes of resuspension and redistribution. The latter appear to be active in this area (Hendricks, 1987).

In this simulation, the maximum sedimentation rate in the region 4 to 8 kilometers downcoast from Transect 8 occurs roughly one simulation cell width (0.25 km) inshore of the 60m isobath. The corresponding longshore variation in sedimentation rate is indicated by the dashed line in Figure 26. Resuspension of this inshore "ridge" of material might also tend to fill in the predicted valley in this region along the 60m isobath.

Figure 27 shows the predicted and estimated sedimentation rates along the cross-shore transect containing stations 6C and 6A. Although there is acceptable agreement between the measured and predicted values near the 60m isobath, the predicted cross-shore distribution of the sedimentation field appears to be substantially "narrower" than the distribution (dashed line - Figure 27) suggested by the accumulation of organic of accumulated organic material at station 6A (305m isobath). This difference between the predicted and observed "widths" of the sedimentation field is a feature common to all the cross-shore comparisons (e.g. 1C-1A, 3C-3A, 6C-6A, 10C-10A).

A number of processes could produce this difference. Measurements of the near-bottom currents in this area show that the movement is generally upcoast and offshore (Hendricks, 1987). Because of the generally small gradients in sedimentation flux in the longshore direction, resuspension of the sediments and redistribution by these currents would be expected to produce only minor changes in the longshore distribution (apart from the smoothing out of the hills and valleys noted earlier). The changes in the cross-shore distribution could, however, be much larger because of the small-length-scales characterizing the cross-shore sedimentation patterns.

A second possibility is related to the shear between the surface (mixed layer) and mid-water flows. The long-term average movement of the surface currents is downcoast, while the net movement of the mid-water currents is upcoast. In order to generate this reversal, the pycnocline surface must, on the average, slope upward towards the coast. Since advective and diffusive transport occurs primarily along surfaces of constant density, this "shoaling" of the isopycnal surfaces reduces the "effective" bottom slope. As a result, the width of the sedimentation field would be expected to increase. At the present time, there is insufficient data available to justify inclusion of the effect into the simulations except possibly on an exploratory basis.

Qualitatively, these comparisons suggest that the advection-dispersion representations and algorithims used in the model provide a reasonable approximation to the average long-term statistical properties of the actual sedimentation process. However, on a quantative basis, the sedimentation pattern predicted by SEDF2D is "narrower" than the accumulation band based on the

core analysis. Although some of the difference between the predicted and observed cross-shore "shapes" of the sedimentation (/accumulation) may be the result of resuspension and redistribution of the deposited material or shoaling of isopycnal surfaces, it appears likely that the total mass deposited along this transect is greater than predicted by the model. Assuming that the cross-shore distribution indicated by the dot-dash curve in Figure 27 is representative of the cross-shore distribution of the "true" seidmentation field, the total mass predicted to settle within this transect by SEDF2D is about 45 percent lower than the (estimated/measured) accumulated mass.

As noted previously, similar differences in the cross-shore distributions are observed at the other transects. This suggests that the total mass of material deposited in the area is approximately 1.7 to 2 times that predicted by SEDF2D. This difference is not inconsistent with the uncertainties in the mass distribution of particle settling speeds, but it was not possible to identify this uncertainty as the source of the observed differences. As noted previously, some other process, such as sediment resuspension or shoaling of the density field, is required to bring the cross-shore distributions into agreement.

VI. SFFT TEST/VALIDATION

VI.1. Overview

Measurements of mid-water currents in the vicinity of the White Point, Orange County, and San Diego outfall areas were examined to determine the characterstics for a time-series of "typical" midwater currents. The properties of the time-series were described in terms of the net flows and the variances for both the longshore and cross-shore directions. "Typical" values for these parameters were found to be:

Vx(avg) = 4.0 cm/sec
Vy(avg) = 0.0 cm/sec
Vx(rms) = 7.7 cm/sec
Vy(rms) = 5.1 cm/sec

where: Vx -> longshore component (+ -> upcoast)
Vy -> cross-shore component (+ -> onshore)

Examination of the individual time-series showed that a record collected from October 7 to November 12 in 1982 at the Orange County outfall area at a depth of 40m (in 55m of water) most closely approximated this set of values. This record had the following characteristics:

Vx(avg) = 4.1 cm/sec
Vy(avg) = -0.3 cm/sec
Vx(rms) = 10.5 cm/sec
Vy(rms) = 4.4 cm/sec

Sedimentation simulations were carried out for this time-series of current measurements using both SFFT and SEDF2D. The "composite" mass distribution of particle settling speeds was used, and the wastefield elevation (above the bottom) was assumed to be 25 meters. A flat bottom cannot be used in SEDF2D, so a slope of 0.4 meters/kilometer was used for those simulations.

In the SFFT simulations, the net cross-shore current was set equal to 0 (using the utility program CFFT). An approximate correction for the net cross-shore compoent of the currents, and the slight bottom slope, in the SEDF2D simulations was carried out by "folding" and averaging the cross-shore probability distributions about a longshore axis passing through the discharge point.

VI.2. Comparison of SFFT Prediction with SEDF2D Prediction for a Flat Bottom

The longshore distributions of depositonal probabilities (integrated along cross-shore transects) for the two simulation models are shown in Figure 28. The (half) cross-shore distributions (integrated along longshore sections) are shown in Figure 29.

In general, SFFT predicts somewhat higher depositonal rates in the immediate vicinity (250-500 meters) of the outfall diffuser than are predicted using SEDF2D. "Downstream" from the outfall, the two depositional rates are quite similar. Sedimentation does not extend as far "upstream" from the outfall in the SFFT simulation as it does in the SEDF2D simulation, and there are some diffferences in the cross-shore distributions. These differences occur primarily when the depositional probabilities are subtantially less than the maximum probabilities.

This comparison indicates that the two depositional patterns, and the associated rates will generally be comparable for the most important regions of the sedimentation field. The differences between the two methods that exist in the immediate vicinity of the outfall can be expected to be reduced when the effects of the finite extent of the diffuser are included in the simulations (the example simulations represent a "point" discharge).

VII. "GENERIC" SEDIMENTATION PATTERN

VII.1. "Typical" Discharge Environment.

In section VI.1., the characteristics of "typical" mid-water currents in the southern California coastal area were identified. A record collected at a depth of 40m (in 55m of water) off Newport Beach (California) from October 7 (JD 280) to November 12 (JD 316), 1982 (see Figure 1) was found to most closely reproduce typical conditons.

This record was used in a SFFT simulation to develop a "generic" sedimentation distribution that could be used to provide rough estimates of sedimentation rates and patterns for areas where time-series of currents were not available--provided that they are expected to be similar to those occurring in southern California coastal waters.

The elevation of the wastefield above the ocean bottom was selected to be 30 meters, and the 301(h) model mass distribution of particle settling speeds for primary or advanced primary treated effluent was used to represent typical particle settling speeds.

VII.2. "Typical" Sedimentation Pattern

The resulting distribution is shown in Figure 30 for an annual mass emission rate of 10,000 metric tons of suspended solids. Depositional rates for other mass emission rates can be obtained by a direct "scaling" by the relative emission rates. The probability matrix listing the depositional probability for each grid cell in this simulation is contained in Appendix B. These probabilities may be converted into deposition rates by multiplying by the annual mass emission rate (in appropriate units, such as gm/yr, or mg/yr) and dividing by the cell areas (3.125 x 10**4 square meters, or 3.125 x 10**8 square centimeters).

VII.3. Sensitivity to Environmental Conditions

VII.3.a. Net Flow Speed

The sensitivity of this generic depositonal pattern to changes in the strength of the mean current was examined by carrying out simulations for net current speeds of 0.0, 2.5, 5.0, and 7.5 cm/sec. The results are shown in Figure 31, which depicts the longshore variation in the deposition integrated across cross-shore transects. The depositional probabilities immediately around the outfall, and for some distance downstream, are not substantially altered by changes in the net flow. The greatest differences occur "upstream" from the discharge, and at substantial distances "downstream".

VII.3.b. Variability - Longshore Flow

A test was also carried out to determine the sensitivity of the distribution to changes in the strength of the fluctuations in the longshore currents. Simulations were carried out for a net speed of 5 cm/sec, with variances for the longshore component of the flow equal to 62, 110, and 192 cm**2/sec**2 (corresponding to rms speeds of 7.9, 10.5, and 13.9 cm/sec, respectively). The resulting longshore variation in the depositional probabilities integrated across cross-shore transects is shown in Figure 32. The results show the same general characteristics as in the simulations for varying net flows--little change in depositional rates in the immediate vicinity of the discharge or immediately downstream, but greater differences upstream from the discharge, or well downstream.

VII.3.c. Variability - Cross-shore Flow

A similar comparison was made for variations in the variance of the cross-shore component of the flow. Simulations were carried out for variances of 11, 19, and 34 cm**2/sec**2 (rms speeds of 3.3, 4.4, and 5.8 cm/sec, respectively). The cross-shore variations in depositional probability (integrated along longshore sections) are shown in Figure 33. As before, the changes in depositional probability in the immediate vicinity of the outfall are minor, with the largest differences occuring near the "tail" of the depositional distribution.

VII.3.d. Wastefield Elevation

The final comparison examined the changes in depositional rates and patterns associated with changes in the wastefield elevation above the ocean bottom. Since the settling time of particles with a particular settling speed is proportional to the settling elevation, to lowest order approximation, they should only be transported one-half as far if the settling elevation is reduced by a factor of two. The validity of this approximation was examined by carrying out simulations for wastefield elevations of 6.25, 12.5, 25, and 50 meters. The dimensions of the grid cells were also increased by a factor of two with each change in settling height (i.e. 0.065 x .125, .125 x .25, .25 x .50, and .50 x 1.0 kilometers, respectively). The resulting longshore and cross-shore variations in depositional probabilities are illustrated in Figures 34 and 35. Depositional rates in the immediate vicinity of the outfall are relatively invariant to these scale changes, however, the spatial extent of the "tails" of the distributions increase with decreasing settling height.

VII.3.e. Summary of Simulation Sensitivity

Overall, distributional rates within 10-15 percent of the "peak"

depositional rate are not substantially altered by changes in the net flow, the strength of the variations, or the wastefield height (after appropriate scaling of the cell dimensions). This suggests that suitable estimates of depositional rates and patterns for sedimentation fields around outfalls with low to moderate mass emission rates of suspended solids can be obtained from the "generic" patterns.

Appendix B contains the probability distribution matricies for each of these simulations. Some details in the two-dimensional distribution of probabilities do accompany changes in the net flow, or in the strength of the variations. These detailed changes can be examined, or estimated for a particular situation, if desired, using these probability matricies.

VIII. MODIFICATION OF "FLAT BOTTOM" DISTRIBUTION FOR A SLOPING BOTTOM

VIII.1. Overview

Depositional patterns generated by SFFT, including the "generic" depositional patterns" discussed in Section VII, are for discharge into an area of constant water depth. Comparison of the depositional patterns generated by the simulation model SEDF2D for the White Point (narrow nearshore shelf) with those for the Orange County discharge (wide nearshore shelf), however, indicates that bottom slope can substantially alter these patterns.

In this section, we address a method that might be used to provide approximate estimates of the changes that may occur in the "flat-bottom" distributions in the presence of bottom slope. This method may provide an estimate of the "real" pattern without demanding the time and resources required to carry out simulations with SEDF2D. The basic approach will be to carry out simulations of the cross-shore distributions of sedimenting particles for a set of different bottom slopes using the sedimentation model SEDF2D. The resulting distributions, combined with dimensional-scaling, indicate the modifications that should be made to the flat bottom simulation results.

VIII.2. SEDF2D Simulations for Varying Bottom Slope

SEDF2D (Ver. 5.1.3) was used to generate the sedimentation pattern around an outfall discharging into an area with a (planar) sloping bottom. Bottom slopes ranged from nearly flat (0.1m/km, or 0.01 percent) to fairly steep (40m/km, or 4 percent). The effective wastefield elevation was 20 meters. The cross-shore distributions for the set of simulations are shown in Figure 36. Sedimentation rates are "normalized" so that a value of unity corresponds to the largest probability oberved in the (nearly) flat bottom simulation.

Several changes in the cross-shore distribution are evident as the slope of the bottom increases. In the case of a flat bottom, the distribution is essentially symmetrical about the discharge depth. As the bottom slope increases, however, deposition is enhanced and sedimentation offshore is depressed. This trend is consistent with the discussion presented in Section III.1.a. regarding modification of the 301(h) model (EPA, 1982) for a sloping bottom, but contrary to the trend predicted by the Koh (1982) model (Section III.1.b.).

As the bottom slope is increased, the "tails" of the cross-shore distributions move closer to the discharge depth, while the "width" the central deposition peak remains roughly constant (except for the maximum simulated bottom slope of 40m/km). Although the number of distributional profiles is small, there is a hint that the representations of the advective transport used in SEDF2D lead to the generation of a second, inshore peak in the

presence of bottom slope. This "secondary" peak moves closer to the discharge depth and increases in magnitude as the slope of the bottom increases. Other simulations show similar features.

The inshore "cut-off" for the deposition of particles corresponds to the isobath representing a depth equal to the wastefield depth. The distance from the isobath corresponding to the diffuser depth to this "effective" coastal boundary is equal to division of the initial wastefield elevation by the bottom slope.

It is not known if the generation of a secondary peak occurs in the ocean, or is simply an artifact of the algorithims used in the simulation model. However, if the coastal boundary "acts" like a "reflective" boundary (as commonly used in estimates of diffusion-driven) dispersion, the depth-dependendence of the sedimentation rate might be expected to result in the generation of such a peak.

VIII.3. Modification of the Generic and SFFT-Generated Flat-Bottom Patterns

Assuming that these cross-shore changes in the depositional pattern predicted by SEDF2D are representative of the real changes, and noting the similarity between the flat-bottom distributions predicted by SEDF2D and SFFT, a rough modification of the depositional pattern predicted by SFFT for a flat bottom to the situation of a sloping bottom can be made using the appropriate profile shown in Figure 36.

This pattern, however, is associated with a wastefield depth of 20 meters. In Section VII.2.d., it was demonstrated that the dominant features of the cross-shore sedimentation distribution for a flat bottom can be estimated for a different settling elevation by a simple scaling of the cell dimensions. It is assumed that a similar scaling approximation can be used in the case of a sloping bottom. In this approximation, the (horizontal) distances shown in Figure 36 should be scaled by the ratio of the actual wastefield elevation to an elevation of 20m (e.g. for a wastefield elevation of 40m, a distance of 1 km in Figure 36 would become 2 km). The labels for each of the profiles (i.e. 5m/km, 20m/km, etc.), however, remain the same. With similar limitations on the validity of the results, this same technique can be applied to the generic sedimentation pattern shown in Figure 30, or to the probability distribution matricies contained in Appendix B.

IX. A MODEL OF PARTICLE SETTLING SPEEDS WITH AGGREGATION - COAG

IX.1. Background

One of the critical inputs into the sedimentation flux models is information on the mass distribution of effluent particle settling speeds. This distribution may vary in time, and reflect the previous and current enviornments experienced by the particles.

Processes that may be expected to influence the distribution include:

1. Physical-chemical aggregation among effluent particles at all stages of the discharge, including transit down the outfall, discharge through the high shear environment of the outfall port, during the initial dilution process (characterized by diminishing shear), and transport and settling in the water column.

2. Analogous aggregation between effluent particles and natural particles (ranging from microscopic phytoplankton cells to "marine snow").

3. Uptake and/or processing by marine biota in the water column, resulting in the formation of fecal pellets, etc.

4. Degradataion and transformation of the particle surface characteristics by wastewater and marine microorganisms.

5. Mechanical break-up of aggregated particles associated with turbulence, including irterrittent turbulent "puffs".

6. Density changes resulting from the combination of changing ambient pressures and adsorbed gasses, or gases generated during micro-biological transformation.

At the present time, the dynamics of these processes and their relative importance in determining the settling characteristics of effluent and natural particles in an ocean environment are poorly understood at best.

The simulations discussed in the preceeding sections utilize information on the settling characteristics of effluent particles from laboratory-based estimates using settling columns. The conditions in these columns deviate from the oceanographic environment in a variety of ways.

One of the prime concerns is that the effects of particle aggregation are not simulated in the columns. The aggregation between small particles, such as found in sewage effluent or sludge, has recently been an area of active research (e.g. Hunt, 1982; Hunt

and Pandya, 1984; Farley and Morel, 1986).

Farley and Morel (1986) reported on a set of experimental, analytical, and simulation studies of particle aggregation. They concluded that the mass rate of removal of particles in a homogeneously mixed column can be described by a three-term series in the particle concentration:

$$\frac{dC}{dt} = B(ds) * C^{2.4} + B(sh) * C^{1.9} + B(b) * C^{1.4} \qquad (27)$$

where:

B(ds),B(sh),B(b) = Proportionality constants for aggregation rates associated with differential settling, shear, and Brownian motion, respectively (see Section IX.2.i)

C = particle mass concentration (e.g. mg/liter)

For particle concentrations in excess of 1-10 mg/l, they suggest that differential settling and shear induced aggregation processes will dominate over those associciated with Brownian motion, resulting in an approximate equation of the form:

$$\frac{dC}{dt} = [\, B(ds)+B(sh) \,] * C^{2} \qquad (28)$$

$$= B * C^{2} \qquad (29)$$

This equation is identical to the quadratic dependence of the aggregation process deduced by Hunt (1982) using different assumptions about the aggregation process.

These results of these studies have the potential to provide significant new "tools" that can be used to estimate the mass distribution of particle settling speeds in the ocean environment. It should be noted, however, that although the studies address some of the concerns regarding the use of simple settling column measurements, major differences still remain between the laboratory environment and the ocean environment. Among these are:

1. Effluent contains particles with a wide range of sizes. The laboratory studies were generally restricted to particles with a narrow size range.

2. A period of time is generally required for aggregation processes to develop and come to "equilibrium". A quantitative relationship between this latency period

and the particle environment has not been developed, and equation (27) is not representative ot this latency period.

3. The initial dilution process contains many elements of an ideal coagulation environment. For example, sea-water is mixed with the effluent, lowering electrostatic barriers to aggregation. Fluid shear is initially high (promoting rapid initial aggregation), but declines in time (reducing the liklihood of breaking up aggregated flocs). This sequence is not simulated in the laboratory environment.

4. Natural particles that may aggregate with the effluent particles may have time-dependent size and density characteristics, depending on whether they represent the remanents of marine "snow" broken-up during entrainment into the initial dilution plume, phyto-plankton cells entrained into the plume or sedimenting into the wastefield from above, or intact marine "snow" encountered by the settling effluent particles.

IX.2. COAG

IX.2.a. Overview

In spite of these differences between the marine and laboratory environments, it is useful to examine the potential role that aggregation processes may play in the sedimentation of effluent particulates. Farley (1986) has developed a sedimentation simulation model of effluent particle sedimentation (DECAL) based on the results of the studies reported by Farley and Morel (1986). In this model, equation (29) is adapted to the ocean discharge by assuming that the upper bound of the wastefield lies at the pycnocline, and that the wastefield and underlying receiving water are rapidly mixed by vertical exchange within the time-scales characterizing the sedimentation process.

There is some question, however, about the validity of the assumption that vertical exchange processes are strong and the water column is rapidly mixed between the pycnocline and the bottom. Figure 37 shows the concentration of ammonia in a section of the water column for almost a two day period as it moves away from the Point Loma (San Diego, CA) outfall (Hendricks and Harding, 1974). Vertical displacements in the position of the wastefield (indicated by elevated ammonia concentrations) associated with internal waves and internal tides are evident, but the structure and vertical extent of the wastefield are essentially maintained. These indications of weak mixing are also consistent with the presence of density stratification in the ambient receiving water.

IX.2.b. Adaptation of Homogeneously Mixed Column Results to a

Density Stratified Water Column

An alternate model, COAG, was developed to address the problems associated with a density stratified water column, and the case of a wastefield that is detached from the ocean bottom in particular. The output from the model is an estimate of the mass distribution of particle settling speeds. This distribution can be used as input to the two sedimentation models SFFT and SEDF2D.

Equation (29) was adapted to a density stratified water column by subdividing a section of the column into a stack of cells. This "stack" extends from the top of the wastefield to the ocean bottom (Figure 38). The water within each cell (or "box") is assumed to be homogeneously mixed, hence equation (29) should apply individually to each cell in the stack. The concentrations of particles within each cell are determined by the inital concentrations, transfers between cells (or through the stack boundaries), and the loss of material due to "decay".

For simplicity, it is assumed that the ocean currents are uniform in strength and direction over the entire stack, and that the simulated "water column" moves with these currents.

IX.2.c. Sedimentation Fluxes

For a cell of unit area and height "h", the flux of mass from a cell through the lower "face" as a result of sedimentation is:

$$J_s = C \cdot V_s \quad . \qquad (30)$$

where:
- Js = flux (mass/area/time)
- C = concentration of particles in the cell
- Vs = particle settling speed

Loss of material from one cell due to sedimentation serves as a source of material for the cell immediately below. The flux of material settling from the lowest cell in the stack constitutes sedimentation rate to the ocean bottom.

IX.2.d. Natural Particles

Farley (1986) addressed the question of aggregation between effluent and natural particles in the sedimentation model DECAL by considering the flux of particles sedimenting down into the wastefield from primary production in the overlying water. His simulations suggest that effluent-natural particle aggregation may significantly alter the total flux, and effluent flux, to the ocean bottom. In COAG, primary production, per se, is not explicitly included--only the flux of natural particles settling into the uppermost cell, the initial distribution of natural particles in the column, and the decay and aggregation charac-

teristics of the particles are specified. However, primary production is one component of the flux into the uppermost cell in the stack--hence it is implicitly included in the simulation.

IX.2.e. Non-Conservative Processes

Time-scales characterizing phytoplankton growth are determined by phytoplankton type (and environmental history), nutrient concentrations, water temperature, and light intensity (in the appropriate spectral bands). For nutrient and light "saturated" conditions, characteristic population "doubling" times are on the order of a day, or comparable with characteristic sedimentation times. The introduction of nutrients into the euphotic zone as a result of the discharge may stimulate phytoplankton growth, or alter the cell density (through nutrient uptake and storage). These processes are ignored in COAG.

In a similar manner, increases in particle mass resulting from the conversion of dissolved nutrients and carbon into bacterial cells is also ignored, as are changes in density associated with the production of gasses, etc.. However, the loss of particulate organic mass as a result of microbial activity is included as a simple, first-order "decay" relationship:

$$m(T) = m(0)\, e^{-kT} \qquad (31)$$

where:
m(T) = mass of the particle at time t=T
m(0) = mass of the particle at time t=0
k = "decay coefficient"

The computations are carried out assuming that the "decay coefficient", k, is independent of position within the cell--and hence water depth. This assumption is not entirely justified since the decomposition rate will depend on temperature and ambient bacterial populations, both of which are known to generally depend on water depth. These effects are ignroed because insufficient information is currently available to develop realistic representations.

Studies by Myers (1974) show that a portion of the organic carbon in effluent particulates is refractory to "decay". The algorithim used in the model divides the organic fraction of the particles into two components: (1) a refractory fraction and (2) the degradable fraction. The first-order decay reaction only applies to the degradable fraction. A similar decomposition of the organic material into a refractory and degradable fraction is used for the natural particulates.

IX.2.f. Initial Wastefield Particle Distribution

Effluent particles are assumed to be homogeneously mixed through-

out the wastefield portion of the stack of cells at the completion of the initial dilution process (i.e. the beginning of the aggregation calculations). The wastefield also contains natural particulates that were entrained into the plume during the initial dilution process. It is assumed that the concentration of "natural" particulates in the wastefield is equal to the average of the natural particle concentration in the cells below the lower bound of the wastefield. This is equivalent to assuming that the initial dilution is proportional to the (vertical component) of the entrainment distance. This entrainment relationship is characteristic of a buoyancy-driven "line" source representation for the outfall diffuser.

The possibility of reentrainment of settling particles into the initial dilution plume as they settle out from the wastefield is ignored.

IX.2.f. Boundary and Initial Conditions

The initial conditions required by the model include the concentration of effluent in the wastefield, the thickness of the wastefield, the height of the water column, and the depth-dependent concentration of natural particles in the water column below the wastefield.

The distribution of natural particle mass in the water column is either (a) fixed or, (b) estimated by carrying out simulations of the sedimentation of natural particles in the absence of effluent particulates. The independent variables for the latter simulation are:

1. The aggregation constant.

2. The decay coefficient for organic material.

3. The refractory fraction of the organic material.

4. The flux of natural particulates settling into the uppermost cell in the water column.

If depth-independent concentrations of natural particulates are not assumed, the simulation is carried out until the water column concentrations of these particles reach their steady-state values. Prior to acheiving steady-state conditions, the concentration in each cell changes until the input of mass associated with sedimentation from the cell above is equal to the loss of mass associated with sedimentation out of the cell and the loss due to decay. In some cases, weeks of simulated time may elapse before this steady-state conditions is achieved.

This long response time suggests that natural particle concentrations in the lower portion of the water column may not achieve steady-state values in the ocean. In this case, the assumption of a constant (depth-independent) concentration may provide an

adequate approximation without requiring the additional natural particle simulation.

In some cases, the flux of natural particles into the uppermost cell of the stack may be unknown, but the flux of natural particulates to the sediments is known. In that case, the value of one or more of the independent variables (flux from the overlying water, aggregation coefficient, etc.) can be adjusted, as deemed appropriate, until simulations fulfilling the desired boundary condition are achieved.

If the distribution of natural particles in the water column (in the absence of a discharge) is simulated. Once steady-state conditions are reached, the profile (including the degradable and refractory fractions) is stored in a file. This file can be used to supply the initial concentrations of natural particulates in the water column at the beginning of each outfall discharge simulation.

IX.2.h. Computational Procedure

The computation begins (T=0) at the completion of the initial dilution process and the formation of the wastefield. At that time, the location of the wastefield in the water column is established (specified as input to the model), the initial concentrations of effluent and natural particles in the wastefield are computed, and the concentrations of of natural particles in the receiving water underlying the wastefield water is set.

The computation then "searches" through the water column to find the cell with the maximum concentration of particles. This initial concentration is used, in combination with the aggregation constant and cell depth, to make a first-order estimate of the time required for all the particles to settle a distance equal to the thickness of a simulation cell. A simulation time step equal to one-tenth of this value is selected for the actual simulations.

At the end of each time step, the loss of degradable and refractory material associated with sedimentation is computed for each cell. The non-refractory mass is "adjusted" for the decay that has occurred during the time step and added to the mass of the underlying cell. The mass of material remaining in the cell is also adjusted to reflect decay.

Material settling out of the bottom cell is considered to be deposited on the ocean bottom, the settling of natural particulates from above the wastefield serves as a source of natural material for the top cell.

This computational sequence proceeds until a specified period of time has elapsed. A summary of the mass that has been deposited on the bottom by sedimentation from the bottom cell is printed at selected time intervals.

The simulations can be executed in either of two modes. In the first mode, sedimentation fluxes are computed for each cell in the wastefield and the underlying receiving water. The "apparent" settling speed of effluent particles deposited on the ocean bottom during each time step is computed from the distance of the wastefield mid-point to the bottom and the total elapsed time since discharge. The summary of deposition at the completion of each time step includes the masses of both the degradable and refractory fractions of both effluent and natural particles, and the associated settling speed.

An alternate method of computation is provided for in the model. In this technique, the settling speed of effluent particles passing through the lower boundary of the wastefield is estimated at each time step from the flux rate and the concentration in the lower wastefield cell (see Equation (30)).

This method does not include the effects of aggregation between particles below the wastefield. However, comparisons of simulations carried out using both methods indicate that the results are generally comparable. Simulations using the second method usually require substantially less computation time.

IX.2.i. The Aggregation Parameter "B"

The aggregation factors are defined in terms of the properties of the environment and the particles as follows (from Farley, 1986):

$$B = f^{1.3} C_a^{0.3} B_{ds} + f^{0.9} B_{sh} / C_a^{0.1} \qquad (32)$$

$$f = 1 + \left(\frac{e}{1+e}\right)\frac{\rho_f}{\rho_p} \qquad (33)$$

$$B_{ds} = 3.12\,(h/S)^{0.32}\,(\alpha_b K_b)^{0.17}\,(\alpha_{ds} K_{ds})^{1.15}/\rho_e^{1.3} \qquad (34)$$

$$B_{sh} = 10\,(S/h)^{0.15}\,(\alpha_b K_b)^{0.1}\,(\alpha_{sh} K_{sh})^{0.75}/\rho_e^{0.9} \qquad (35)$$

$$K_b = \frac{2KT}{3\mu}\ \left[\text{in } \frac{cm^3}{sec}\right] \qquad (36)$$

$$K_{ds} = (6/\pi)^{1/3}\,\frac{g}{12\nu}\,\frac{\rho_e-\rho_f}{\rho_f}\ \left[\text{in } \frac{1}{cm\text{-}sec}\right] \qquad (37)$$

$$K_{sh} = (G/\pi)\ \left[\text{in } \frac{1}{sec}\right] \qquad (38)$$

$$\frac{S}{h} = \left(\frac{1}{6\pi^2}\right)^{1/3}\frac{g}{3\nu}\,\frac{\rho_e-\rho_f}{\rho_f}\,\frac{1}{h}\ \left[\text{in } \frac{1}{cm^2\text{-}sec}\right] \qquad (39)$$

$$\rho_e = (1-e)\,\rho_p + e\,\rho_f \qquad (40)$$

where:
C_a = average particle concentration
ρ_f = fluid density
ρ_p = particle density
e = particle porosity
$\alpha_b, \alpha_{ds}, \alpha_{sh}$ = collision efficiencies
T = absolute temperature
ν = kinematic viscosity
μ = dynamic viscosity
g = gravitational acceleration
G = fluid shear
h = cell thickness

In general, there is only a weak to moderate dependence on the cell thickness, "h". The rate equation, (29), is specified in terms of particle concentration, C, however, instead of particle mass. As a result, vertical flux rates are not independent of cell thickness. For example, the "flux-rate" based analog (B*) to the "aggregation parameter", is related to the concentration-rate based aggregation parameter (B) by a factor equal to the cell thickness:

$$dm/dt = - B^* C^2 \qquad (41)$$

$$B^* = B \cdot H \qquad (42)$$

where:
H = the cell thickness
m = mass/unit area

This means that if a homogeneously mixed segment of the water column of thickness, H, is subdivided into two homogeneously mixed cells, each of thickness H/2, the flux out of the bottom cell will be one-half the flux before the column was subdivided unless B* is based on the total height of the two cells, instead of the height of each cell. Thus, the flux equations are not scale independent. For internal consistency, the flux-based aggregation parameter, B*, must be computed on the basis of the total thickness of the mixed layer (i.e. 2 x H/2 = H in this example), to ensure that the flux rates are independent of the number of cells used to represent the wastefield.

This requirement does not present any conceptual or computational difficulties when distinct, completely mixed, layers are simulated. However, the region of the water column below the wastefield (and the upper region in the absence of the wastefield) generally is not completely mixed. Thus there are some conceptual difficulties in choosing an appropriate value for B* (or, to a lesser degree, B). Again, for internal consistency, all simulations carried out with COAG have used flux-rate aggregation parameter values based on the total thickness of the wastefield.

IX.2.j. Simulations

Mass distributions of the effluent particle settling speeds have been generated for wastefield thicknesses of 15m and 30m, and wastefield concentrations of effluent particles of 0.6 mg/l, 2.5 mg/l, and 3.3 mg/l. The concentration of natural particles was assumed to be 0.3 mg/l. The water was assumed to have a temperature of 15 deg.-Celsius. The values of the other quantities entering into the aggregation parameter equations are from Farley (1986).

The resulting mass distributions of particle settling speeds, based on the flux rates from the bottom of the wastefield, are shown in Figure 39 . The strong dependence of the mass distribution of particle settling speeds on both wastefield thickness and particle concentration is obvious. A doubling of the wastefield thickness increases the effective particle settling speeds by about a factor of two. A factor of 4.2 change in particle concentration (0.6->2.5) results in a factor of about 4 change in the settling speeds.

In all cases, approximately 30 percent of the particles have essentially a unique settling speed; about 50 percent of the particles have a settling speed within 20 percent of the dominant (highest) speed; and 80 percent of the particles have settling speeds that differ by a factor of about 3 (or less) from the maximum speed.

IX.2.h. Simulation of White Point Sedimentation with SEDF2D and Settling Speeds from COAG

Each settling speed sub-group used in the previous SEDF2D simulations for White Point contains a range of setting speeds that varies by a factor of about 3 (actually 3.16). Thus the range of settling speeds estimated for the White Point discharge using the COAG simulations spans approximately one SEDF2D settling speed subgroup. In the early 1970's, the concentration of suspended solids in White Point effluent was about 330 mg/l, in the mid-seventies, improved treatment reduced this concentration to about 245 mg/l (SCCWRP, 1972; Schafer, 1974-1982). For a wastefield effluent particle concentration of 2.5 to 3.3 mg/l (corresponding to an initial dilution of 100:1) and a wastefield thickness and elevation equal to 30m, the predicted settling speeds range from about 0.01 to 0.032 cm/sec.

The sedimentation pattern associated with the SEDF2D sub-group of particles with this range of settling speeds for the White Point outfall simulations was examined. The longshore distribution of sedimentation rates along the 60m isobath is shown in Figure 40. Also shown are the estimated values at each of the coring stations (see Section V.2.).

The peak sedimentation rate is estimated to be about 3300

mg/cm**2/yr. For a (concentration-based) refractory fraction of organic material of 75 percent, the cores in that area indicate sedimentation rates of about 400-550 mg/cm**2/yr. Thus the predicted sedimentation rates are about 7 times greater than the values estimated from the cores in the immediate vicinity of the 90-inch outfall. Twelve kilometers "downstream" from the outfall (Station 1C), however, the sedimentation is predicted to fall off to about 1 mg/cm**2/yr, or only about 1/70 of the rate estimated from the core at that station.

Sedimentation rates in the immediate vicinity of the outfall should be relatively insensitive to measurement errors in the current speeds, their temporal variability, or the large-scale flow characteristics of the ocean currents. Thus the difference between the predicted and estimated sedimentation rates near the outfall suggests that: (1) the refractory fraction of organic material may be less (e.g. 0.3 instead of 0.75) than estimated in the Myers (1974) studies, (2) resuspension may have dispersed a substantial fraction of the deposited material, (3) the wastefield may be thinner and form higher in the water column or, (4) the settling speeds obtained from the COAG simulation may not be representative of the true distribution. At the present time, the correct reason(s) cannot be determined.

Figure 41 shows the cross-shore distribution of the sedimentation flux using the COAG-generated mass distribution of particle speeds for an initial wastefield concentration of effluent particles of 2.5-3.3 mg/l. As in the simulation generated using the mass distribution of particle speeds measured in settling column, the predicted wastefield width is less than the width inferred from the cores. In the present case, however, the total sedimentation flux is substantially greater than inferred from the core measurements.

Figure 42 shows the distribution of sedimentation flux along the 60 meter isobath using the next (slower) sub-group of effluent particle settling speeds (corresponding roughly to an initial wastefield concentration of effluent particles of about 0.6 mg/l). In this case, the predicted distribution is similar to the measured distribution. Figure 43 illustrates the predicted cross-shore distribution of sedimentation flux. Although a minor "secondary" peak is predicted to occur offshore, the general characteristics are similar to those obtained using the settling column based mass distribution of particle settling speeds.

A comparison of the simulations carried out for the White Point area using estimates of the mass distribution of effluent particle settling speeds from settling column studies and from the aggregation model COAG indicates that:

(1) the longshore distribution of sedimentation flux using the settling column settling speed information is in relatively good agreement with the rates estimated from the accumulation of organic material in the sediments along this isobath

(2) if particle settling speeds are estimated using COAG, the effluent concentration of particles, and an initial dilution of 100:1, the predicted sedimentation in the vicinity of the outfall is much greater than observed in the sediments; farther downstream (7-12 km), the predicted rates are much lower than observed

(3) longshore sedimentation flux distributions based on the particle settling speed distribution predicted by COAG for an initial wastefield effluent particle concentration of 0.6 mg/l is similar to the distributions predicted using the settling column information, or the measured distribution. Initial wastefield concentrations of effluent particles of 0.6 mg/l would, however, require "typical" initial dilutions of about 400:1 to 550:1

(4) all the settling speed distributions lead to cross-shore sedimentation flux distributions that are significantly "narrower" than the fluxes based on accumulation rates

(5) COAG simulations predict that the settling particles will have an almost unique settling speed, whose value depends on the initial wastefield concentration of particles (and hence the initial dilution generated by the outfall) and the wastefield thickness. The large-scale sedimentation flux patterns based on settling speed distributions predicted by COAG are sensitive to the initial particle concentation.

(6) existing data on the characteristics of the sediments is insufficient to determine the best method for estimating particle settling speeds.

X. CONCLUSIONS

Two numerical simulation techniques have been developed to estimate the sedimentation of effluent particulates around ocean outfalls. Both methods take into account the temporal characteristics of the ocean flows, and require one, or more, time-series of measurements of the mid-water currents. Other information required for a simulation includes: (1) the height of the wastefield above the ocean bottom and, (2) the settling characteristics of the effluent particles.

One of these methods, SFFT, was used to develop a set of "generic" sedimentation patterns. The sensitivity of these "generic" sedimentation rates to variations in the net current speed, variability in the longshore and cross-shore components of the flow, and the settling elevation were tested. It was found that the sedimentation rates and pattern in the immediate vicinity of, and downstream from, the outfall were not especially sensitive to the flow characteristics, and the dependence on settling elevation could be approximately accounted for by a simple dimensional scaling of the generic pattern. These generic patterns should provide useful estimates for areas where appropriate current information are unavailable and the mass emission rates of suspended solids are "small".

One of the simulation models, SEDF2D, can be used to estimate sedimentation in the presence of spatially variable bathymetry--provided that the water depth increases monotonically with increasing offshore distance, and "abrupt" changes in the bathymetry do not occur. Simulations may still be generated in many cases if these conditions are not fulfilled, however, sedimentation rate artifacts may be generated in the vicinity of these "non-conforming" regions of the discharge area.

Sedimentation pattern changes as a function of increasing bottom slope were examined using SEDF2D. The results can be used to provide an approximate method for modifying the generic sedimentation pattern, or predictions generated using SFFT, for areas with "simple" variations in bottom depth.

The simulations generated by SEDF2D for the White Point outfall area were tested by comparing the predicted sedimentation rates and patterns with those estimated from a set of sediment cores collected within the sedimentation field. Sedimentation associated with this outfall system tends to follow the 55-60 m isobath (the depth of the outfall diffusers). In general, there was good agreement between the predicted and "observed" sedimentation rates along this isobath. However, the cross-shore "width" of the predicted sedimentation field was less than that inferred from the core analysis--a difference that may result from resuspension and redistribution of the sediments.

As a result of the narrower width, the predicted total mass of effluent particulates deposited within the simulation area is only about 50-60 percent of the mass estimated from the core

analysis. Uncertainty in the mass distribution of effluent particle settling speeds could account for part, or possibly all, of this difference.

All the previous analysis was developed using effluent particle settling speed characteristics obtained from laboratory-based settling column studies. A separate simulation model, COAG, was developed to adapt results on particle aggregation kinetics developed from laboratory studies (Hunt, 1982; Farley and Morel, 1986) to typical discharge conditions in the ocean. The resulting predictions for the mass distribution of effluent particle settling speeds for White Point effluent were used to provide an alternative prediction for the sedimentation rates and patterns in that area.

These initial simulations with COAG-based particle settling speeds predicted sedimentation patterns in which the predicted rates near the outfall were nearly an order-of-magnitude greater than the "measured" rates near the discharge, while the "far downstream" (e.g. approx. 10 km) flux rates were predicted to be an order-of-magnitude (or more) smaller than the rates estimated from the core values.

Simulations with sedimentation patterns comparable to those obtained with settling column settling speeds could be generated using COAG if the initial concentration of effluent particulates in the wastefield, or the thickness of the wastefield, was reduced by about a factor of four. Although this reduced concentration, or wastefield thickness, seems unlikely, the results indicate the sensitivity of the COAG-based sedimentation patterns to the details of the initial dilution process.

In summary, three methods ("generic", SFFT, SEDF2D) were developed to estimate initial sedimentation rates and patterns of effluent particles around ocean outfalls. These "tools" should provide improved estimates compared with the methods presently used in EPA evaluations of outfall-related sedimentation--particularily for areas where hydrodynamical-numerical model techniques are inappropriate or impossible to implement.

XI. REFERENCES

Cardoni, J.J., D.R. Bingham, and N.D. Baratta, 1986. Determining settling velocities of wastewater in sea water. Proc. of Water Poll. Control Federation - Nov. 1986. Los Angeles, CA.

Emery, K.O., 1964. The Sea Off Southern California - A Modern Petroleum Habitat. J. Wiley and Sons, NY, NY. 1964.

EPA 1982. U.S. Env. Protect. Agency, Revised Section 301(h) Technical Support Document. EPA 430/9-82-011. Nov., 1982.

Farley, K.J. 1985. A simplified deposition calculation (DECAL) for organic solids accumulation near sewage outfalls. Draft Report TC-3953-02. Prepared for Marine Operations Div., Office of Marine and Estuarine Protection, U.S.-Env. Protection Agency, Washington, D.C. 20460.

Faisst, W.K., 1976. EQL Rept. No. 13, Env. Qual. Lab, Calif. Inst. of Tech., Pasadena, CA.

Farley, K.J,, and F.M.M. Morel 1986. Role of coagulation in the kinetics of sedimentation. Env. Sci. and Tech., Vol. 20, No. 2, 1986.

Hendricks, T.J. 1983. Numerical model of sediment quality near an ocean outfall. Final Report, NOAA Grant# NA80RAD00041. Nat. Oceano. and Atm. Adm. (NOAA), ERL/PMEL, Seattle, WA. Oct., 1983.

Hendricks, T.J., 1987. Final Report - Part 2: Development of methods for estimating the changes in marine sediments as a result of the discharge of sewered municipal wastewaters through submarine outfalls. U.S.-EPA, Marine Research Division, Newport, OR. (In preparation).

Hendricks, T.J. and J.M. Harding, 1974. The dispersion and possible biological uptake of ammonia in a wastefield, Point Loma, May 1972. TM-210, So. Calif. Coastal Water Res. Proj., Long Beach, CA. Feb. 1974.

Herring, J.R. and A.L. Abati, 1978. Effluent particle dispersion. In: Coastal Water Res. Proj. Ann. Rept.-1978. So. Calif. Coastal Water Res. Proj., Long Beach, CA.

Hunt, J.R., 1982. Particle dynamics in seawater: Implications for predicting the fate of discharged particles. Env. Sci. and Tech., Vol. 16, No. 6, 1982.

Hunt, J.R. and J.D. Pandya, 1984. Sewage sludge coagulation and settling in sea water. Env. Sci. and Tech., Vol. 18, No.2, 1984.

Koh, R.C.Y., 1982. Initial sedimentation of waste particulates

discharged from ocean outfalls. Env. Sci. and Tech., Vol. 16, No. 11, 1982.

Okubo, A., 1971. Ocean diffusion diagrams. Deep Sea Res., Vol. 18.

Myers, E.P., 1974. The concentration and isotopic composition of carbon in marine sediments affected by sewage discharge. Ph.D. Dissertation, Calif. Inst. of Tech., Pasadena, CA. 178pp.

SCCWRP, 1973. The ecology of the southern California bight: Implications for water quality management. So. Calif. Coastal Water Res. Proj., Long Beach, CA. Mar. 1973.

Schafer, H.A. 1974->1982. Characteristics of municipal wastewater. In: Coastal Water Research Project Annual and Biennial Reports (1974 through 1982). So. Calif. Coastal Water Res. Proj., Long Beach, CA.

Stull, J., R. Baird, and T. Heesen, (In Press). Relationship between declining discharges of municipal wastewater contaminants in marine sediment profiles. In: Oceanic Processes in Marine Pollution, Vol. 5, Urban Wastes in Coastal Marine Environments. D. Wolfe, ed., Robt. Krieger and Co., Malabar, FL.

Winand, C.D., 1983. Longshore coherence of currents on the Southern California Shelf during the summer. Jou. Phys. Oceano., Vol. 13, No. 1.

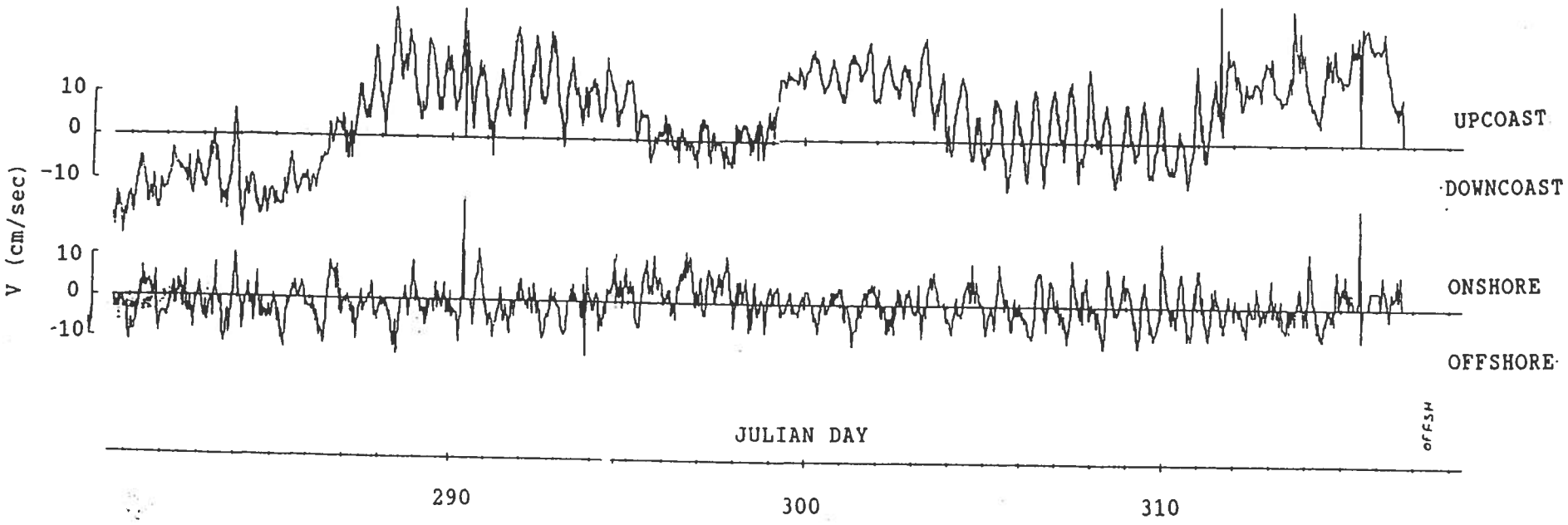

Figure 1. "Typical" mid-water currents.

Newport Beach, Oct. 7 to Nov. 12, 1982, 40m deep in 55 m of water.

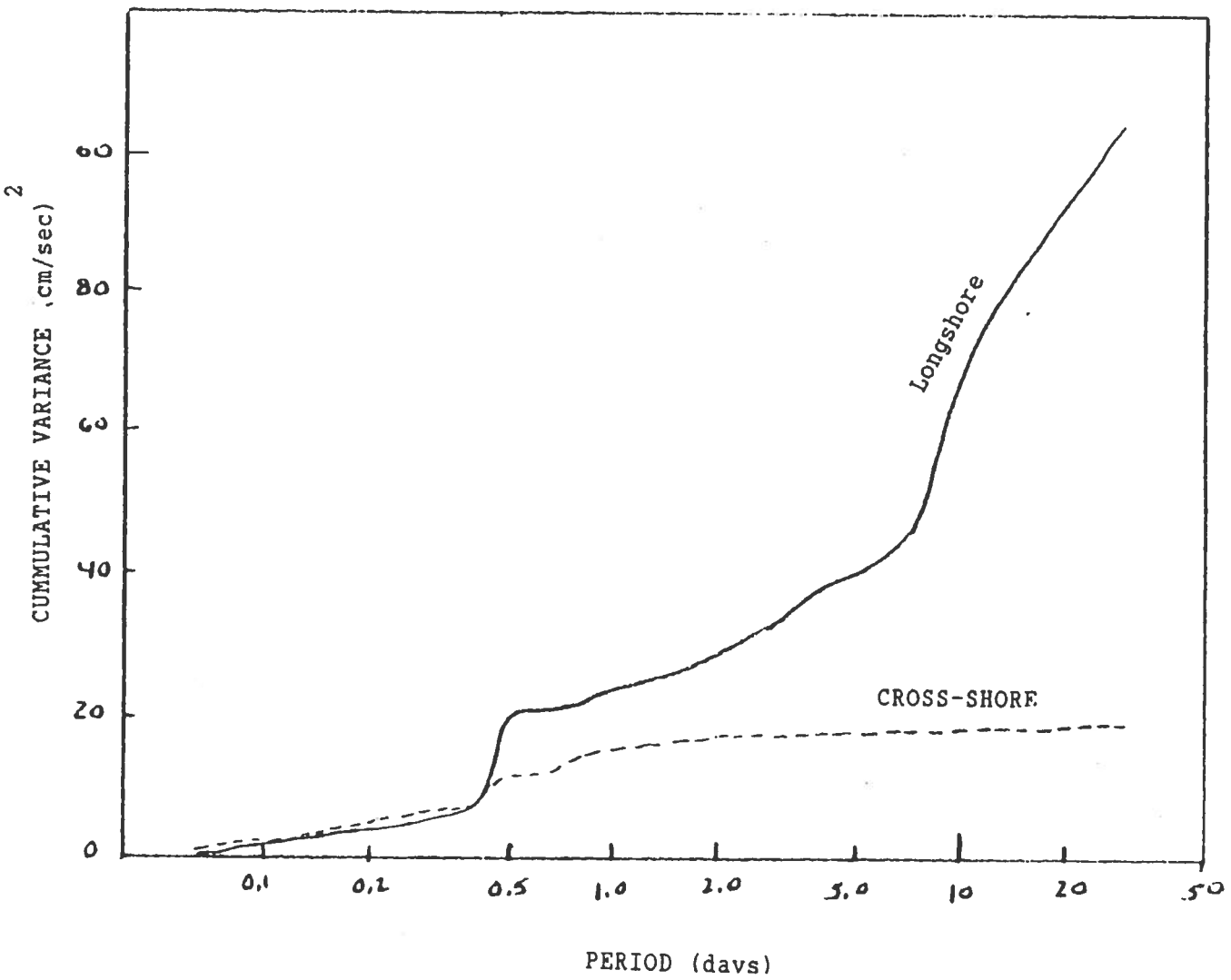

Figure 2. Temporal dependnce of current variability.

Newport Beach, JD280-316, 1982, 40m/55m.

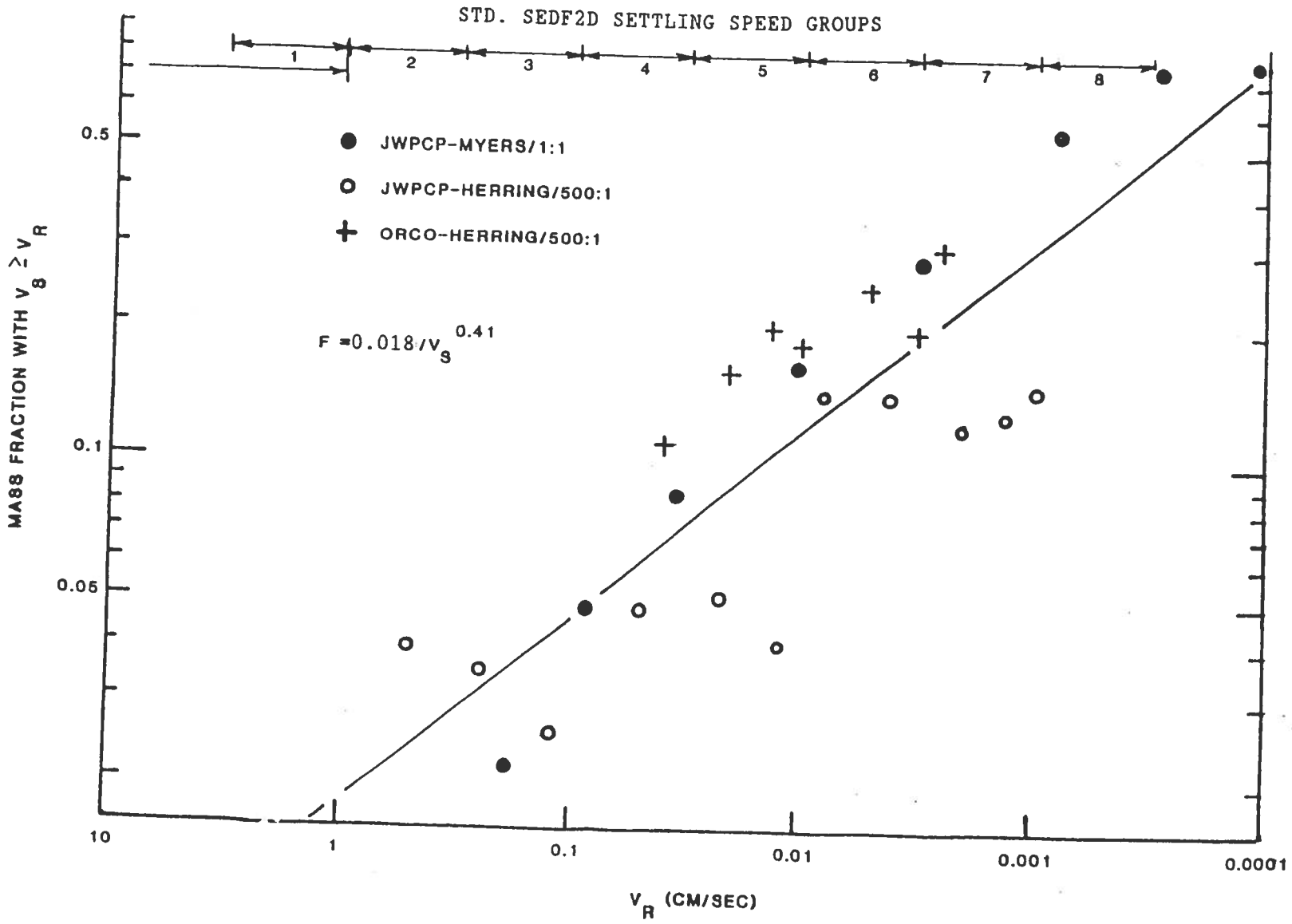

Figure 3. Settling speed characteristics of effluent particles.

(Adapted from Myers,1974, and Herring and Abati, 1978).

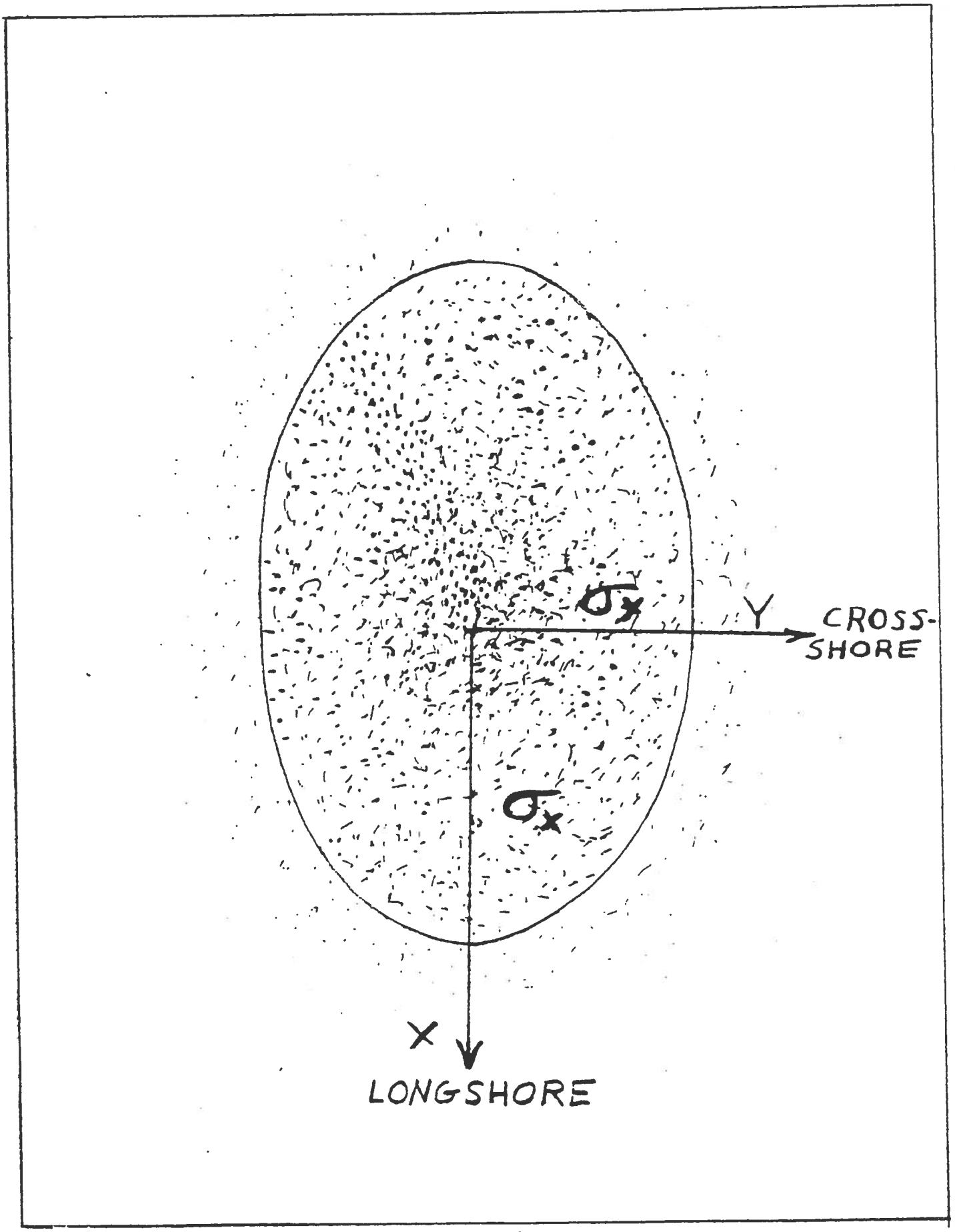

Figure 4. Particle dispersion - single release.

Variances of similarity distribution in longshore and cross-shore directions.

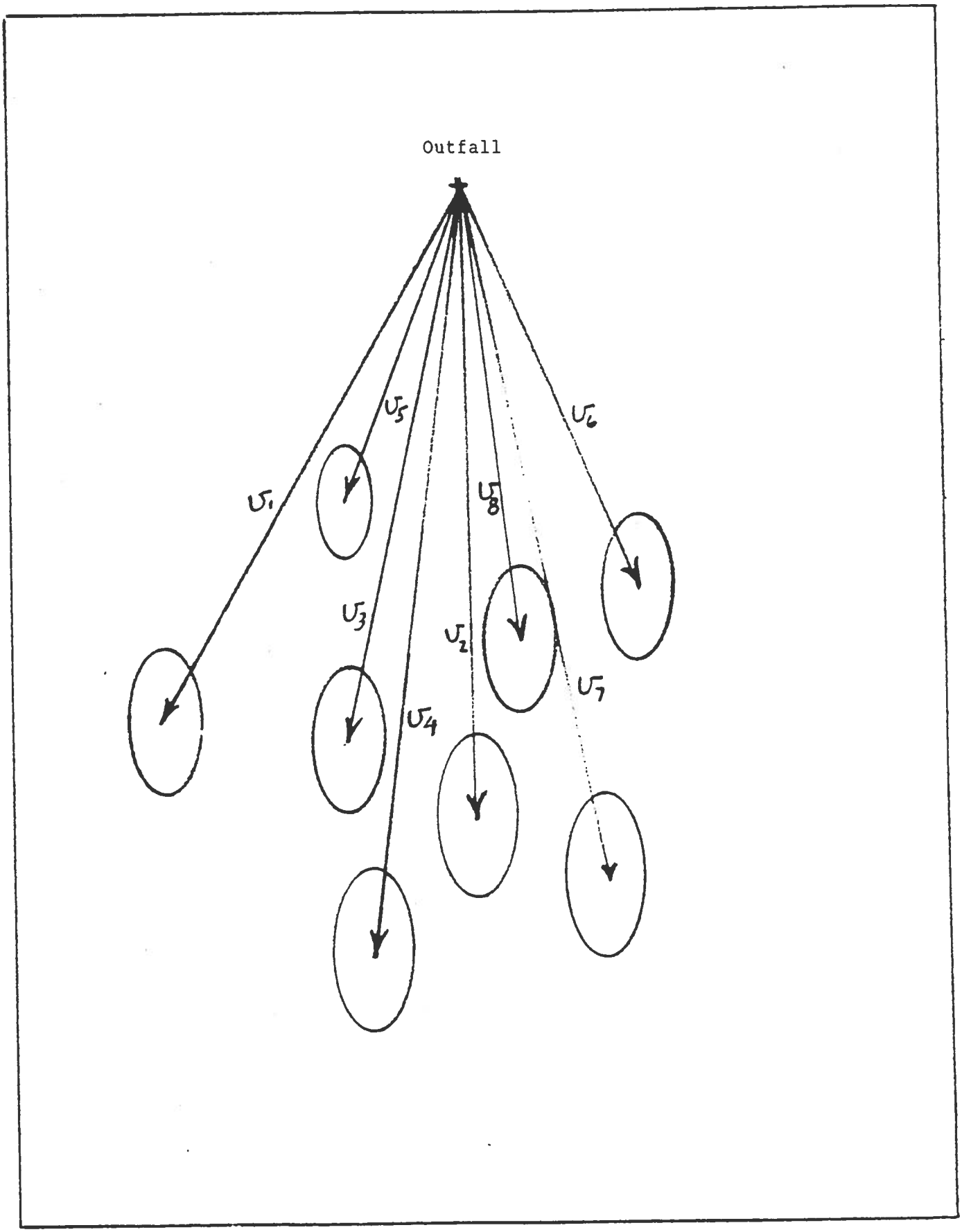

Figure 5. Packet dispersion - multiple releases.

V_j designates the "mean" velocity for the jth release.

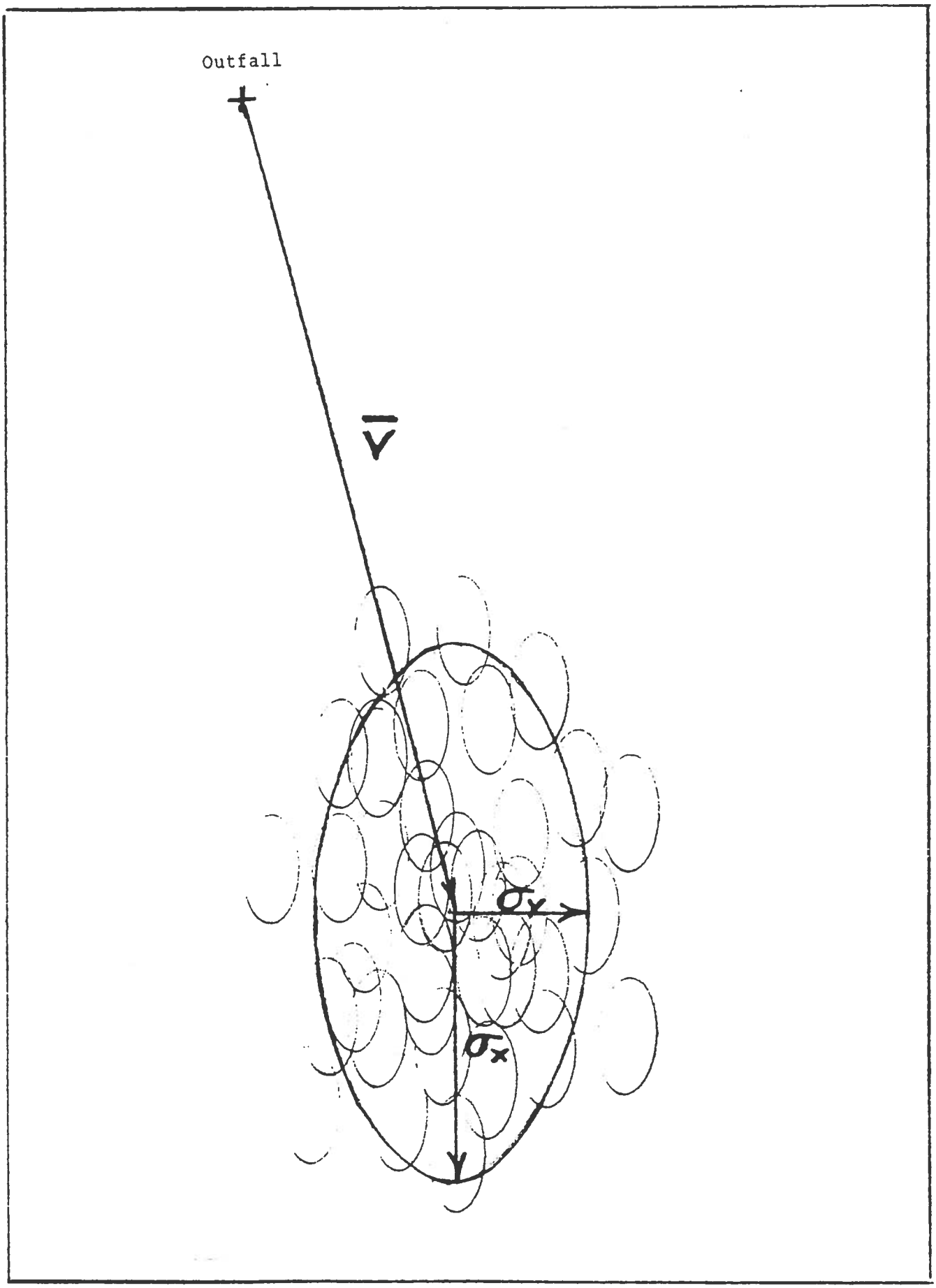

Figure 6. Ensemble dispersion and motion.

$\bar{V}$ represents the ensemble mean velocity; σ_x, σ_y the variances of packet dispersion.

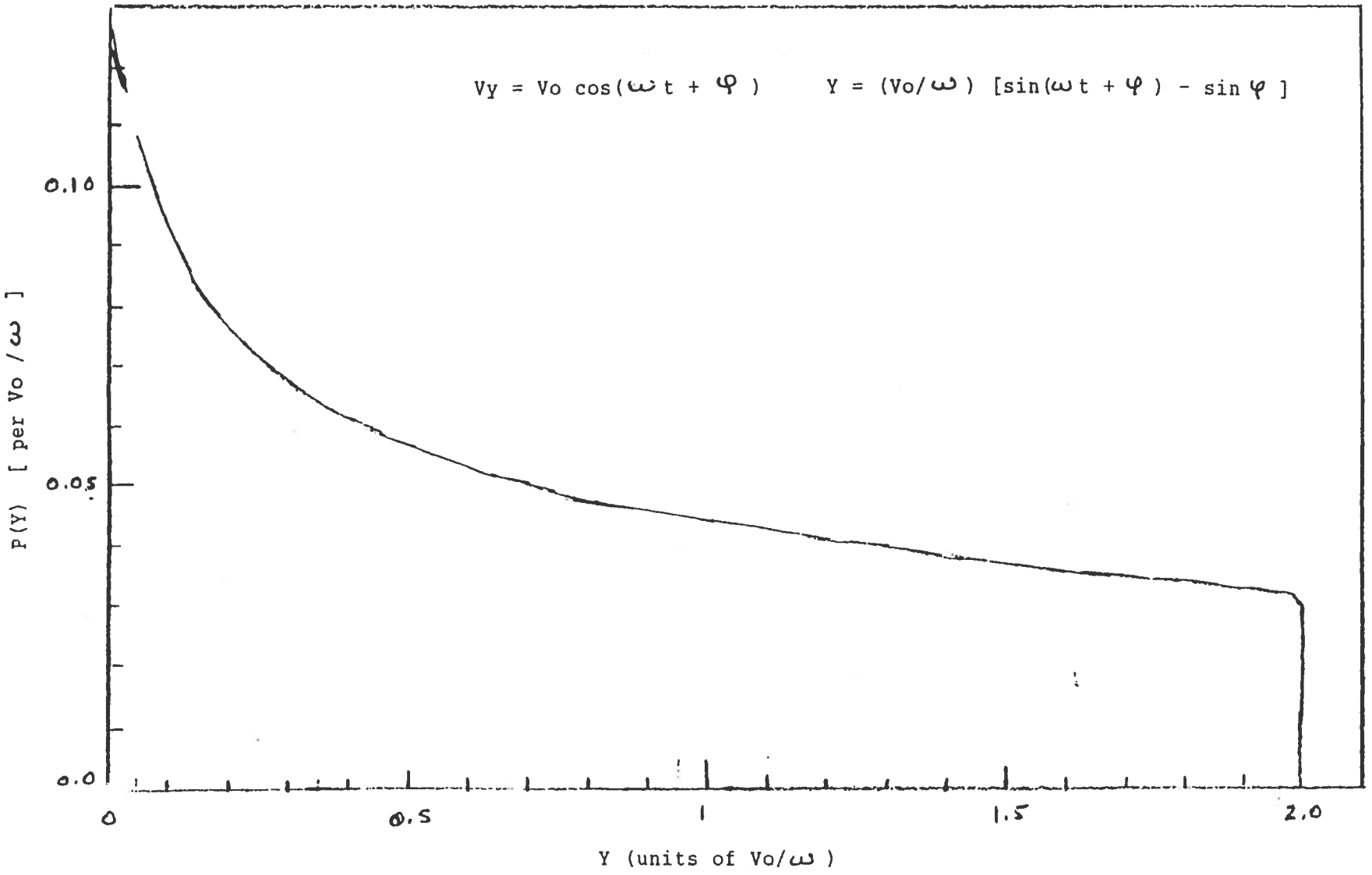

Figure 7. Probability distribution for a sine function.

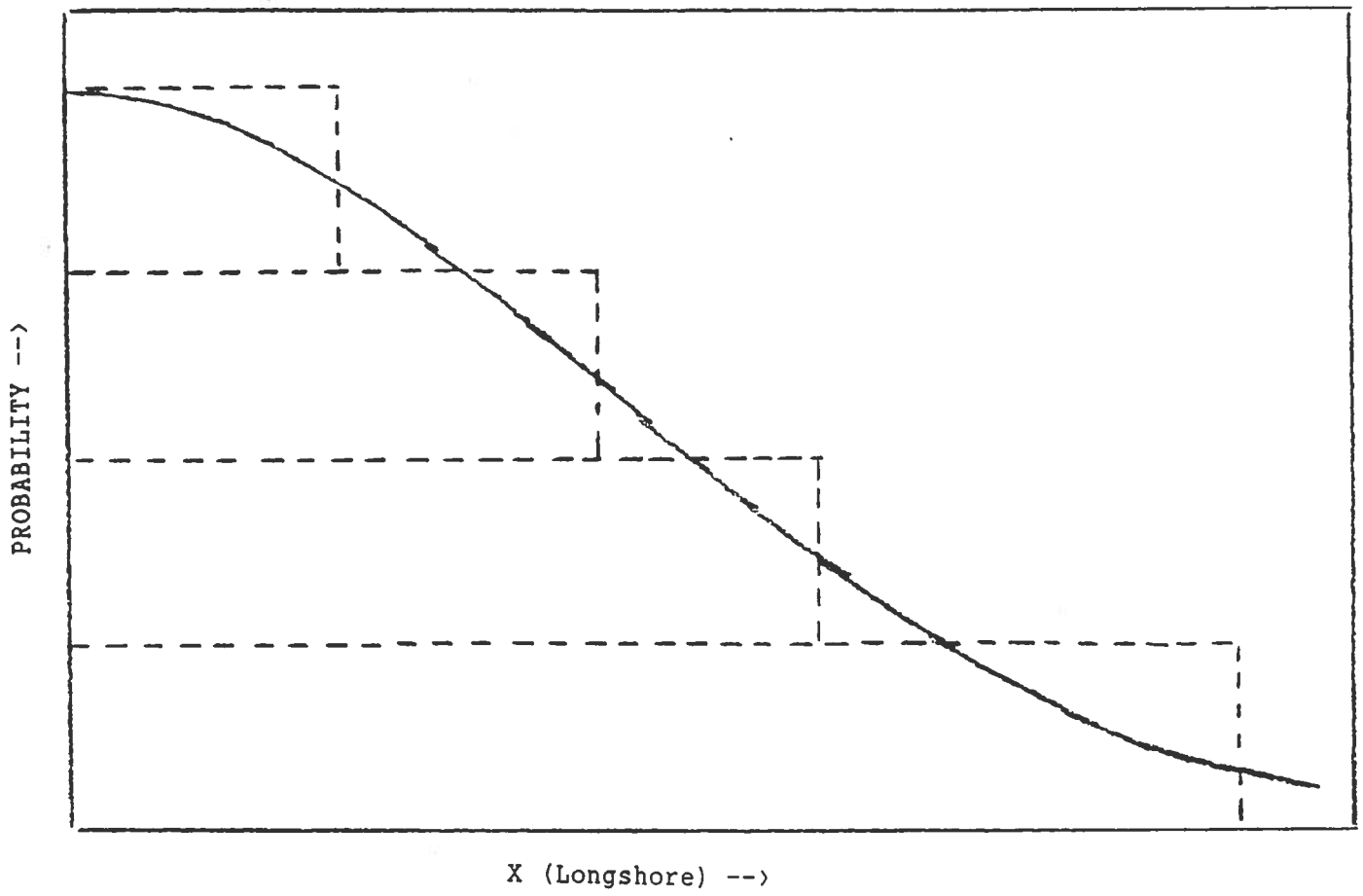

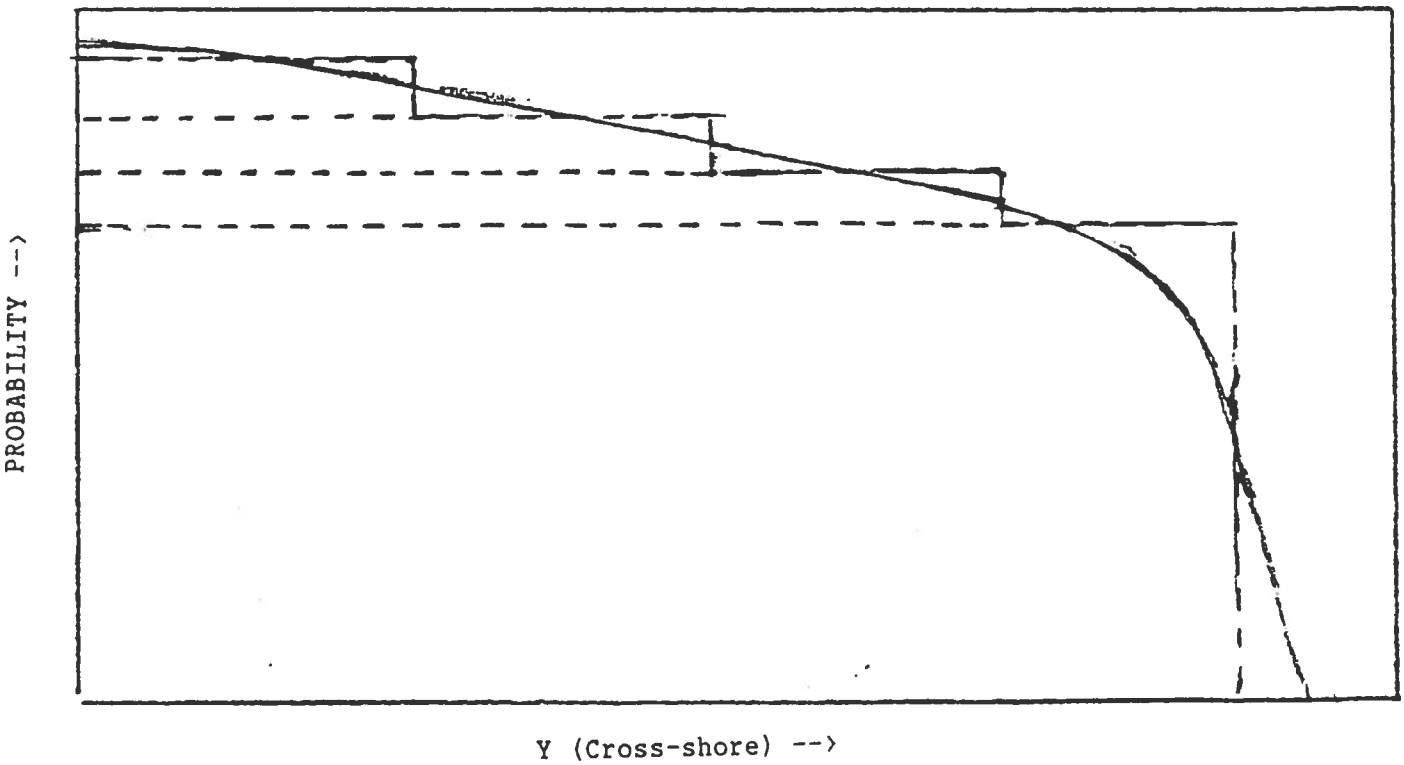

Figure 8. "Top-hat" approximation.

(a) Gaussian probability distribution, (b) top-hat approximation

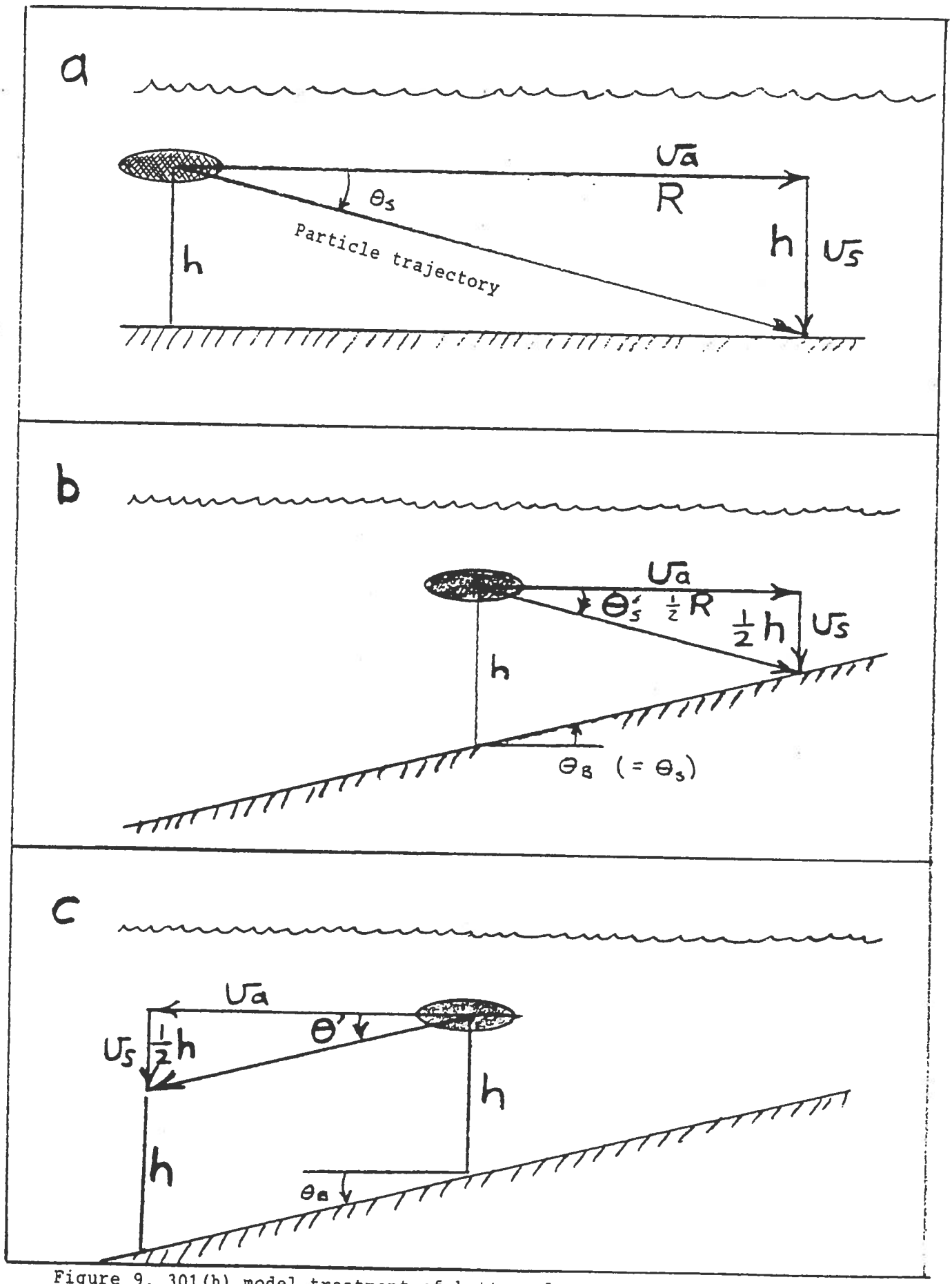

Figure 9. 301(h) model treatment of bottom slope.

R = transport distance, Va = ambient current speed
θ_B= bottom slope angle, Vs = particle settling

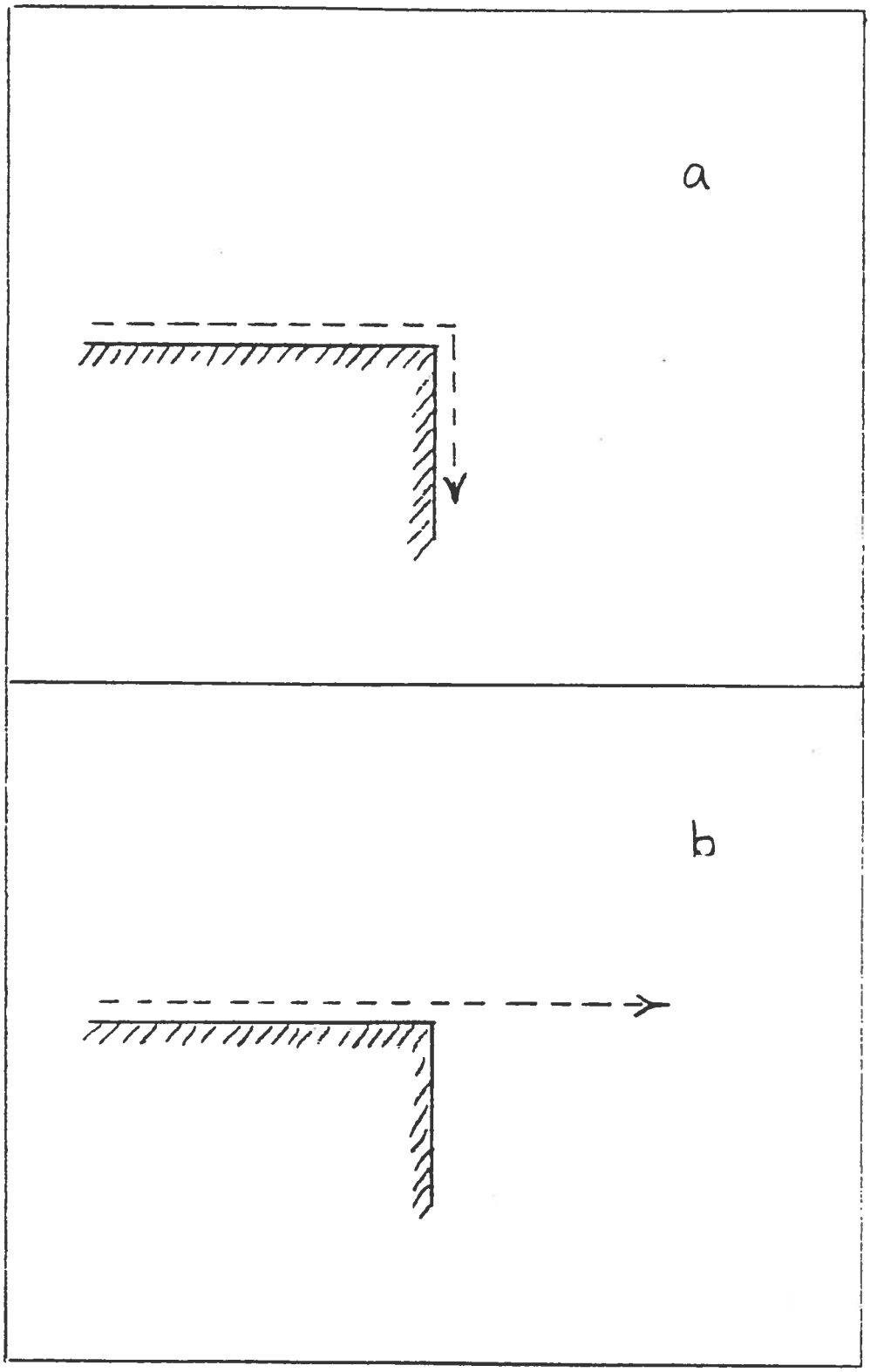

Figure 10. Divergent flow.

(a) attached flow (no viscosity); (b) separated flow (viscous).

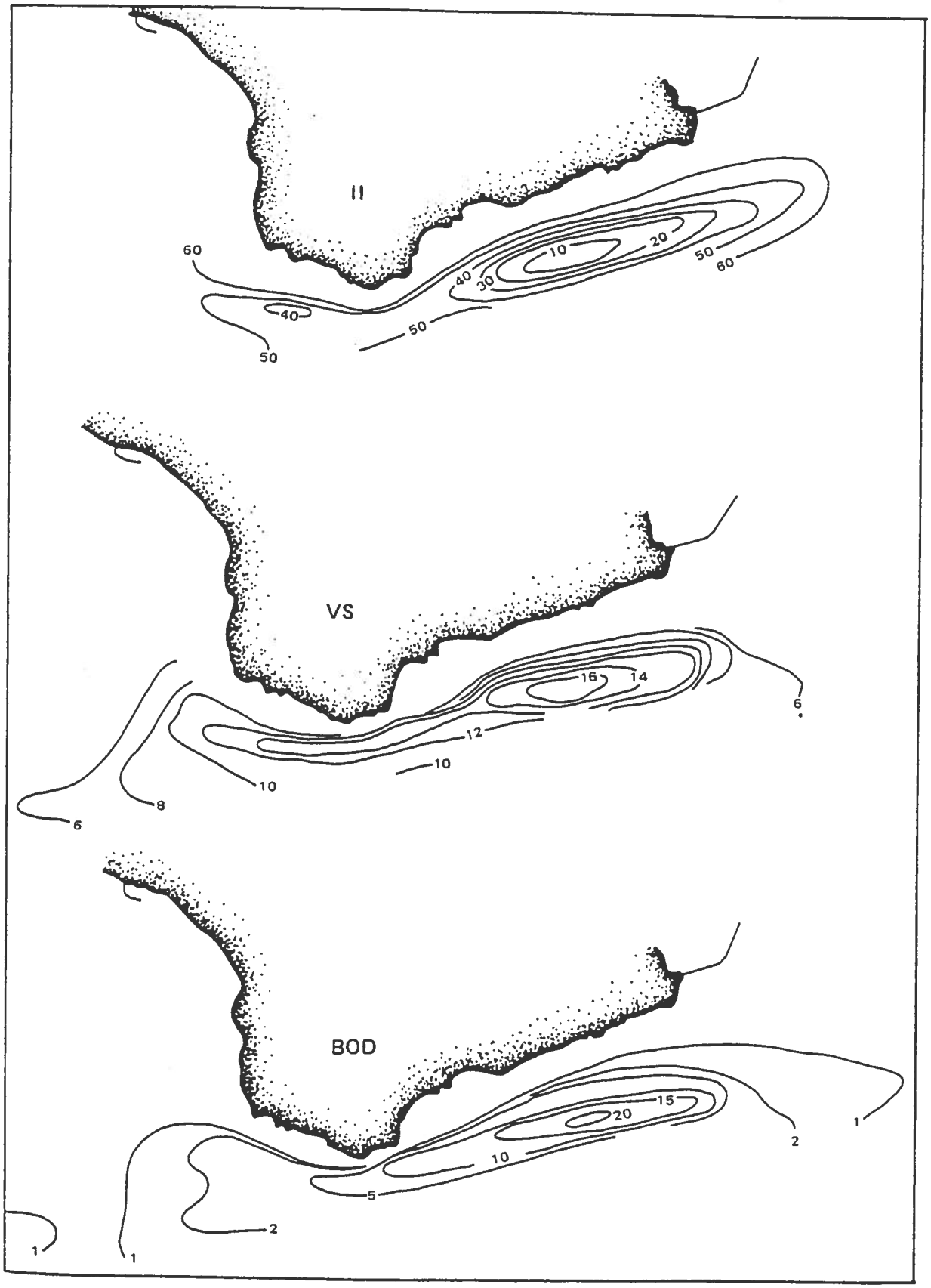

. Figure 13. Observed Patterns of Infaunal Index, Sediment Volatile Solids, and Sediment BOD–White Point Area, II = Infaunal Index; VS = Volatile Solids (percent); BOD = Biological Oxygen Demand (gm/Kg).

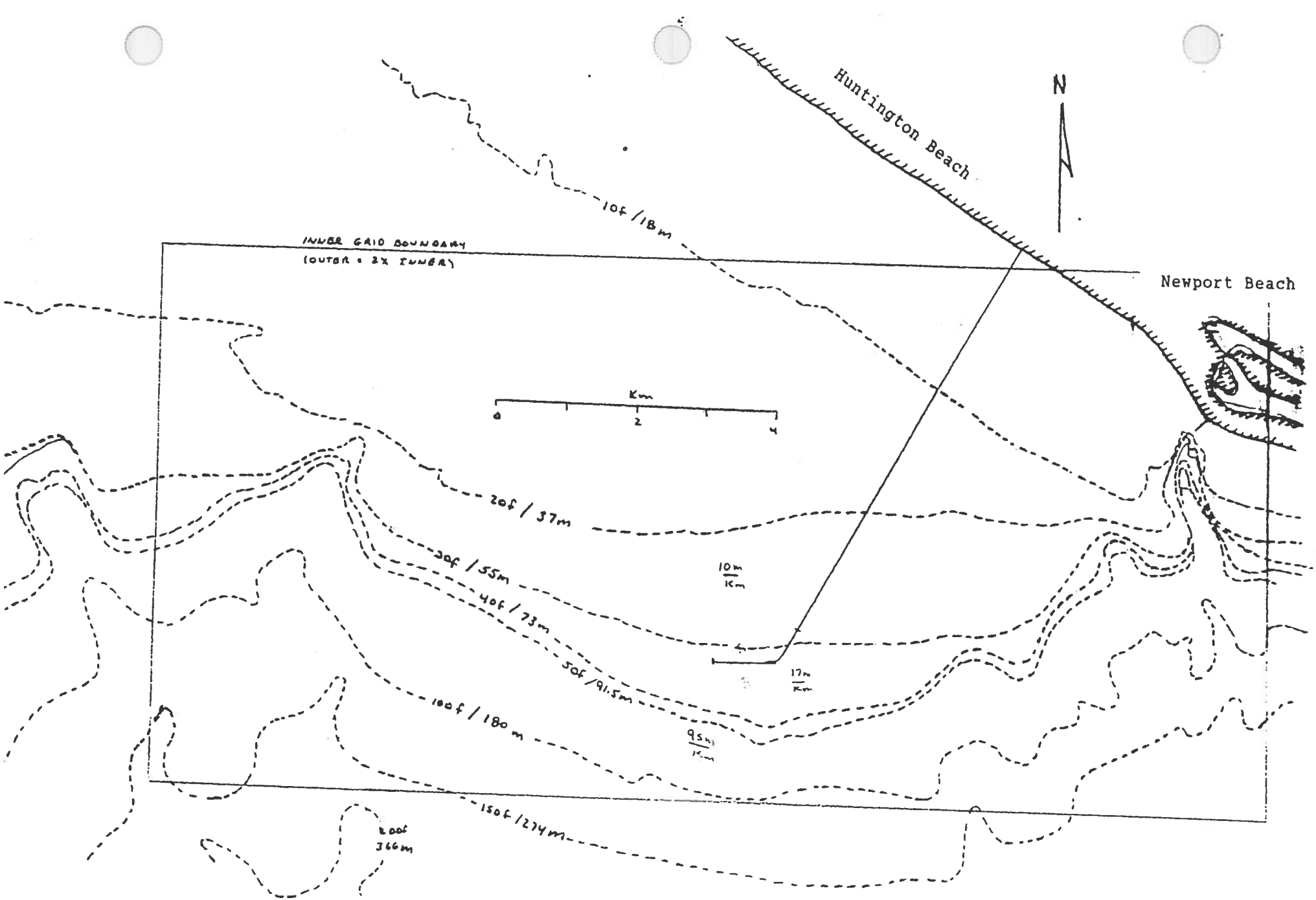

Figure14. Orange County outfall area.

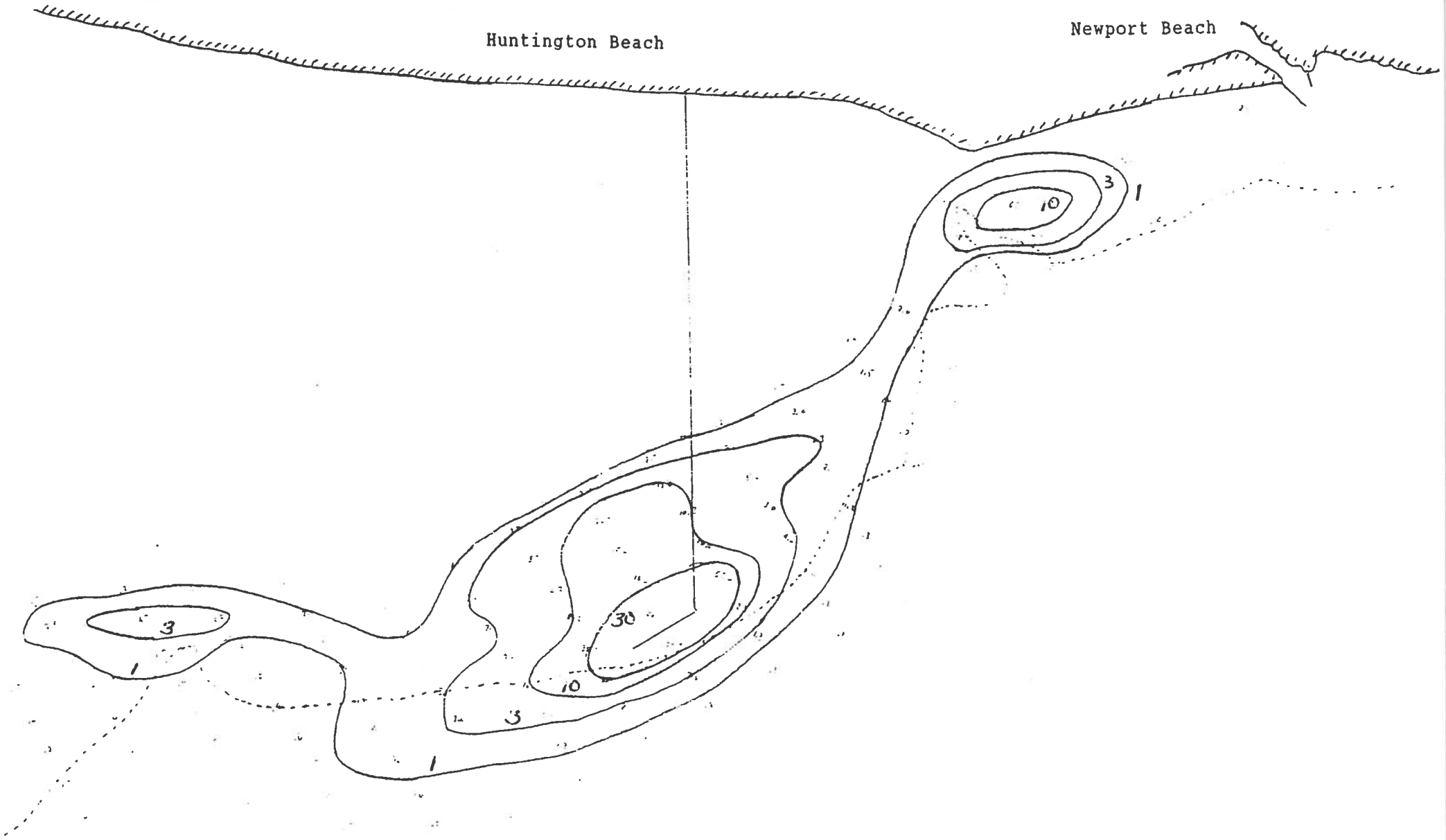

Figure 15. Predicted sedimentation rates for the Orange County outfall.

Contours in mg/cm^2/yr; mass emission rate = 33,000 m-tons/yr.

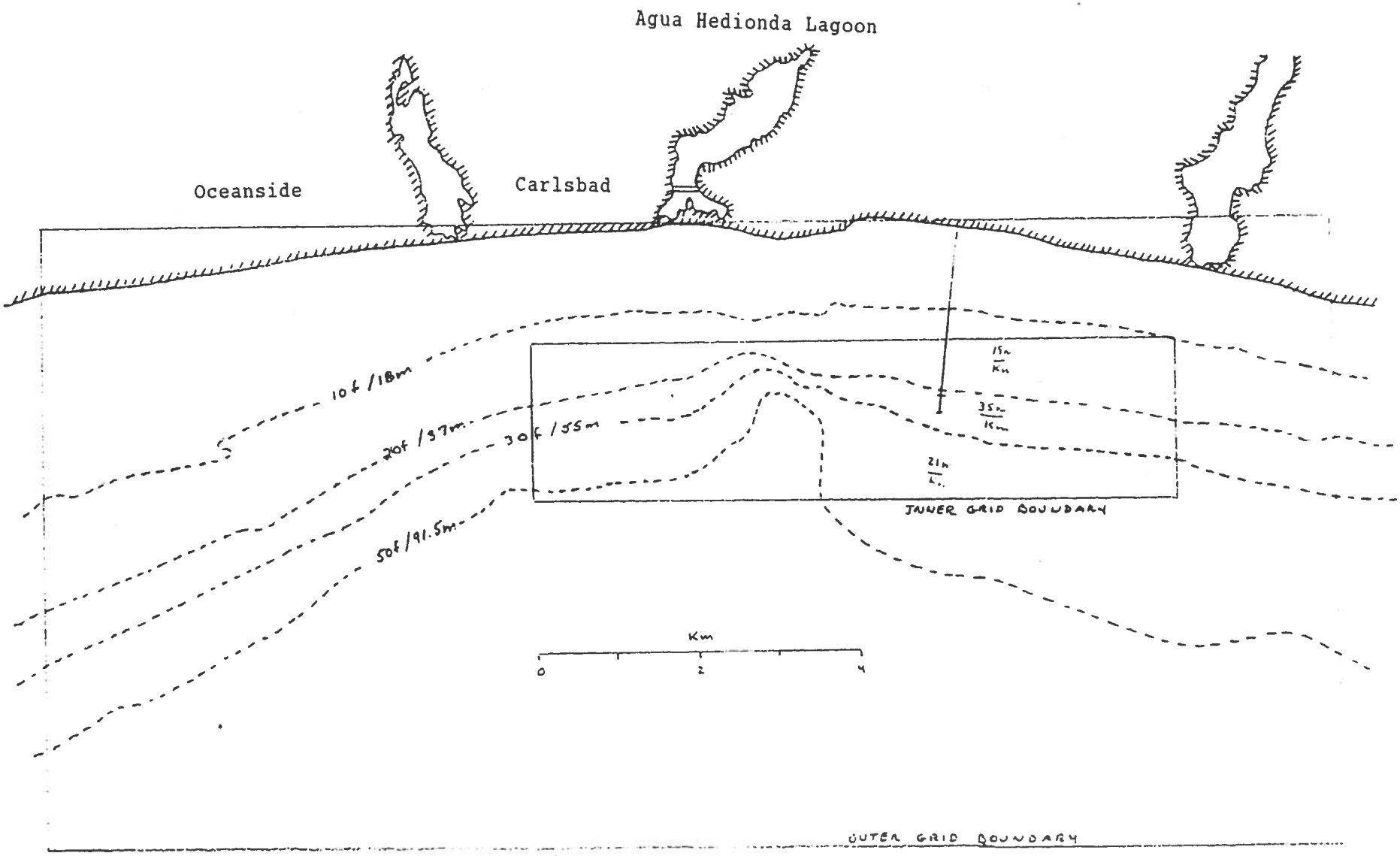

Figure 16. Encina outfall area.

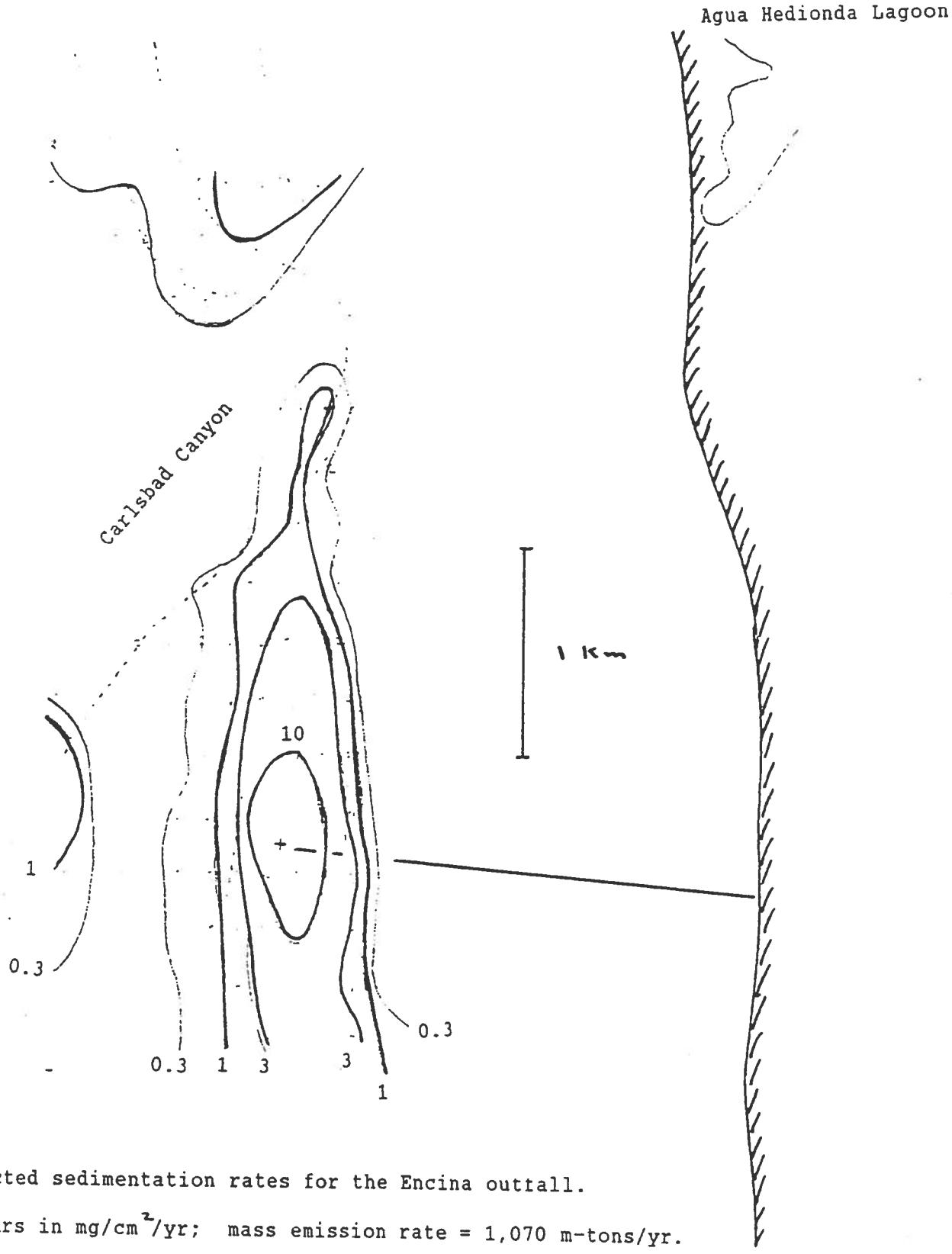

Figure 17. Predicted sedimentation rates for the Encina outfall.

Contours in mg/cm^2/yr; mass emission rate = 1,070 m-tons/yr.

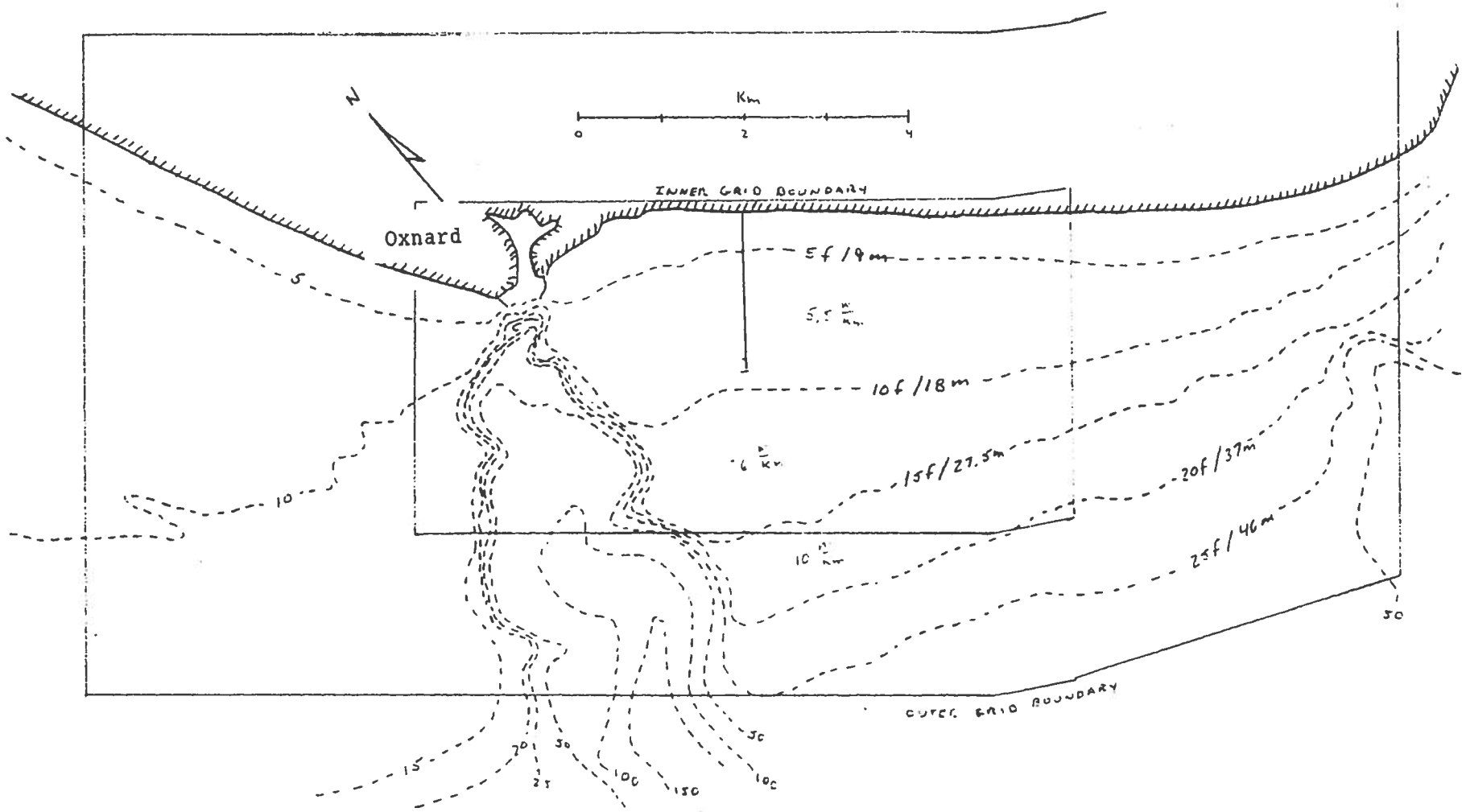

Figure 18. Oxnard outfall area.

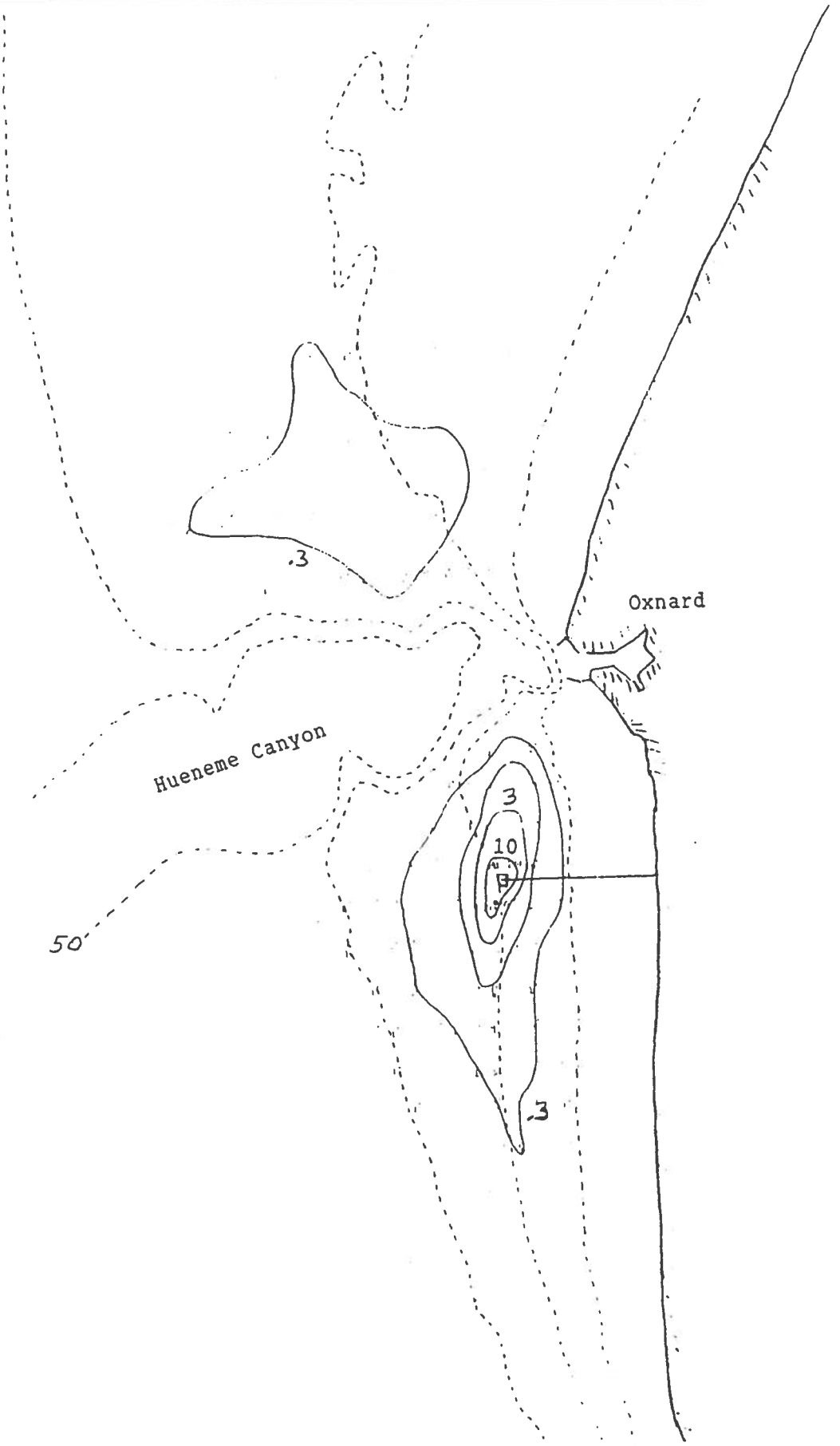

ure 19. Predicted sedimentation rates for the Oxnard outfall.

Contours in mg/cm^2/yr; mass emission rate = 925 m-tons/yr.

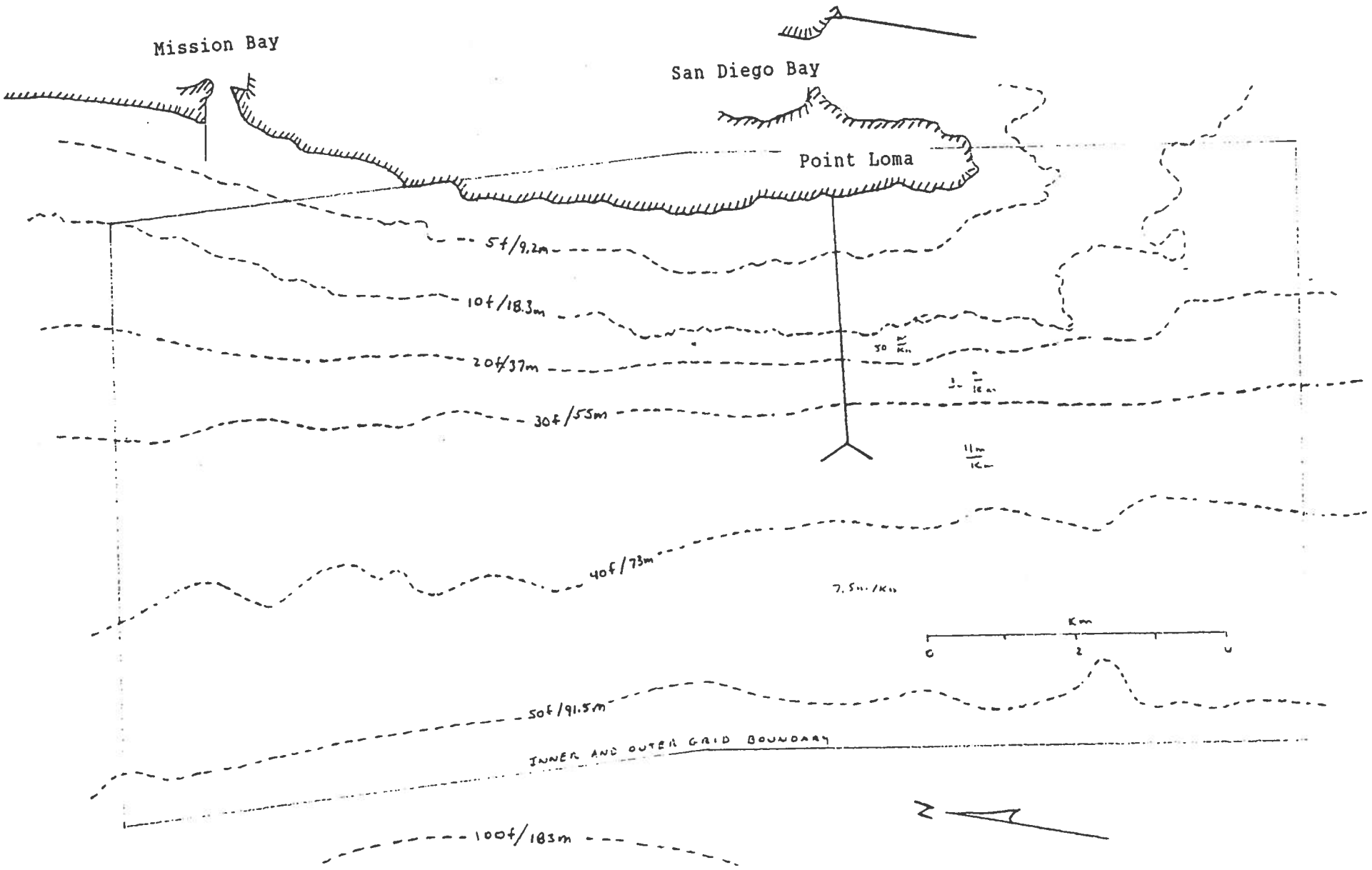

Figure 20. San Diego outfall area.

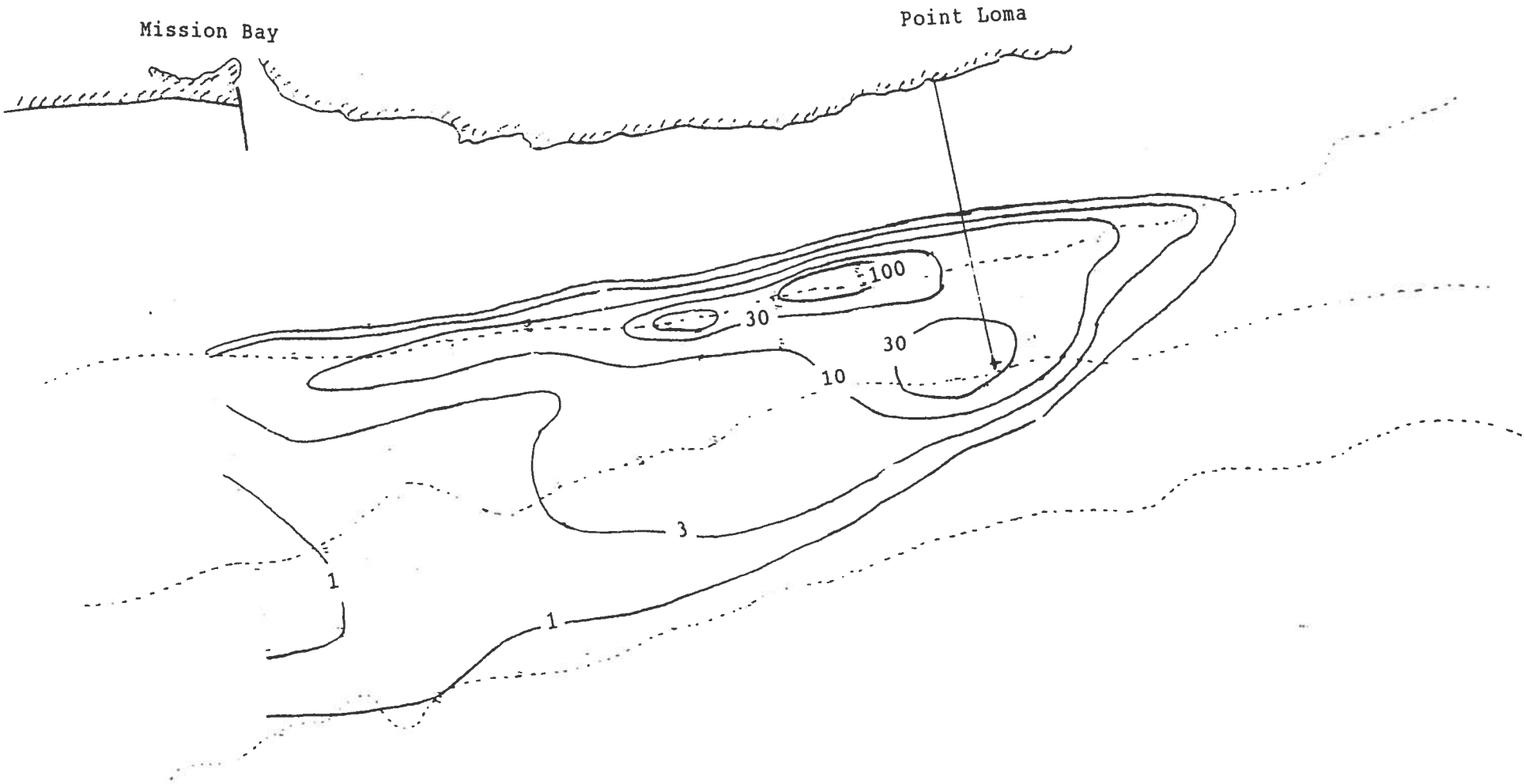

Figure 21. Predicted sedimentation rates for the San Diego outfall.

Contours in mg/cm^2/yr; mass emission rate = 17,600 m-tons/yr.
Currents for period from JD164 to JD226, 1985.

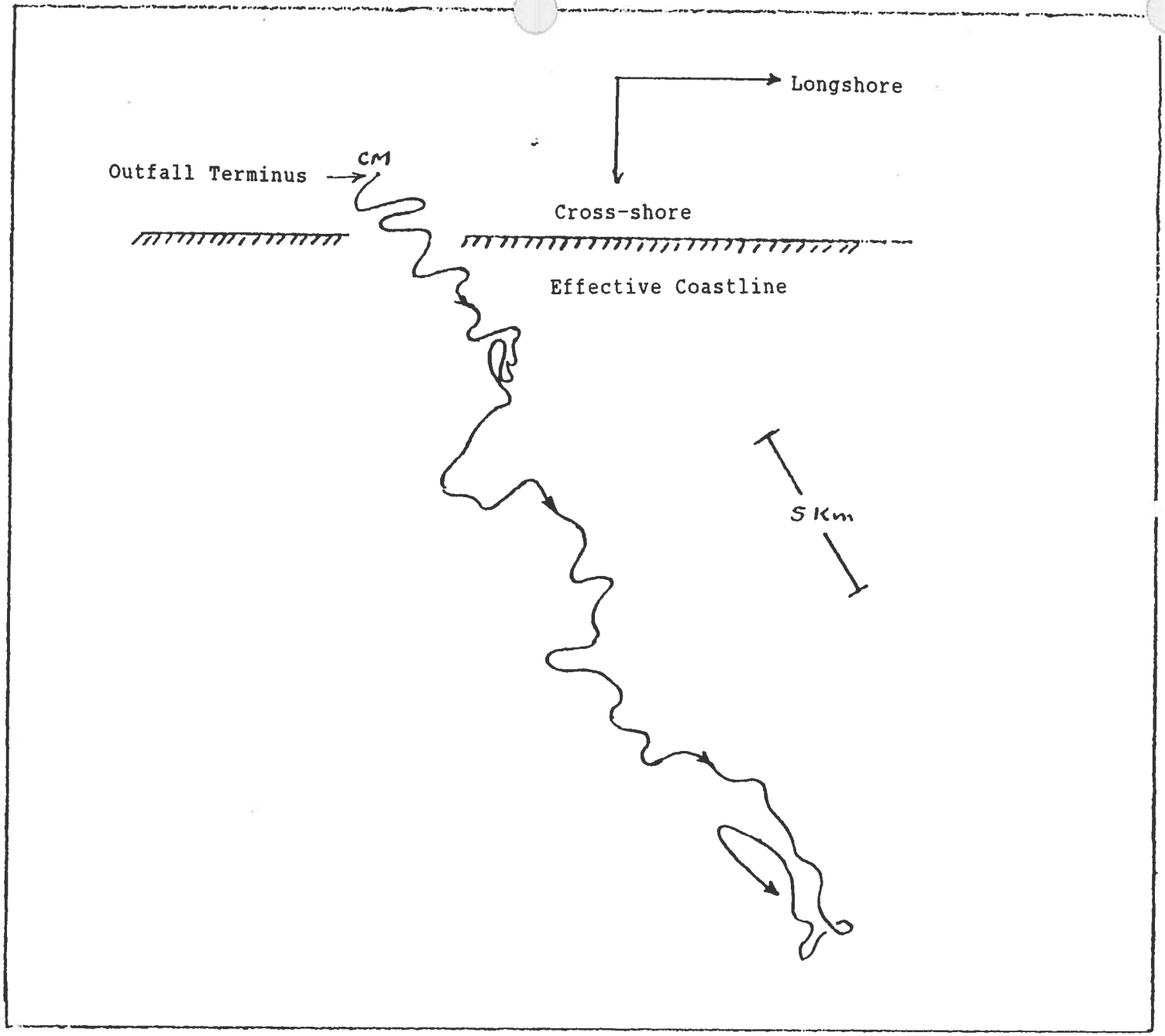

Figure 22. PVD for San Diego from JD 213 to JD 226,. 1985.

Meter depth = 40 m; water depth = 62 m. Shaded line indicates the approximate location of the "effective" coastline. The origin of the PVD represents the location of the outfall diffuser.

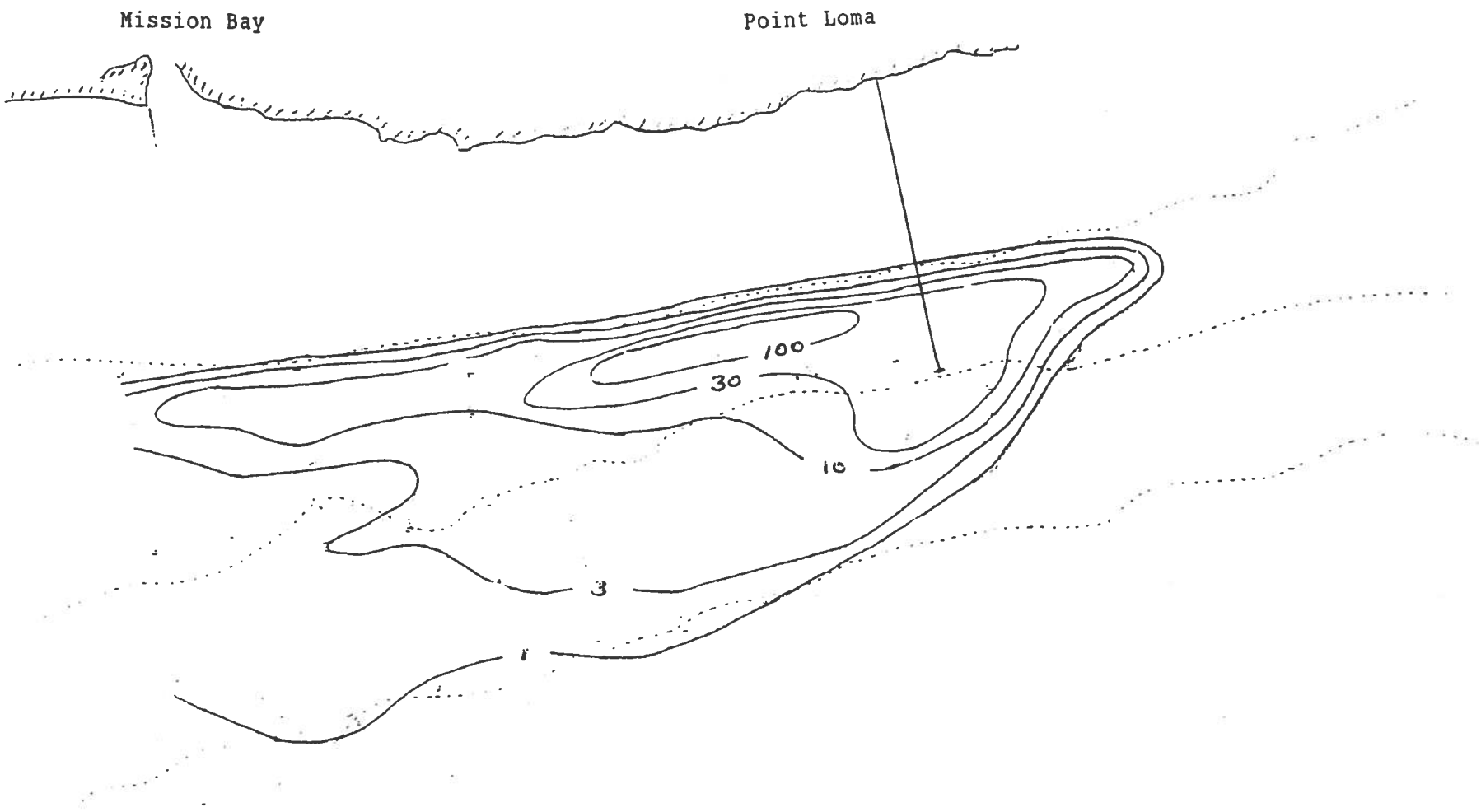

Figure 23. Predicted sedimentation rate for the San Diego outfall - JD 199->226.

Contours in mg/cm^2/yr, mass emission rate = 17,600 m-tons/yr.
Currents from JD 199 to JD 199 (1985) fail to fulfill assumptions implicit in SEDF2D.

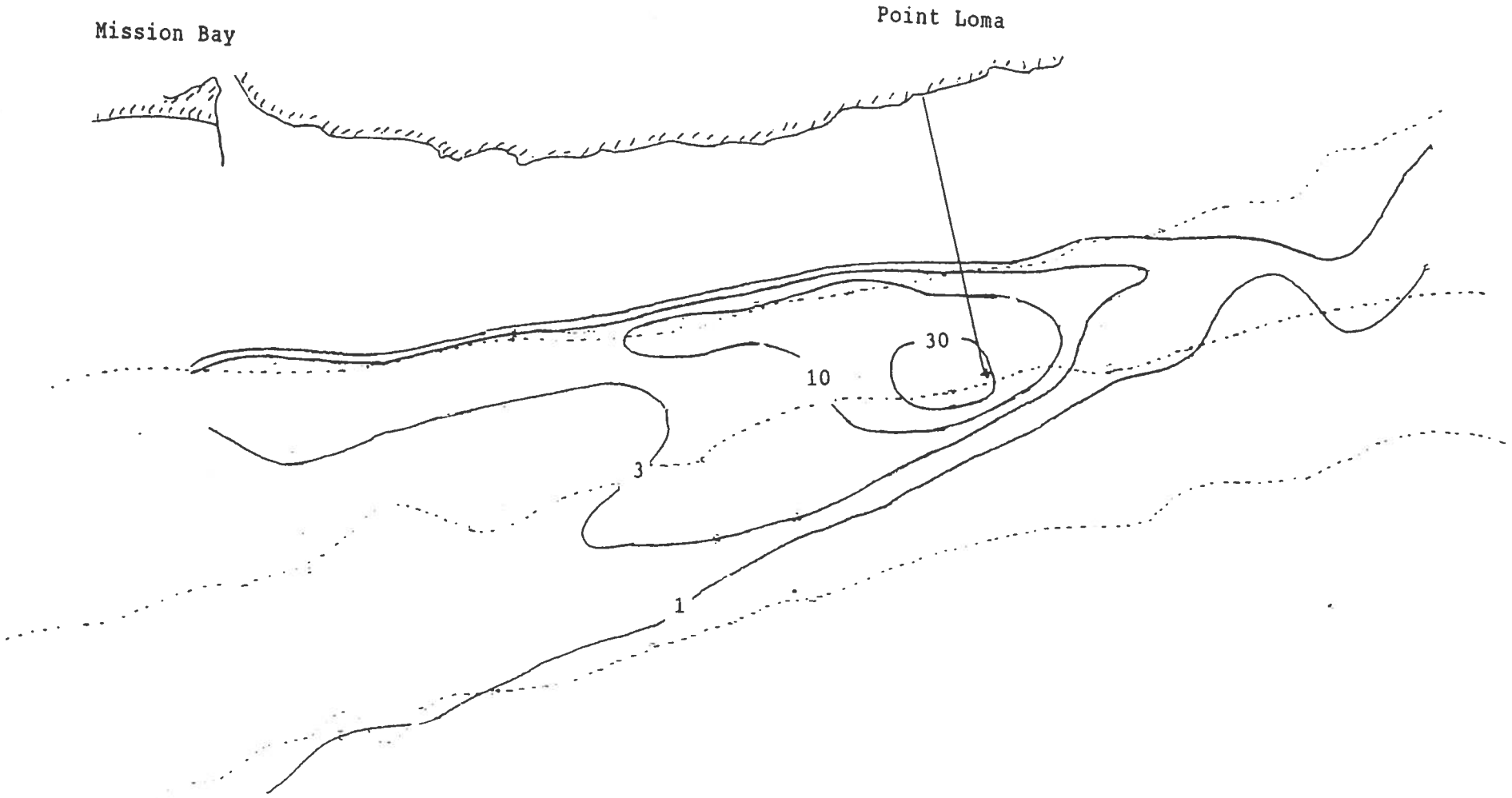

Figure 24. Predicted sedimentation rates for the San Diego outfall - JD164->199.
Contours in mg/cm^2/yr, mass emission rate = 17,600 m-tons/yr.
Currents from JD164 to JD199, 1985.

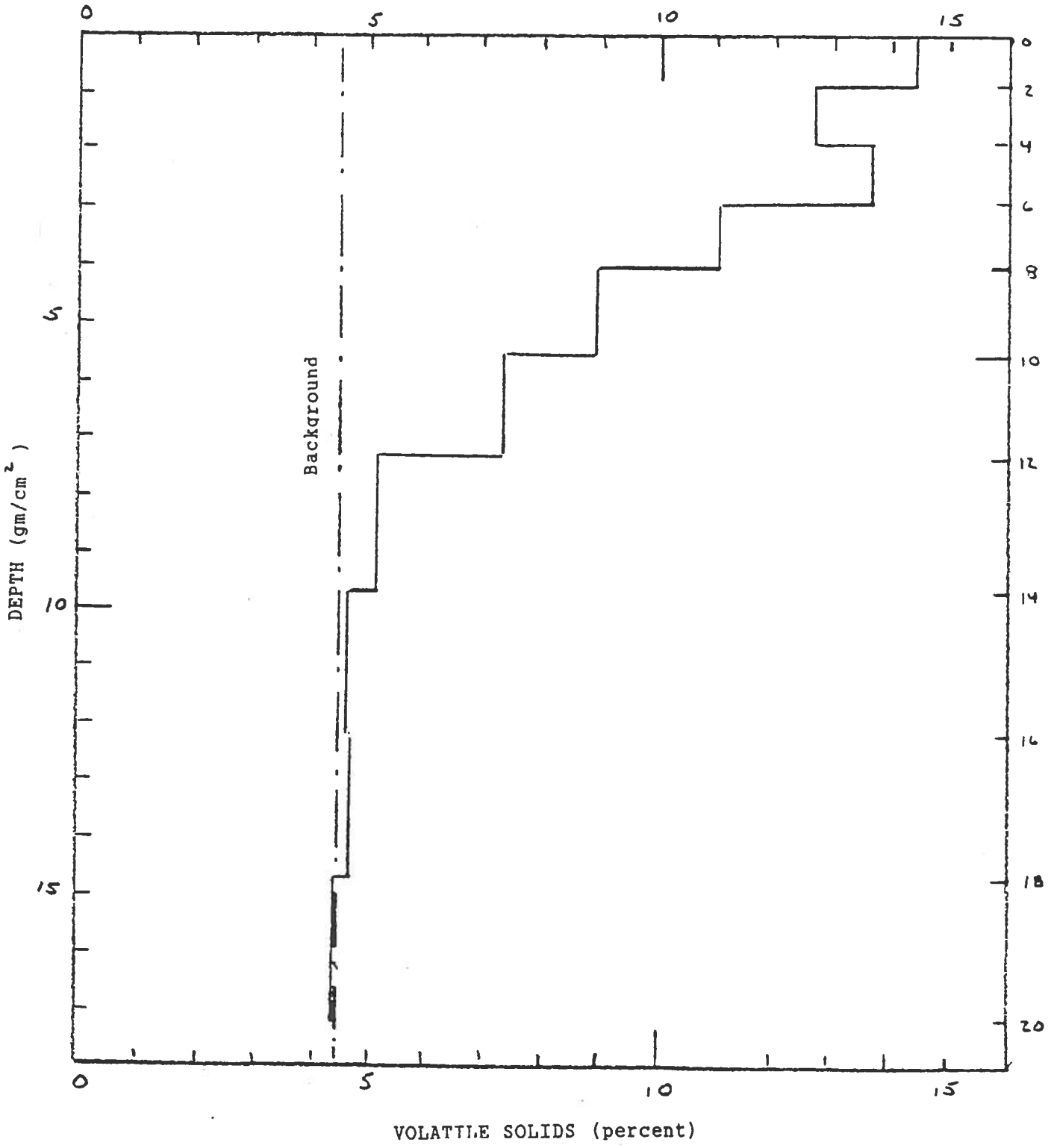

Figure 25. Profile of sediment volatile solids - Core 9C (White Point). Depth expressed in (dry) grams/cm^2.

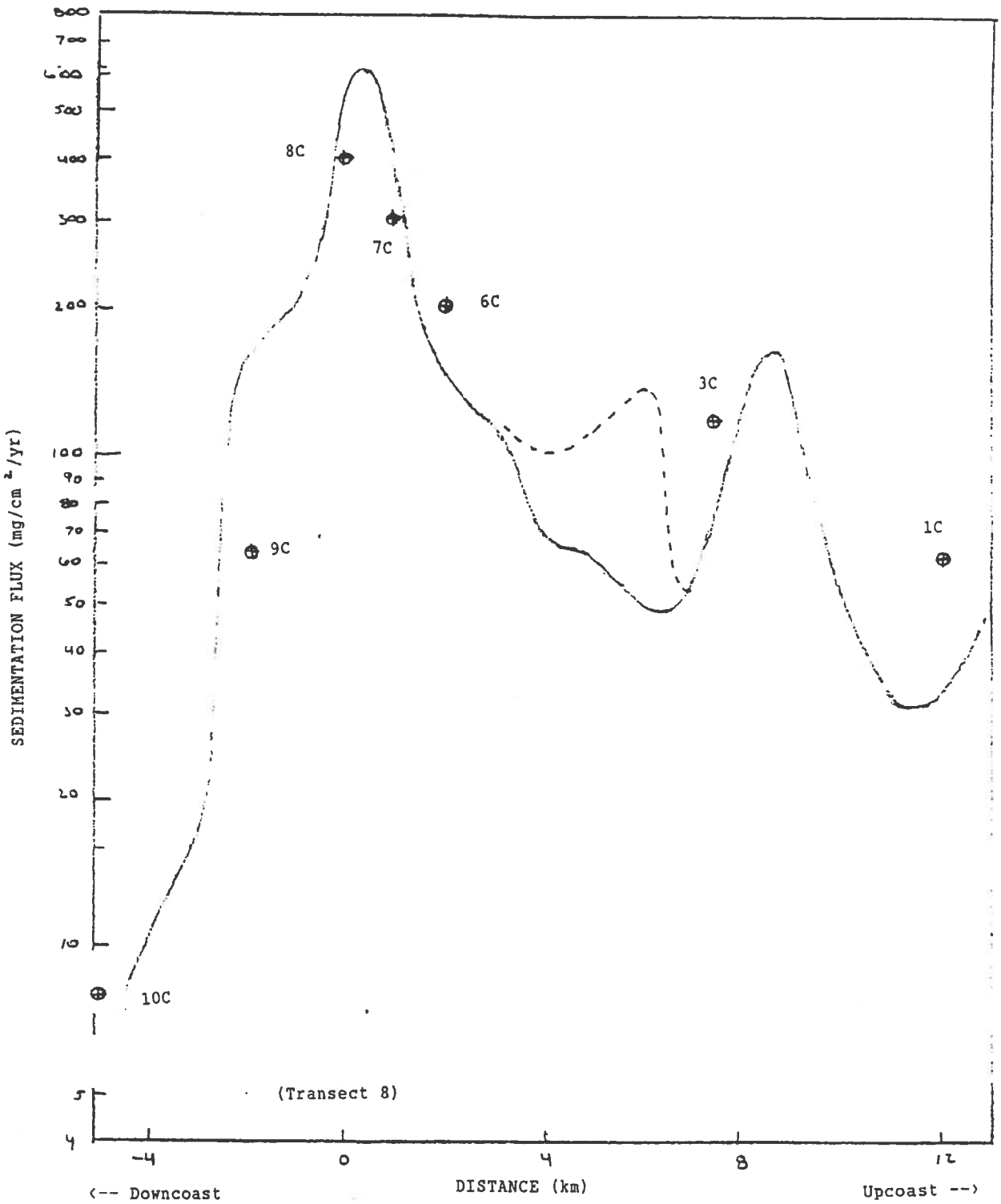

Figure 26. Sedimentation rate - 60 m isobath.

—— predicted rate ; - - - rate where maximum occurs inshore of the 60m isobath; ⊕ rate estimated from sediment cores.

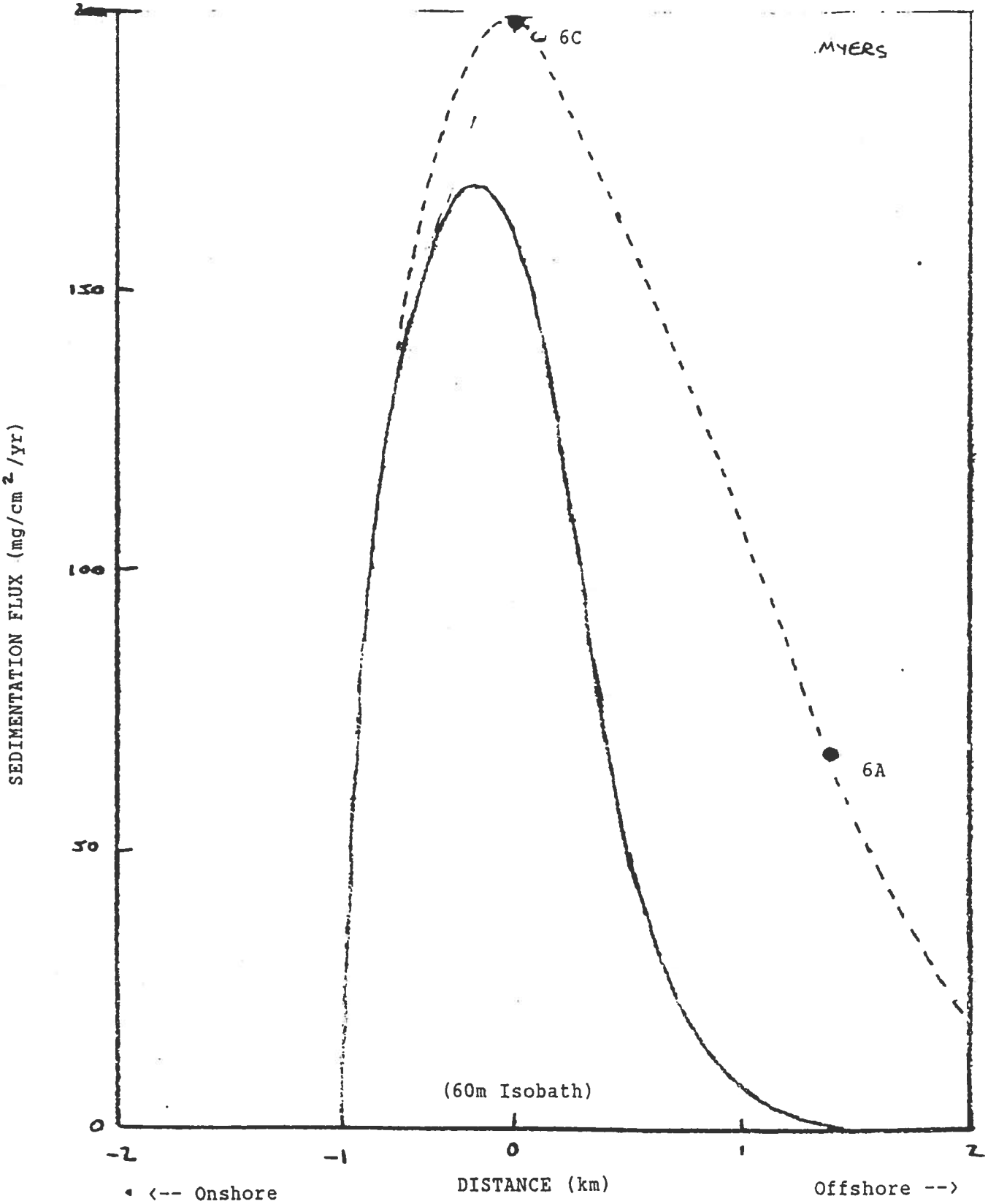

Figure 27. Predicted cross-shore sedimentation rates - Transect 6 (White Point)

—— predicted distribution; - - - estimated distribution (from cores)

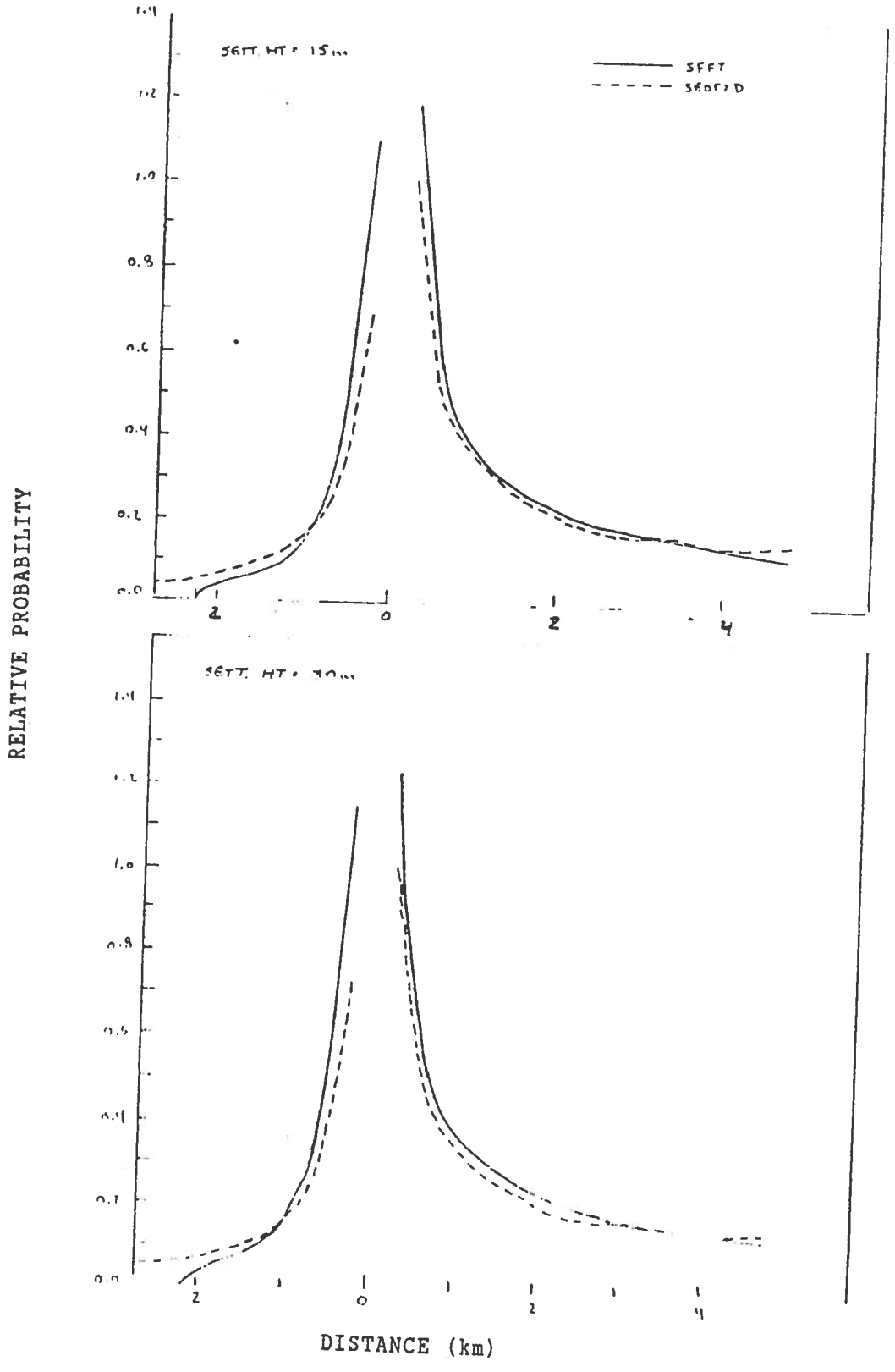

Figure 28. Comparison of longshore sedimentation distributions predicted by SFFT and SEDF2D.

Rates integrated along cross-shore transects and normalized to the maximum value (for a cell) in SFFT.

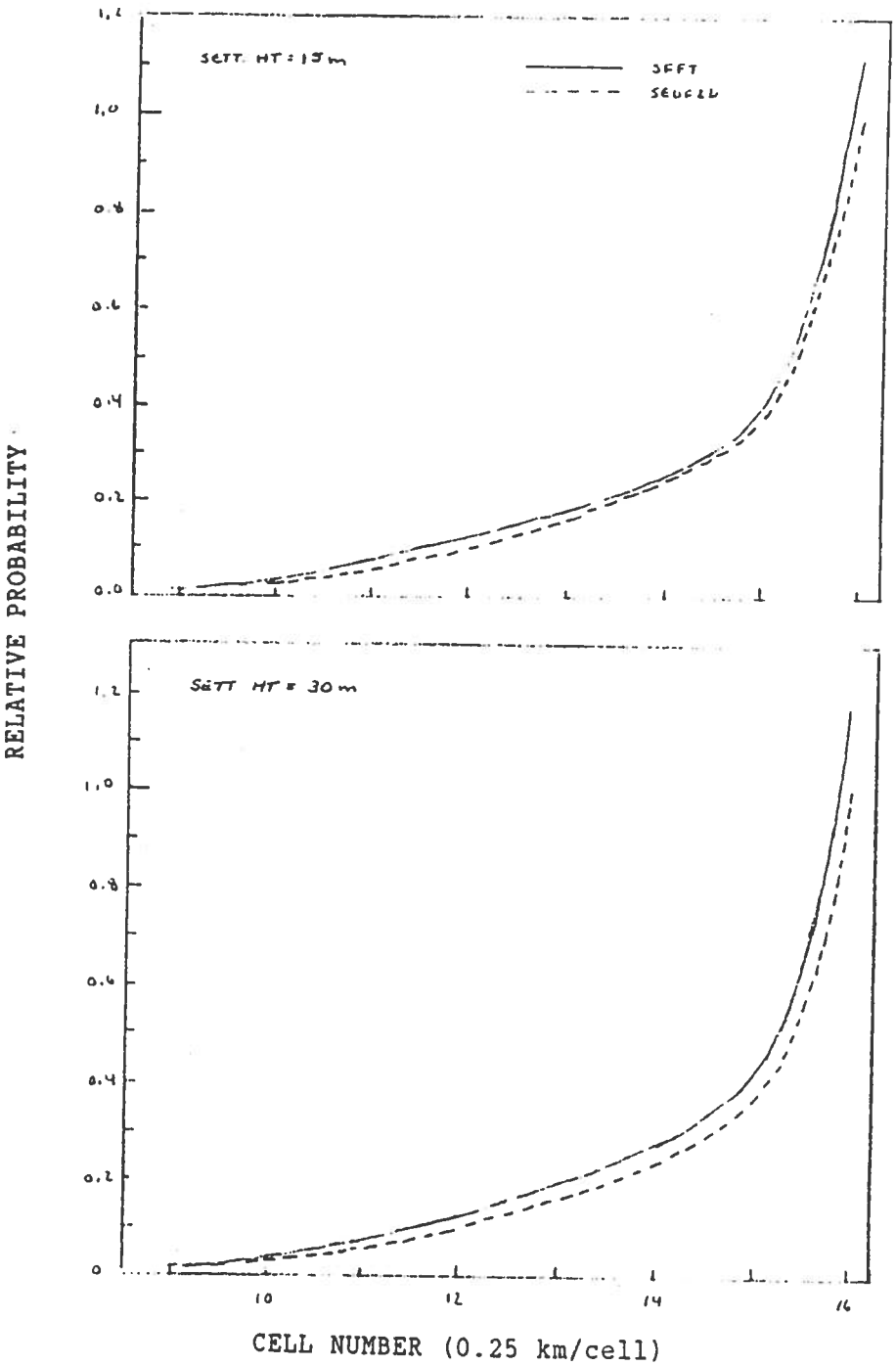

Figure 29. Comparison of cross-shore sedimentation distributions predicted by SFFT and SEDF2D.

Rates integrated along longshore transects and normalized to the maximum value (for a cell) in SFFT.

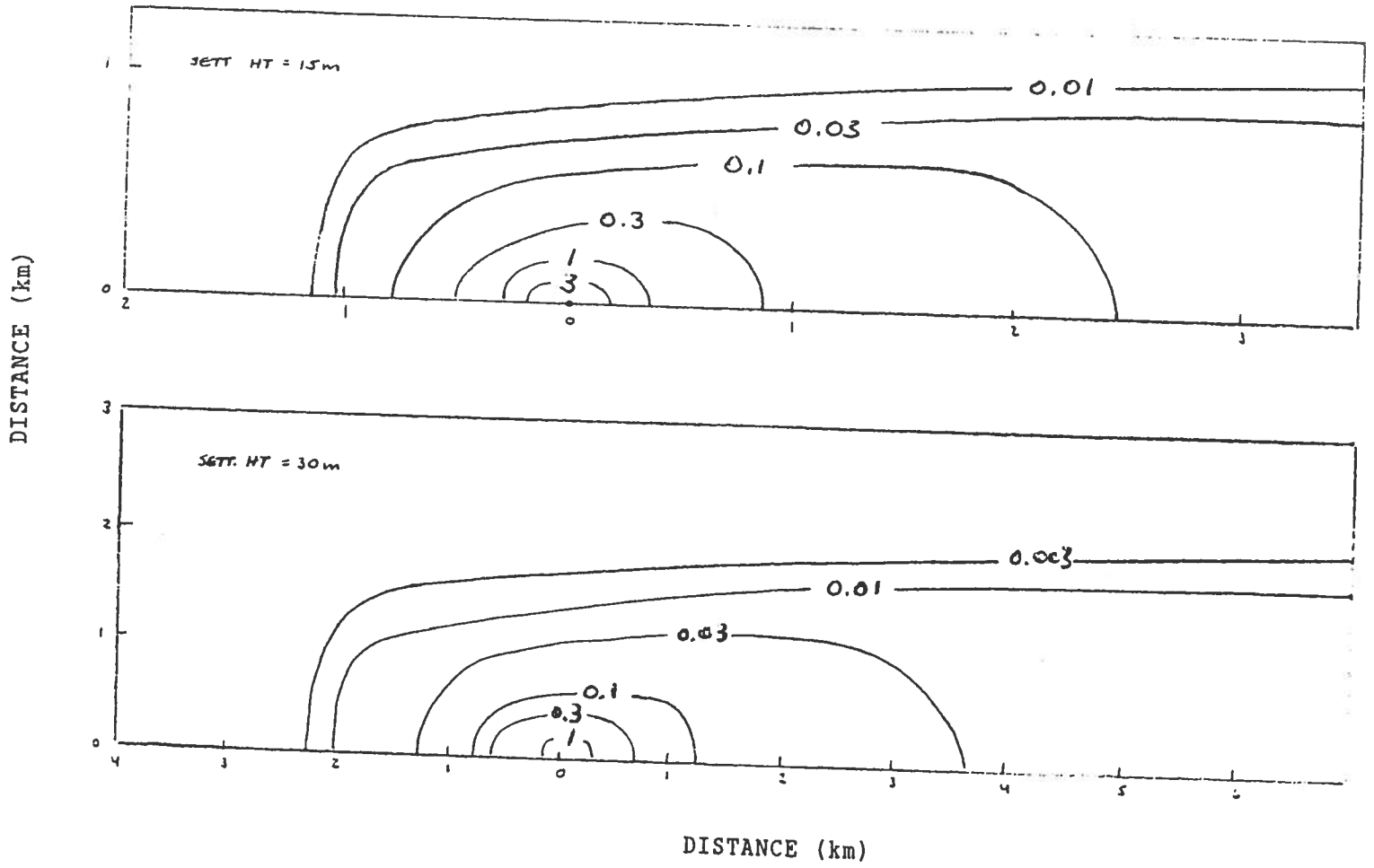

Figure 30. "Generic" sedimentation pattern.

Values are the fraction of the discharged mass (in percent) deposited in a cell 0.5 km long by 0.25 km wide. Multiply this fraction by 8 times the mass emission rate (in units of 1000 metric-tons/year or suspended solids) to get the corresponding sedimentation rates in mg/cm**2/yr.

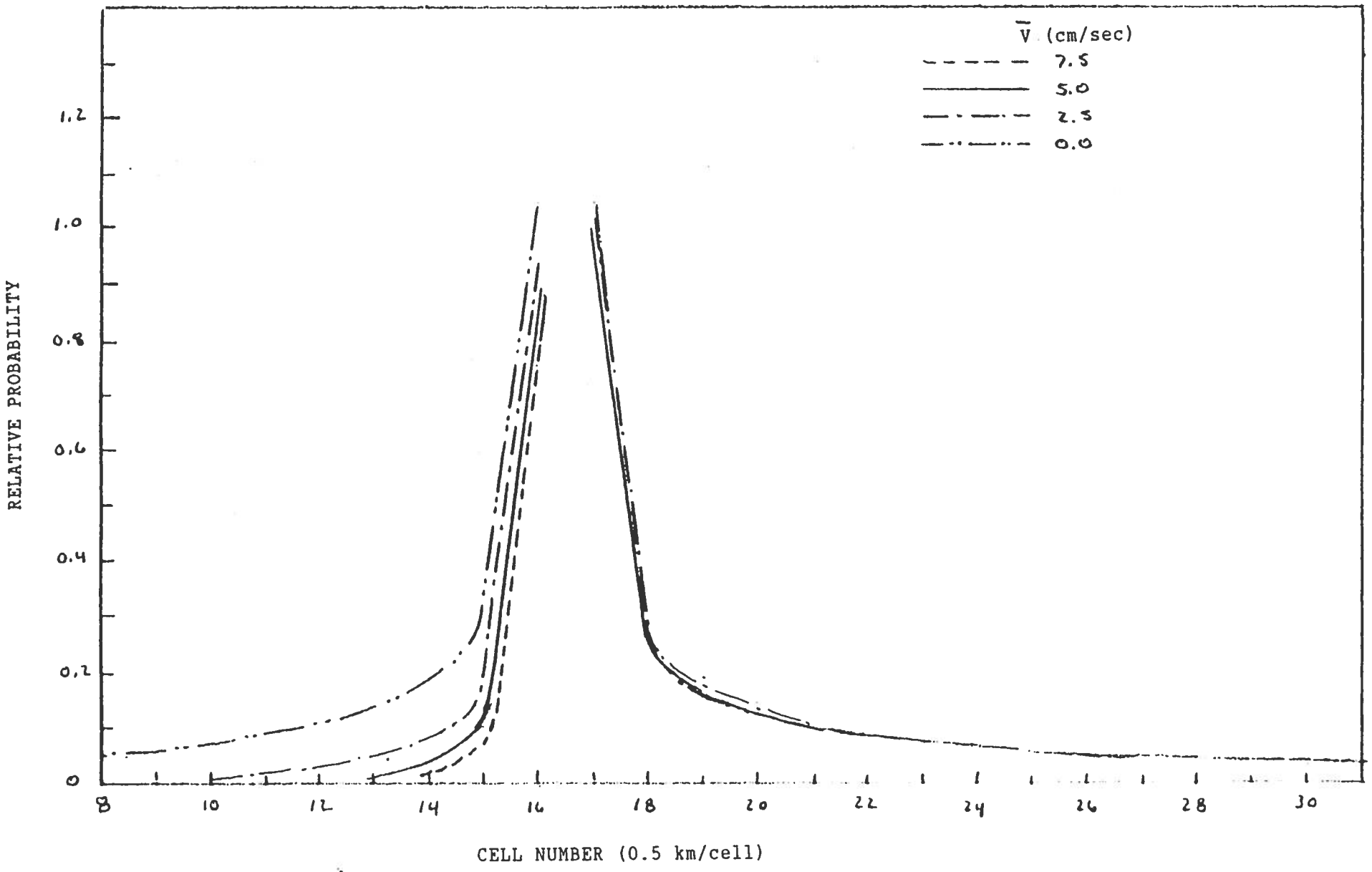

Figure 31. Longshore distribution dependence on net current speed (SFFT).

Current speeds in cm/sec; cell length = 0.50 km; values normalized to maximum cell value for a net current speed of 5.0 cm/sec.

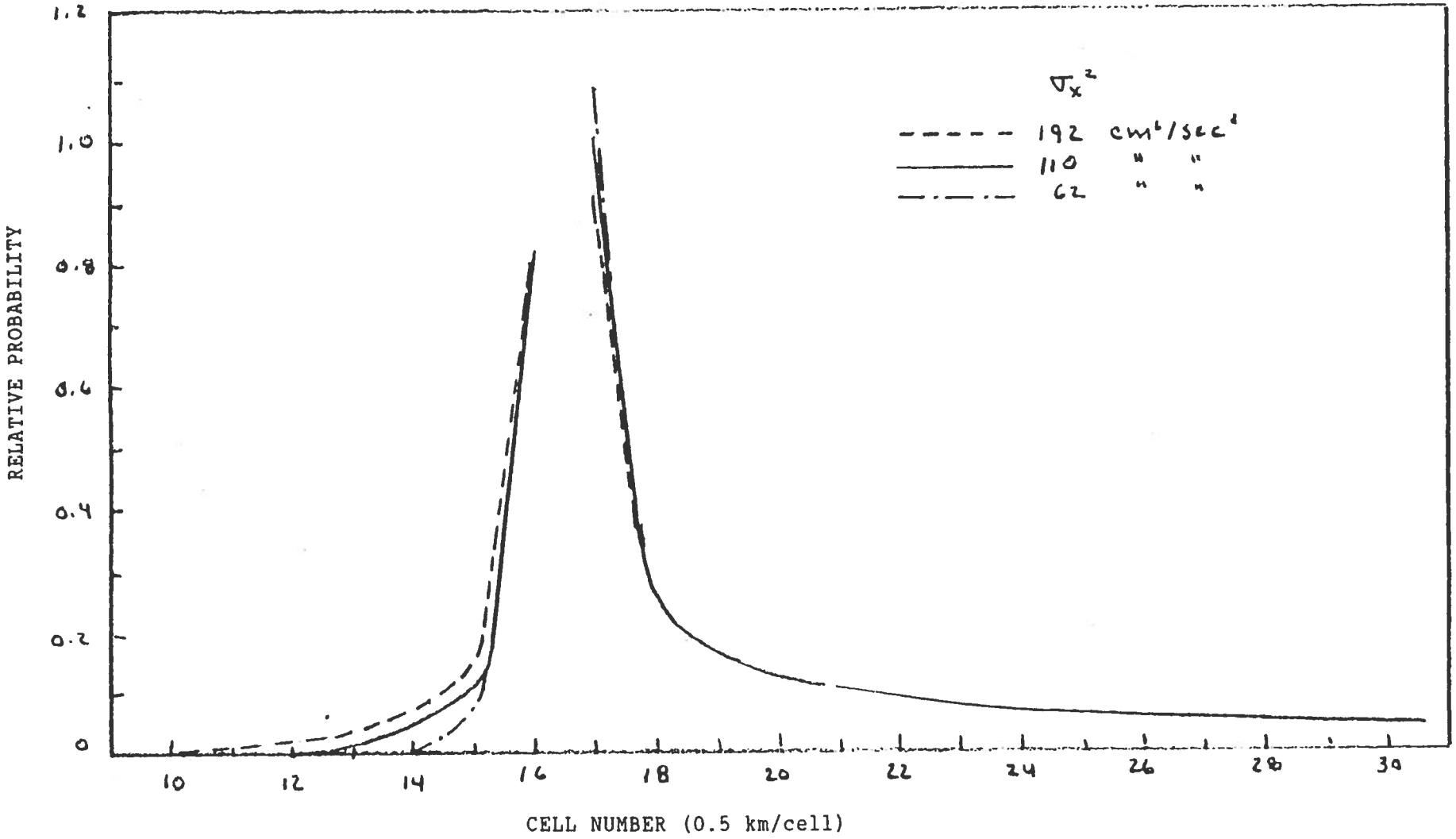

Figure 32. Longshore dependence on longshore variability in the currents (SFFT).

Probabilities normalized to maximum cell value for σ_x^2 = 110 cm²/sec², V = 5.0 cm/sec, H = 25 m. Cell length = 0.5 km.

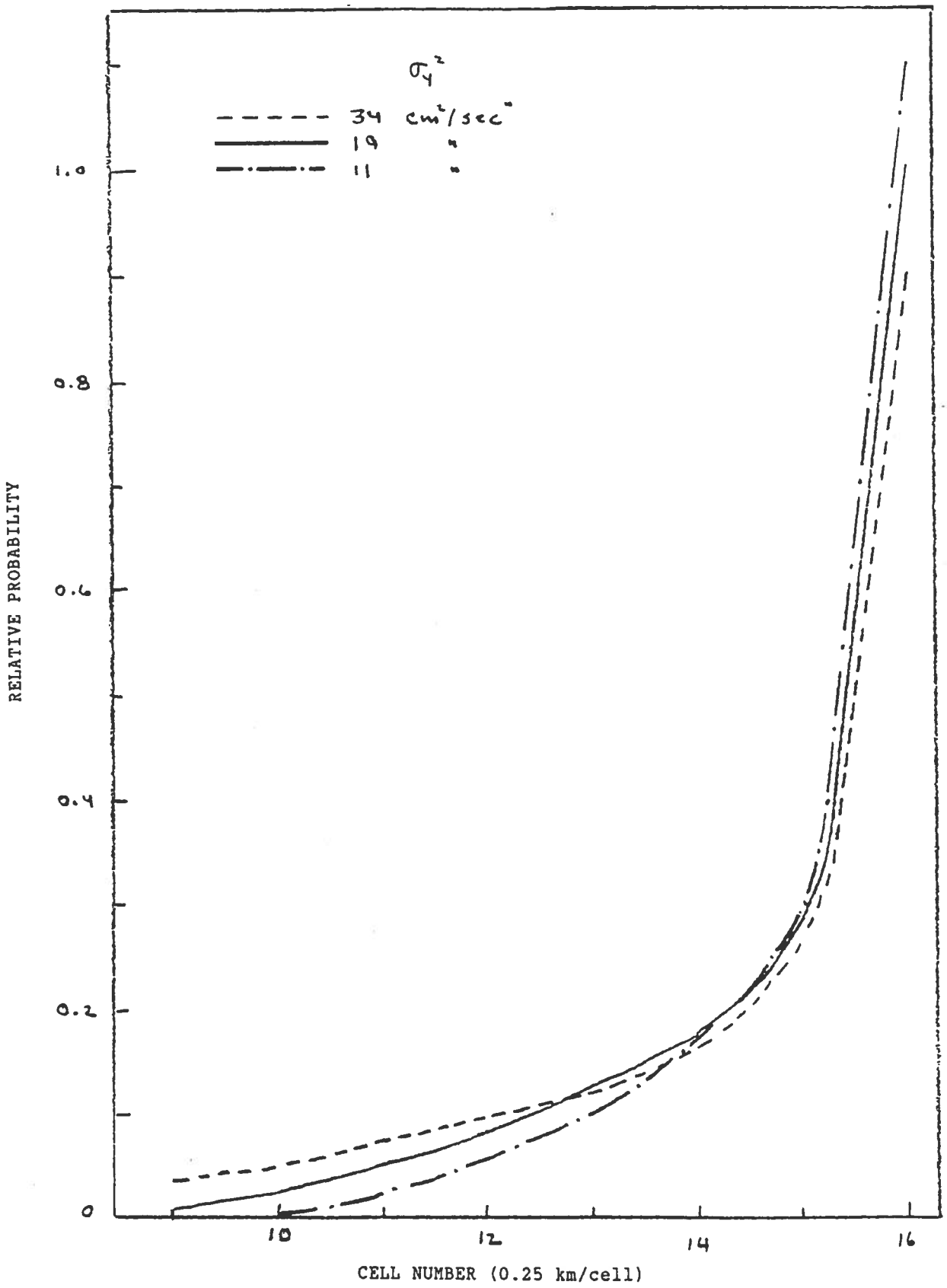

Figure 33. Cross-shore dependence on cross-shore variability in the currents (SFFT).

Probabilities normalized to maximum cell value for σ_y^2 = 19 cm²/sec², V = 5.0 cm/sec, H = 25m. Cell width = 0.25 km.

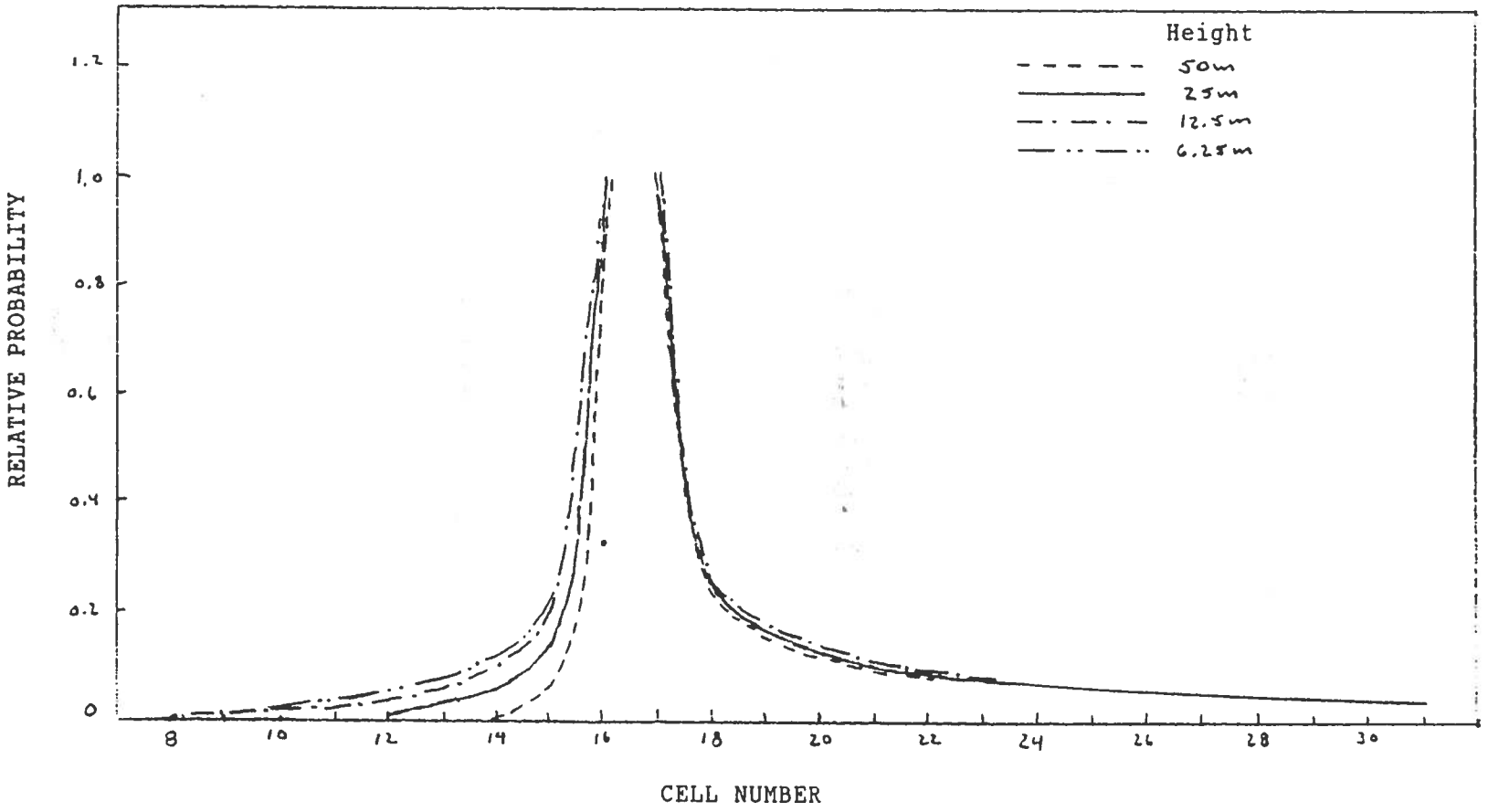

Figure 34. Longshore dependence on settling height (SFFT).

Probabilities normalized to maximum cell value for V = 5 cm/sec, σ_x^2 = 110 cm^2/sec^2, σ_y^2 = 19 cm^2/sec^2, H = 25 m. Cell length (km) = 0.02 times the settling height (in m).

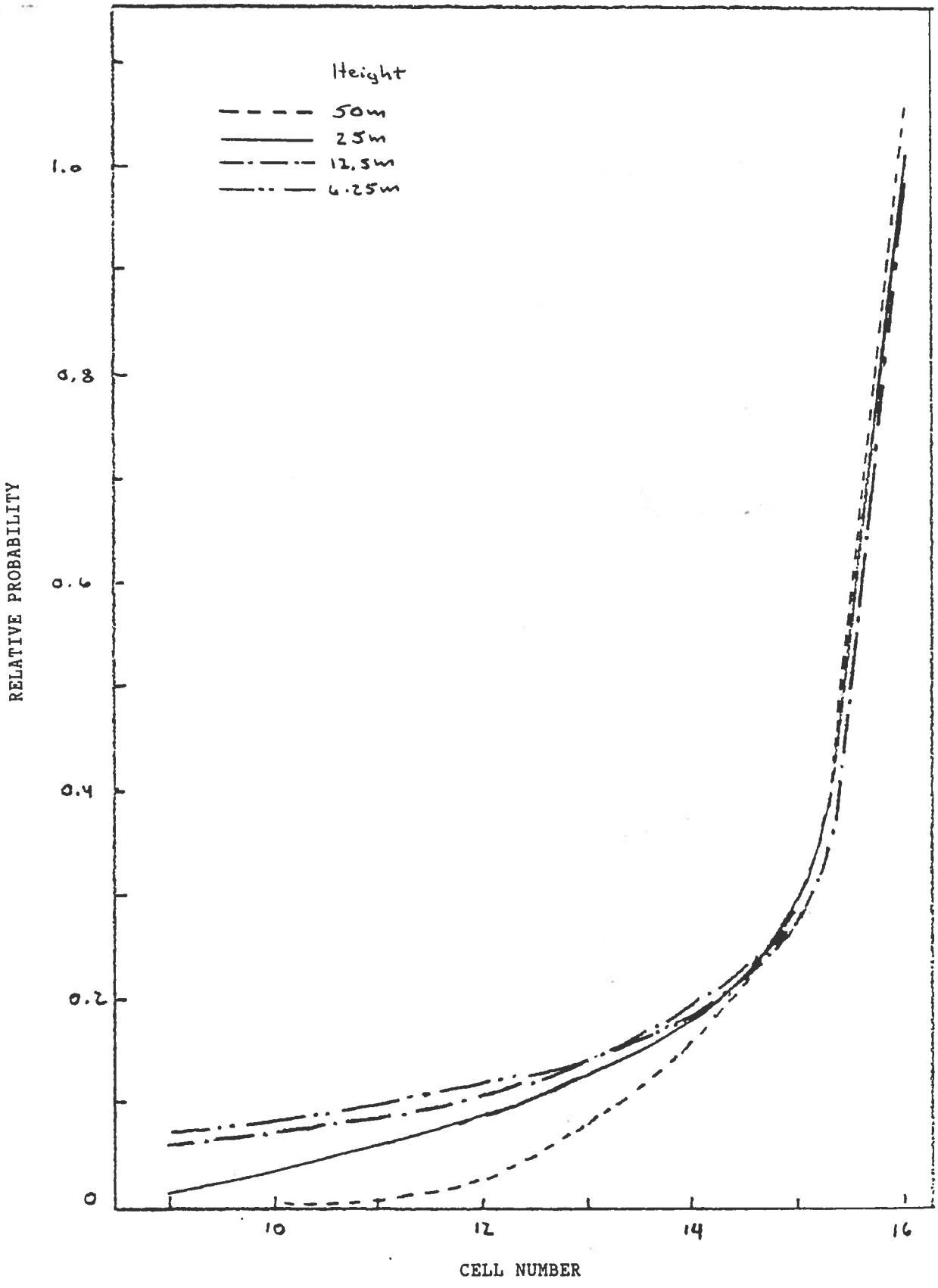

Figure 35. Cross-shore dependence on settling height (SFFT).

Probabilities normalized to maximum cell value for $\bar{V}$ = 5 cm/sec, σ_x^2 = 110 cm^2/sec^2, σ_y^2 = 19 cm^2/sec^2, H = 25m. Cell width (km) = 0.01 times the settling height (in m).

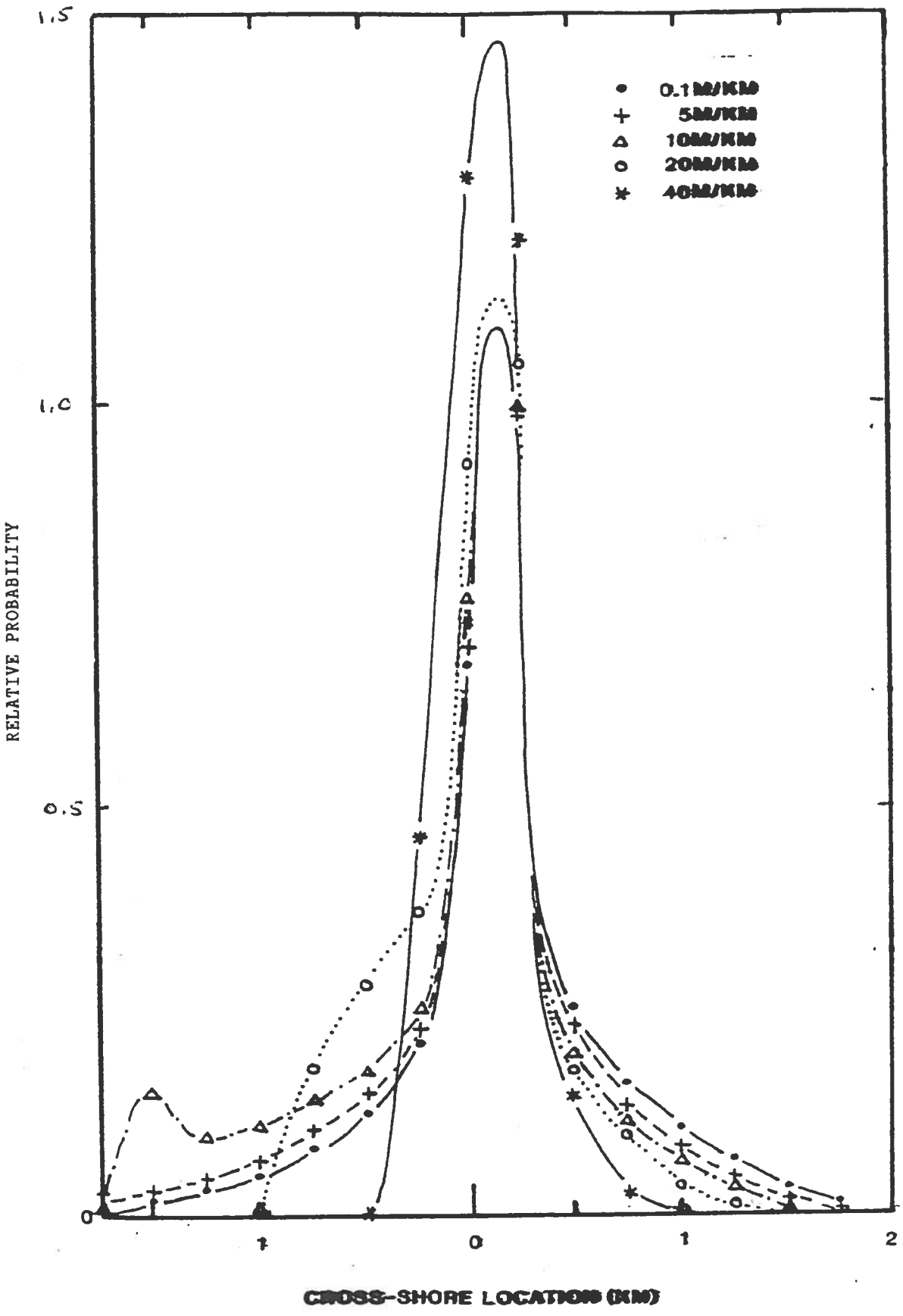

Figure 36. Cross-shore dependence on bottom slope.

Values normalized to maximum (cell) value for a slope of 0.1m/km.
Settling height = 25 meters.

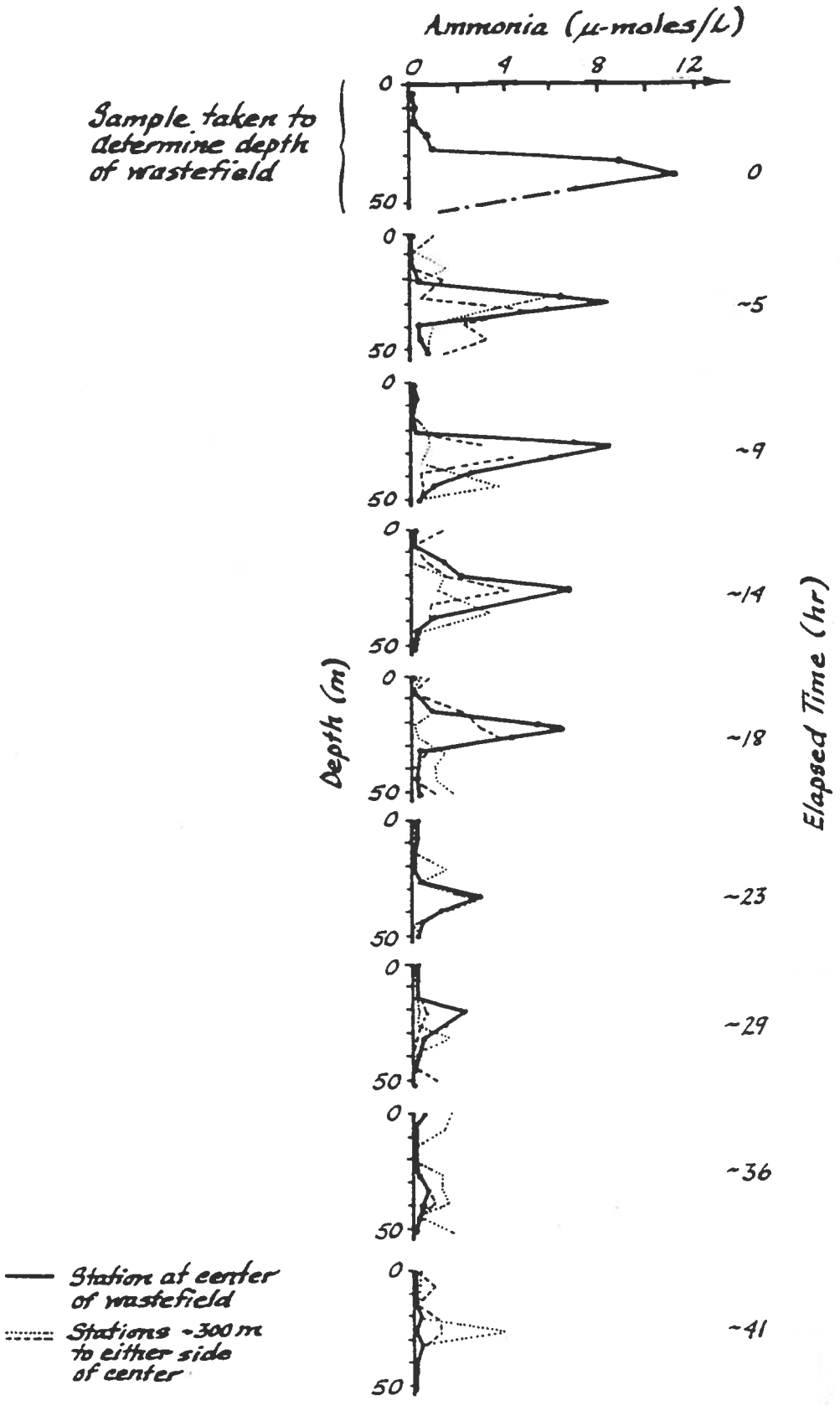

Figure 37. Wastefield Profile (ammonia concentration) - Point Loma, May 1972.

COAG – PARTICLE SETTLING SPEED MODEL

(ADAPTED TO OCEAN DISPOSAL CONDITIONS FROM FARLEY & MOREL, 1986)

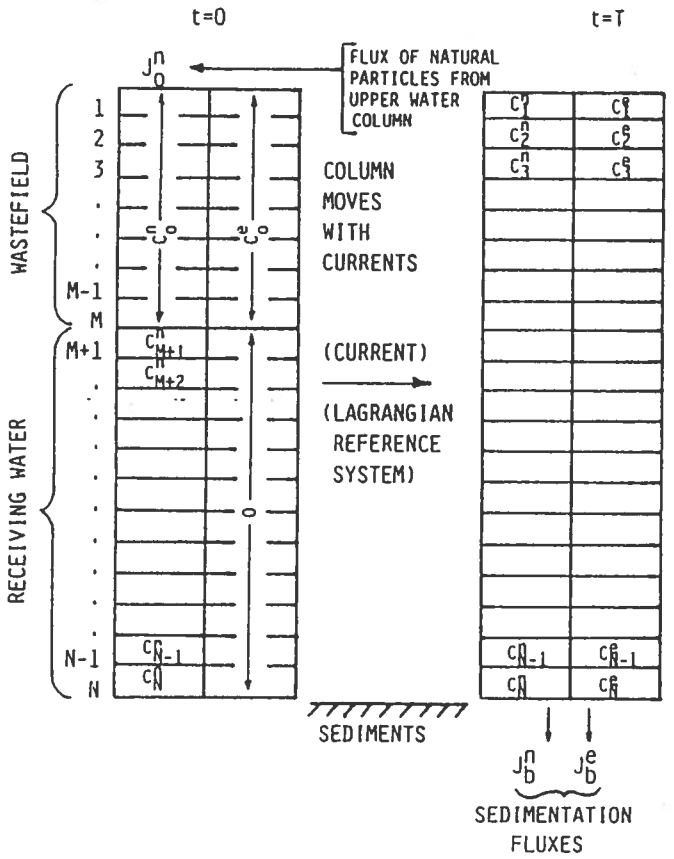

INITIAL CONDITIONS

NATURAL PARTICLES*

$$C_1^n \rightarrow C_M^0 = \frac{1}{N-M} \sum_{j=M+1}^{N} C_j^n \equiv C_0^n$$

EFFLUENT PARTICLES

$$C_1^e \rightarrow C_M^e = C_0^e$$

$$C_{M+1}^e \rightarrow C_N^e = 0$$

* $C_{M+1}^n \rightarrow C_N^n$ CONCENTRATIONS DETERMINED BY SIMULATING NO EFFLUENT PARTICLE CASE UNTIL STEADY STATE IS ACHIEVED. $C_1^n \rightarrow C_M^n$ REPRESENT ENTRAINMENT OF DILUTION WATER INTO THE PLUME.

RATE EQUATION

CHANGE IN MASS IN CELL "J" = - 1) MASS LOST TO CELL "J+1" BY SEDIMENTATION + 2) MASS INPUT BY SEDIMENTATION FROM CELL "J-1" - 3) MASS LOST DUE TO DECAY

1)
$$\left.\frac{\partial c_j^e}{\partial t}\right]_2 = -B_e^e c_j^{e\,2} - \left[\frac{c_j^e}{c_j^e + c_j^n}\right] 2B_e^n c_j^n c_j^e$$

$$\left.\frac{\partial c_j^n}{\partial t}\right]_2 = -B_n^n c_j^{n\,2} - \left[\frac{c_j^n}{c_j^n + c_j^e}\right] 2B_n^e c_j^e c_j^n$$

WHERE: $B_e^n = B_e^n$

(SEE REF. FOR DEFINITION OF "B" COEFFICIENTS)

2)
$$\left.\frac{\partial c_j^e}{\partial t}\right]_1 = -\left.\frac{\partial c_{j-1}^e}{\partial t}\right]_2$$

$$\left.\frac{\partial c_j^n}{\partial t}\right]_1 = -\left.\frac{\partial c_{j-1}^n}{\partial t}\right]_2 \quad J \neq 1$$

$$\left.\frac{\partial c_1^e}{\partial t}\right]_1 = 0$$

$$\left.\frac{\partial c_1^n}{\partial t}\right]_1 = J_o^n$$

3)
$$\left.\frac{\partial c_j^e}{\partial t}\right]_3 = -\lambda_e c_j^e$$

$$\left.\frac{\partial c_j^e}{\partial t}\right]_3 = -\lambda_n c_j^n$$

Figure 38. Definition of COAG method and simulation grid.

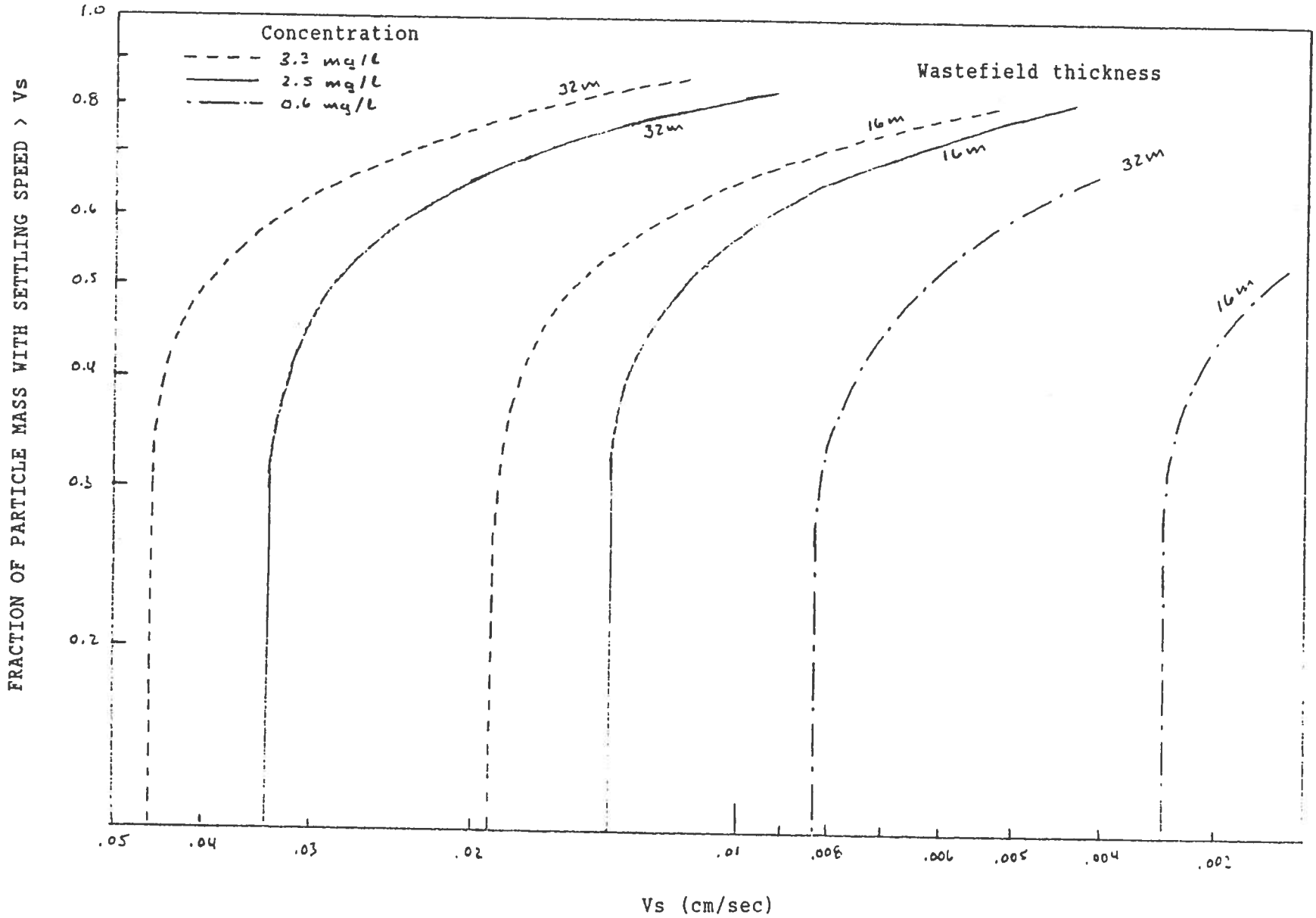

Figure 39. White Point settling speed distribution (COAG).

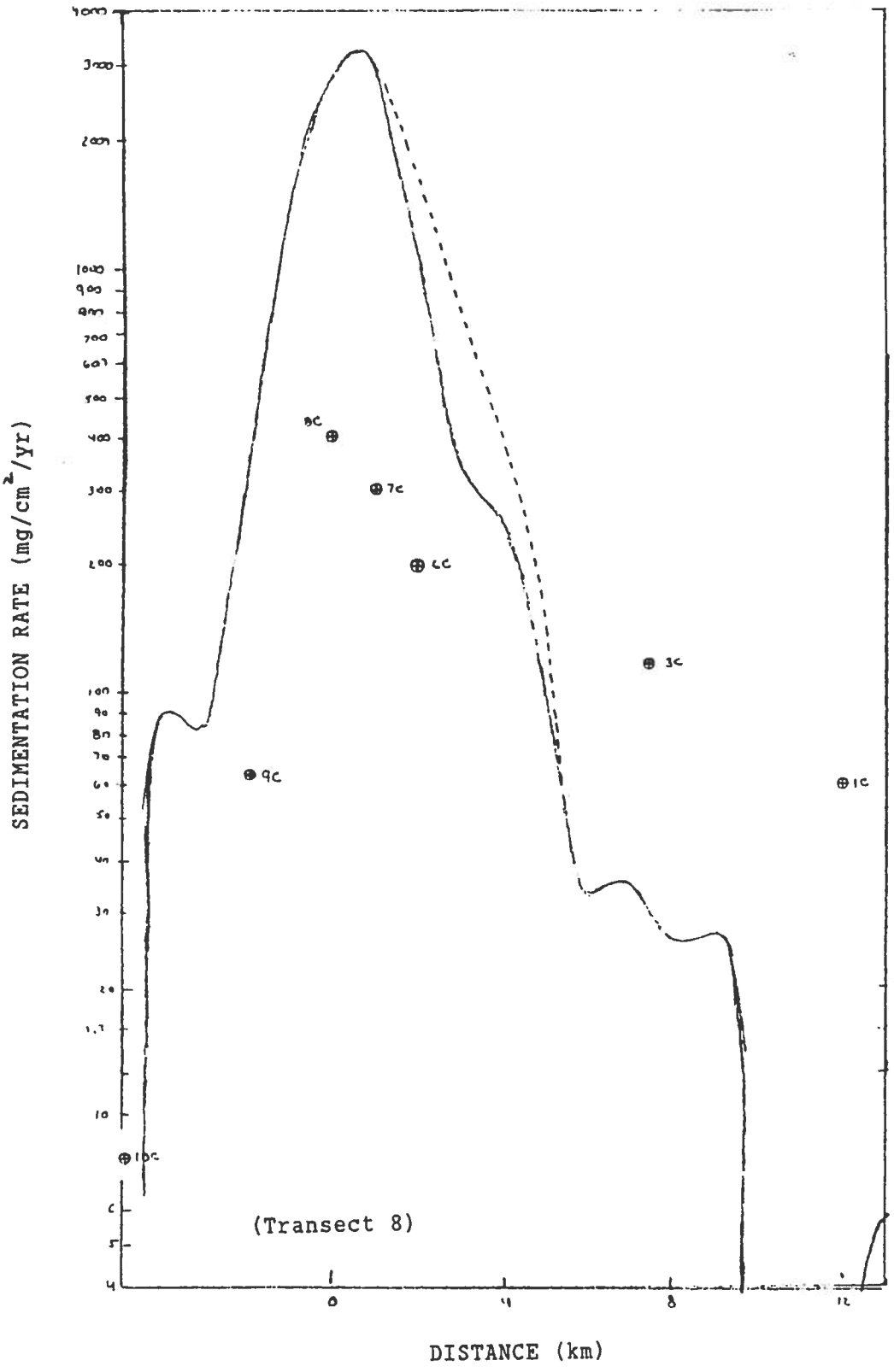

Figure 40. Longshore sedimentation distribution for 60m isobath - White Point.

COAG settling speed distribution for C=2.5 mg/l, H=32 m. —— indicates SEDF2D predicted distribution (60m isobath), - - - indicates predicted rate if inshore of 60m. ⊕ indicates rate estimated from cores.

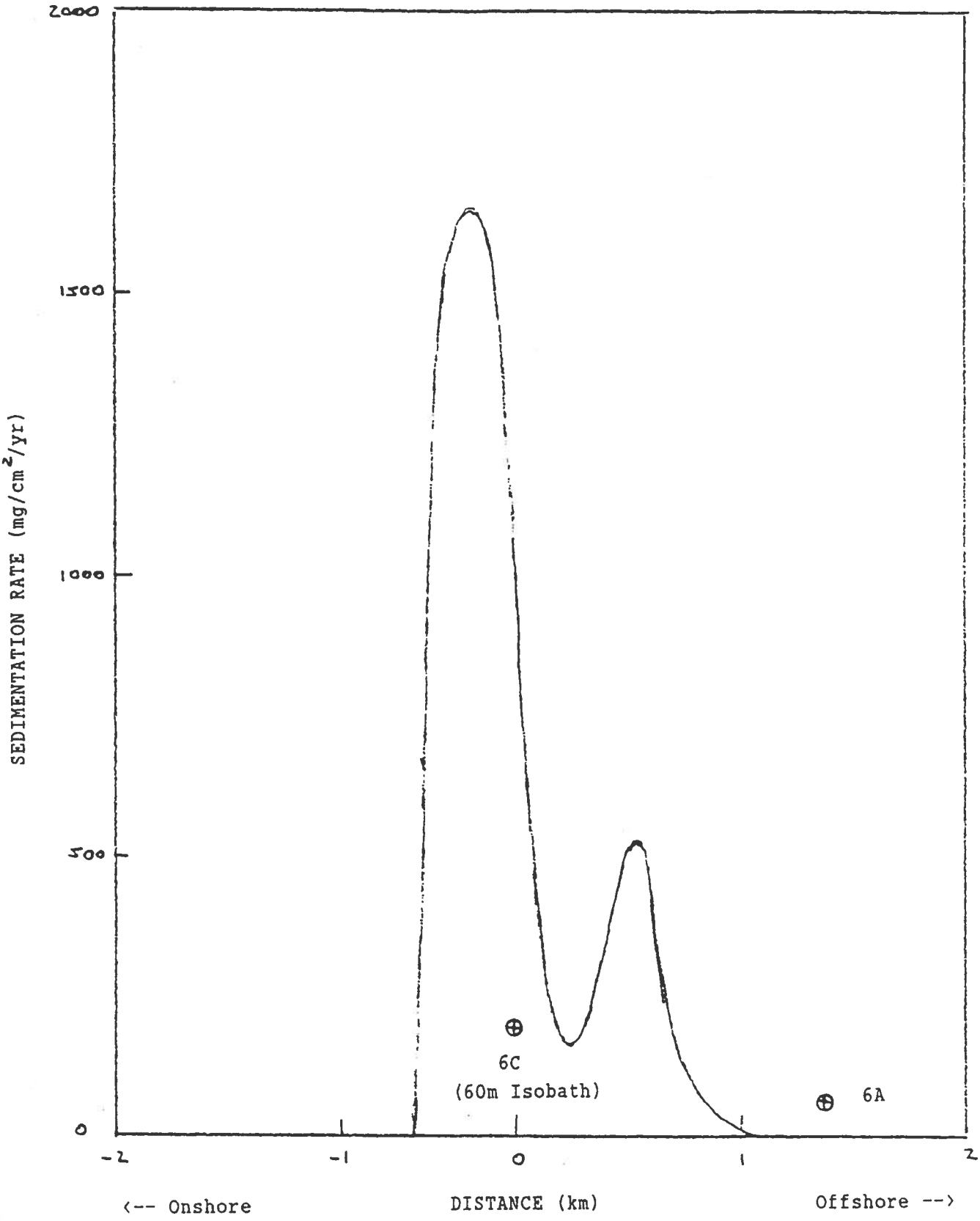

Figure 41. Cross-shore sedimentation distribution for Transect 6 - White Point.

COAG settling speed distribution for C=2.5 mg/l, H=32m. —— indicates SEDF2D predicted distribution (60m isobath), - - - indicates predicted rate if inshore of 60m. ⊕ indicates rate estimated from cores.

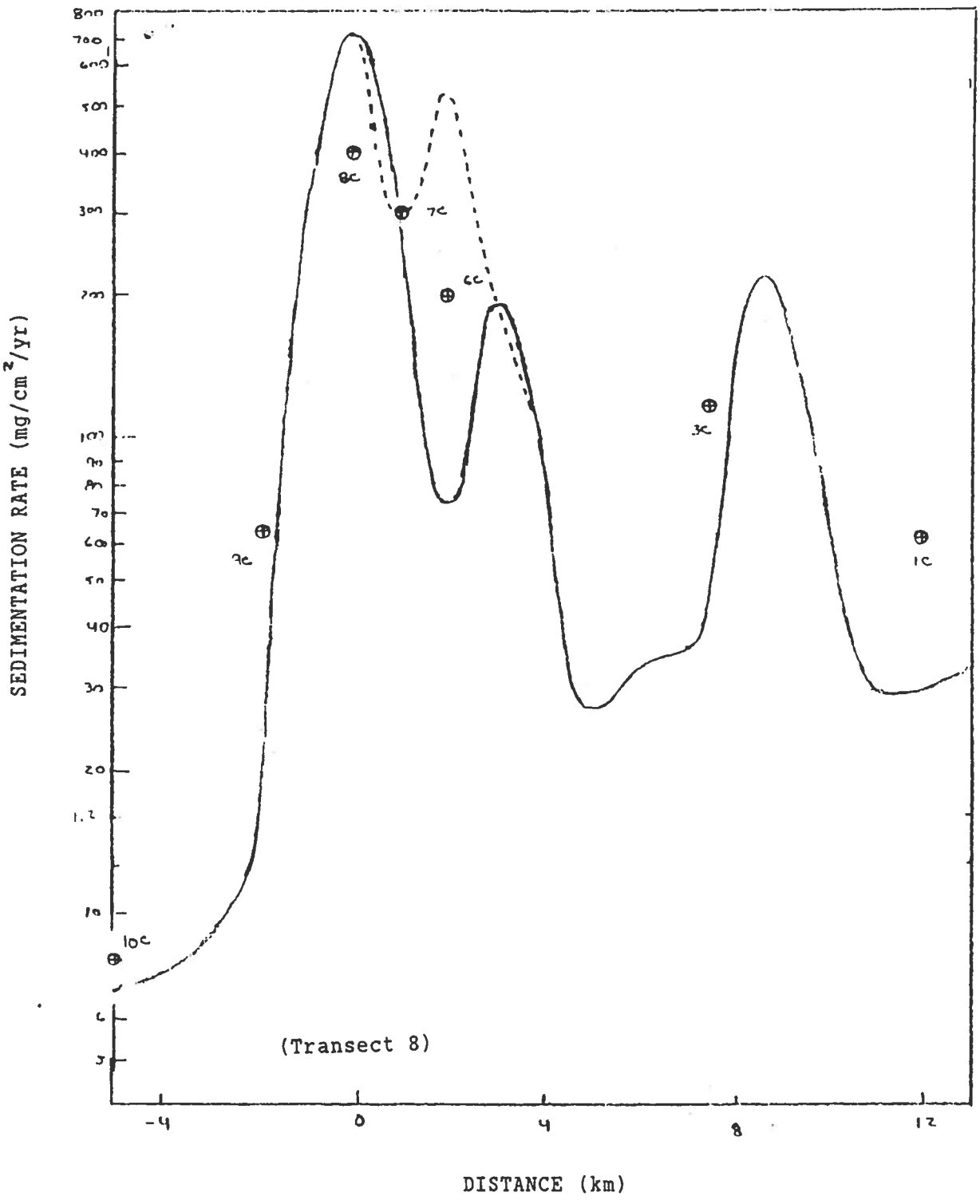

Figure 42. Longshore sedimentation distribution for 60m isobath - White Point.

COAG settling speed distribution for C=0.6 mg/l, H=32 m. —— indicates SEDF2D predicted distribution (60m isobath), - - - indicates predicted rate if inshore of 60m. ⊕ indicates rate estimated from cores.

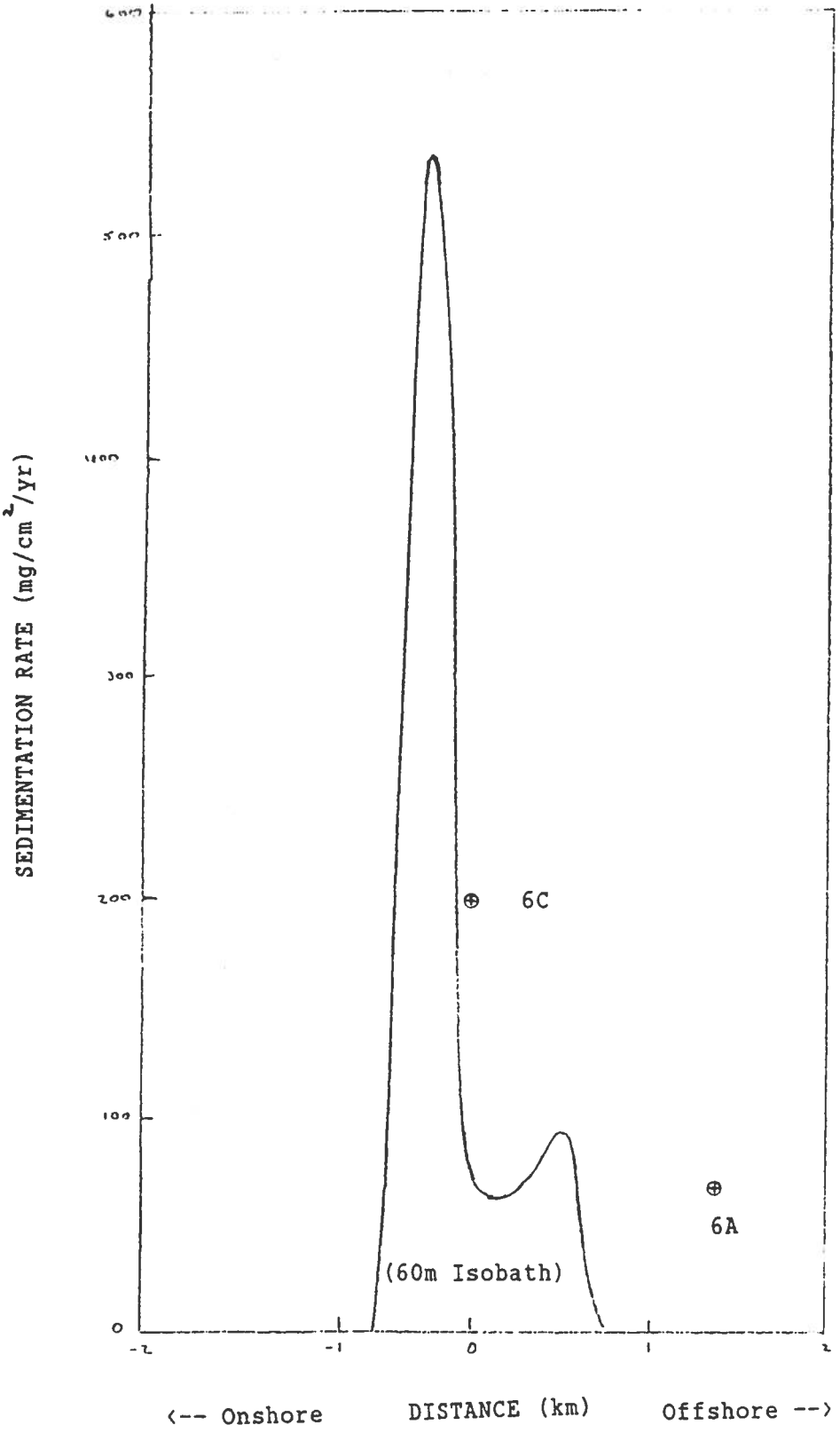

Figure 43. Cross-shore sedimentation distribution for Transect 6 - White Point.

COAG settling speed distribution for C=0.6 mg/l, H=32m. —— indicates SEDF2D predicted distribution (60m isobath), - - - indicates predicted rate if inshore of 60m. ⊕ indicates rate estimated from cores.